SUPPLEMENT SERIES

Astron. Astrophys. Suppl. Ser. **124,** 205-253 (1997)

Physical and chemical variations within the W 3 star-forming region

II. The 345 GHz spectral line survey⋆

F.P. Helmich[1,2] and E.F. van Dishoeck[1]

[1] Leiden Observatory, P.O.-Box 9513, 2300 RA Leiden, The Netherlands
[2] SRON Laboratory Groningen, P.O.-Box 800, 9700 AV Groningen, The Netherlands

Received February 28; accepted September 30, 1996

Abstract. Results are presented of the 345 GHz spectral survey toward three sources in the W 3 Giant Molecular Cloud: W 3 IRS4, W 3 IRS5 and W 3(H_2O). Nearly 90% of the atmospheric window between 334 and 365 GHz has been scanned using the James Clerk Maxwell Telescope (JCMT[1]) down to a noise level of $\sim$ 80 mK per resolution element. These observations are complemented by a large amount of data in the 230 GHz atmospheric window. From this data set physical conditions and beam-averaged column densities are derived for more than 14 chemically different species (over 24 different isotopes). The physical parameters derived in Paper I (Helmich et al. 1994) are confirmed by the analysis of the excitation of other species, although there is evidence that the silicon- and sulfur-bearing molecules exist in a somewhat denser and warmer environment. The densities are high, $\geq 10^6$ cm^{-3}, in the three sources and the kinetic temperatures for the bulk of the gas range from 55 K for IRS4 to 220 K for W 3(H_2O). The chemical differences between the three sources are very striking: silicon- and sulfur-bearing molecules such as SiO and SO_2 are prominent toward IRS5, whereas organic molecules like CH_3OH, CH_3OCH_3 and CH_3OCHO are at least an order of magnitude more abundant toward W 3(H_2O). Vibrationally excited molecules are also detected toward this source. Only simple molecules are found toward IRS4. The data provide constraints on the amount of deuterium fractionation and the ionization fraction in the observed regions as well. These chemical characteristics are discussed in the context of an evolutionary sequence, in which IRS5 is the youngest, W 3(H_2O) somewhat older and IRS4, although still enigmatic, the oldest.

Key words: ISM: molecules — ISM: clouds — ISM: individual: W 3 IRS5, W 3 IRS4, W 3(H_2O) — surveys — radio lines: ISM

1. Introduction

Spectral line surveys are a very powerful method to obtain a detailed physical and chemical overview of star-forming regions. The best-studied example is provided by the Orion-KL object, where various surveys have revealed a very rich chemistry and significant changes in physical and chemical conditions over small ($\lesssim$10″(0.02 pc)) scales (Sutton et al. 1995; Blake et al. 1984; Sutton et al. 1985; Blake et al. 1986, 1987; Jewell et al. 1989; Ziurys & McGonagle 1993; Turner 1991; Greaves & White 1991; Groesbeck 1994). Another well studied object, which also shows a remarkable number of lines and a rich chemistry, is the Sgr-B2 Giant Molecular Cloud (GMC) (e.g., Cummins et al. 1986; Sutton et al. 1991; Turner 1991; Hjalmarson & Bergman 1992). This region, however, has the disadvantage of its large distance and its location in the southern hemisphere. Sgr-B2 is close to the Galactic Center and thus 18 – 19 times farther away than Orion, so that the linear resolution in single-dish observations is much lower. For distant high-mass star-forming regions like W 49A the situation is even worse.

With the availability of large-aperture submillimeter telescopes, the more recent line surveys have shifted to the higher frequency atmospheric windows. The main advantage over the earlier lower frequency data is that only the warmer and denser gas is sampled by the higher excitation lines, so that there is less confusion with the colder,

Send offprint requests to: E.F. van Dishoeck

⋆ Tables 7–12 are also available in electronic form at the CDS via anonymous ftp to cdsarc.u.strasbg.fr (130.79.128.5) or via http://cdsweb.u-strasbg.fr/Abstract.html

[1] The James Clerk Maxwell Telescope is operated by the The Joint Astronomy Centre on behalf of the Particle Physics and Astronomy Research Council of the United Kingdom, the Netherlands Organisation for Scientific Research, and the National Research Council of Canada.

more extended molecular cloud material. Also, the beam sizes are smaller, only $15 - 20''$, compared with $> 1'$ in the early work, so that the observations are much more sensitive to the chemistry on the smallest scales.

The 345 GHz window is a good region in which to perform such surveys, because of its high frequency coupled with good atmospheric transmission. The number of completed projects in this window has recently increased considerably and includes a number of high-mass star-forming objects such as Orion-KL, Orion-S, G34.3 and NGC 6334 (Groesbeck 1994; Sutton et al. 1995; Schilke et al. 1996; Macdonald et al. 1996; McCutcheon et al., in preparation). In addition, more selected settings covering about half the window have been performed for lower-mass objects like IRAS 16293–2422 (van Dishoeck et al. 1995; Blake et al. 1994). Due to the improved sensitivity of receivers and stability of backends it is now possible to do such surveys almost routinely down to low noise levels. Because a large frequency range is covered, these data allow a fairly complete census of the molecules present in the gas, especially of the heavier linear and asymmetric rotor molecules. The surveys automatically cover the optically thin lines of the rarer isotopomers and often contain several transitions of the molecule, so that both the excitation and the column densities of these species can be determined accurately. Combination with lines from lower or higher frequencies can lead to a detailed analysis of the physical parameters of the gas. The disadvantage of the well-studied Orion-KL and Sgr-B2 objects is that the line crowding is so large that an easy identification of the lines is often not possible, and that the contribution of different lines to a blend is hard to estimate, especially in double side-band spectra. CLEANing or maximum entropy techniques are needed to extract the best information out of these spectra.

On the chemical modeling side, there has also been considerable advancement in recent years. The survey data have led to a better appreciation of the importance of gas-grain interactions in star-forming regions, since large abundances of complex organic molecules are difficult to form by ion-molecule gas-phase reactions alone. The preferred current picture is one in which molecules freeze out onto the grains during the cold collapse phase, and are released back into the gas phase (perhaps in modified form) after the star has formed due to radiative heating and shock disruption of the grains. The evaporated molecules subsequently drive a rapid gas-phase chemistry leading to complex organic molecules for a limited amount of time (Blake et al. 1987; Millar et al. 1991; Charnley et al. 1992; Caselli et al. 1993; Shalabiea & Greenberg 1994). These models have been tested against millimeter observations of gas-phase species. Unfortunately, no information on the composition of the ice mantles for the same lines of sight is available.

We present here a 345 GHz line survey obtained with the JCMT of three sources in the W 3 Giant Molecular Cloud: IRS4, IRS5 and W 3(H_2O). Our main motivation for choosing these objects stems from the fact that IRS5 and IRS4 are sufficiently bright at near- and mid-infrared wavelengths to permit ground-based and ISO absorption line observations of solid state features. Thus, information on the chemical composition of *both* the gas phase and the ices will be available for the first time to constrain the models. A second motivation is that the three sources originate from the same parent cloud, and are observed in similar detail with the same telescope. Thus, evolutionary effects can be studied much more accurately. Another advantage is that although W 3 is five times farther away than Orion (at 2.3 kpc; Georgelin & Georgelin 1976), it is still much closer than Sgr-B2, which is almost twenty times more distant than Orion. The $\sim 15''$ JCMT beam corresponds to ~ 0.16 pc, keeping the linear scales within reasonable bounds. Finally, the line blending for these sources is not as severe as in Orion, allowing easier identification and line fitting.

The first results of this project were presented in Helmich et al. (1994); Paper I hereafter). The analysis of this survey actually goes one step further than that of previous surveys. Specifically, the detailed excitation processes of each molecule are considered, rather than just its excitation temperature. Thus information on the kinetic temperature, density and source size for each species is obtained. Observations of a few molecules (H_2CO, CH_3OH and SO_2) showed that the three sources have very different chemical and physical characteristics. Helmich et al. tentatively linked these to the evolutionary stage of the regions. In this paper, the work of Paper I is extended, and all molecules detected toward the three sources are discussed and analyzed. These data support the original conclusions of Paper I, although specific questions about the evolutionary state of the objects remain. Part of the survey data toward W 3 IRS5 have also been analyzed by de Boisanger et al. 1996) to determine the ionization fraction of this source. The observations and analysis of the HDO lines are presented separately in Helmich et al. (1996).

The paper is divided as follows. In Sect. 2, a log of the observations and technical details are given. In Sect. 3, background information on the three sources is presented. In Sect. 4, the method of analysis is presented, and the results are analyzed per molecule in Sect. 5. Sect. 6 discusses the general trends, whereas conclusions are given in Sect. 7. The tables and figures with the observed lines are found at the end of the paper.

2. Observations

Observation time was granted for a total of ~ 50 shifts spread over a number of observing runs between January 1992 to November 1994 on the 15 m JCMT on Mauna Kea, Hawaii. The program was originally set up to observe only specific lines, but was changed after the first successful run to a complete spectral scan of the three

sources. The approach of systematic stepping through the 345 GHz window with 500 MHz bandwidth was therefore adopted only after the first run. In contrast with other surveys, no redundancy was built in, mainly because of time limitations. For more than half of the allocated time, no observations at 345 GHz or higher frequencies were possible due to weather conditions. As a result, many frequency settings in the 230 GHz window were observed as well during the bad weather periods.

At 345 GHz, the facility receiver B3i (Cunningham et al. 1992) was used in all runs, whereas at 230 GHz the Schottky receiver A1 was employed in January 1992, and the SIS-receiver A2 (for characteristics see Davies et al. 1992) in all subsequent observing runs. All three receivers provide an instantaneous bandwidth of 500 MHz. The intermediate frequency of 1.5 GHz for receivers B3i and A2 results in a separation of the two sidebands of 3 GHz, whereas for A1 the difference is 7.88 GHz. The line crowding is such that there is little ambiguity in the assignment of the side band, and line identification is aided by the slightly different $V_{\rm LSR}$ of the three sources. From repeated observations of the same line in different settings and side bands, the side band ratio was found to be close to unity in most runs, except in November 1993, when a potential problem was identified after the run by the JCMT staff. Although only a few measurements were done at this time, the spectra for W 3(H_2O) were re-observed in order to determine the side-band ratio. The difference turned out to be small, so no corrections were made.

The JCMT beam is $15''$ at 345 GHz and $21''$ at 230 GHz. Pointing was checked every $1.5-2$ hours on the continuum of the nearby compact H II region W 3(OH), and was found to be within $3''$ in most cases and somewhat larger under the worst observing conditions. In most observations, a $+180''$ beam-switch in the azimuth direction was used. Experiments show that this is sufficient for the higher-lying transitions of almost all molecules (see Paper I). Only for ^{12}CO a larger switch must be employed. Some of the CO $3-2$ profiles toward W 3(H_2O) and W 3 IRS4 clearly suffer from artificial "absorption" due to emission at the off position.

Calibration was done in the standard way, using the chopper-wheel method (see Kutner & Ulich 1981). In general, the absolute calibration is uncertain by $20-30\%$, which is confirmed from repeated observations of the same lines. Occasional problems did occur, however, especially during warming up of the cold load in August 1993. Because the program was spread out over many observing sessions, it cannot claim the high internal accuracy of some other surveys. However, in some crucial cases it is believed that the internal accuracy is better than 10%, while in the worst cases it should be within 50%.

As described in Paper I, a significant dip due to a mismatch in the mixer was found in the B3i spectra taken in January 1992. This dip was effectively removed by a flat-field provided by the JCMT staff. It also influenced the calibration since the whole bandwidth was used as a total power detector in those data. After 1993 the dip was removed by a channel-by-channel calibration of the backend, so that no further flat fielding was necessary.

As the backend, the facility's 2048 channel acousto-optical spectrometer (AOSC) was used in 1992. It provides a 500 MHz bandwidth and a channel spacing of 250 kHz, with an effective resolution of 2 channels corresponding to 0.65 and 0.43 km s^{-1} at 230 and 345 GHz respectively. The Digital Autocorrelation Spectrometer (DAS) built in Dwingeloo, The Netherlands was used after 1992. The DAS offers the possibility of observing at different bandwidths of 125, 250, 500 and 920 MHz (receiver permitting). In the survey, the 500 MHz bandwidth mode has mostly been used (0.328 km s^{-1} resolution at 345 GHz), with occasional higher resolution settings at 125 and 250 MHz bandwidth. Since the DAS is calibrated channel-by-channel, not only the dip in the B3i spectra is removed, but also the uncertainties in the calibration of lines at the edges of the band. The availability of the DAS in the later runs greatly improved the detection and reliability of the strengths of weak lines.

Integration times of 30 min (ON + OFF) were chosen for each frequency setting on each source. With typical system temperatures of ~ 1000 K at 345 GHz, this results in a 1σ noise level in $T_{\rm A}^*$ of $50-60$ mK per resolution element (1 resolution element equals 2 channels in 500 MHz bandwidth mode) and $30-40$ mK per resolution element at 230 GHz ($T_{\rm sys} \approx 500$ K). For comparison, the rms in the 345 GHz Orion line survey of Groesbeck (1994) and Schilke et al. (1996) is 80 mK, whereas the 230 GHz survey of Sutton et al. (1985) and Blake et al. (1986) had an rms of $0.20-0.30$ K The strongest CO, HCO^+ and HCN lines in this survey are a factor of $\sim 2-4$ weaker than those in Orion; thus, within a factor of 2, the chemistry is probed in comparable detail.

The beam-efficiency for extended objects varied considerably over the three years of observation. The 345 GHz efficiency was measured to be 0.45 in February 1994 when adjustments were being made to the dish surface, whereas it was 0.60 in June and November 1994 when the adjustments had been completed. The efficiency at 230 GHz varied from 0.5 in August 1992 to 0.72 in June and November 1994. A complete list of efficiencies used is given in Table 1. These are the values for small sources as determined from observations of planets. For the W 3 sources, it may not always be justified to use the efficiency for extended objects rather than the value for point sources, but generally the difference between the two values is smaller than the uncertainties in calibration between different runs. In addition, some molecules may be more extended than other species, and there is no systematic method to correct for this. Only a single position was observed for the three sources.

Table 1. Beam efficiencies, number of settings

Observing run	$\eta_{\rm MB}$ RxA1 230 GHz (21″)	$\eta_{\rm MB}$ RxA2 230 GHz (21″)	$\eta_{\rm MB}$ RxB3i 345 GHz (15″)	# of settings
January 1992	0.7	–	0.6	23
August 1992	–	0.5	–	12
December 1992	–	0.63	0.53	4
July 1993	–	0.63	0.53	15
August 1993	–	0.63	0.53	4
November 1993	–	0.63	0.53	2
December 1993	–	0.63	0.53	3
February 1994	–	0.53	0.45	11
June 1994	–	0.72	0.6	16
November 1994	–	0.72	0.6	1

3. The W 3 sources

As introduction and background information for the following sections, an overview will be given of the W 3 region. First the early detections and models will be noted, then the three individual sources will be discussed. A sketch of the region is shown in Fig. 1; it consists of the Giant Molecular Cloud (GMC) core containing IRS4 and IRS5, with a smaller core containing the W 3(OH) and W 3(H_2O) clumps located $\sim 16'$ to the south-east.

The W 3 sources have been popular research objects for many years. Since the discovery of its radio continuum radiation by Westerhout in 1958, W 3 has been the subject of many radio studies. Several H II regions were discovered (e.g. Wynn-Williams 1971; Harris & Wynn-Williams 1976; Colley 1980) and identified with the near-infrared sources of Wynn-Williams et al. (1972). While some of the infrared sources clearly coincide with ionizing radiation of their H II regions, others are hardly associated with any free-free continuum radiation at all. One of these sources (IRS5) has a very deep silicate absorption band at 10 μm (Willner et al. 1982), as well as solid water and methanol bands (Allamandola et al. 1992). Not only is this a clear sign of a very young source, but it is also indicative of large amounts of dust and molecular gas in front of the luminous source. The far-infrared continuum of the W 3 core has been measured e.g. by Werner et al. (1980), Jaffe et al. (1984) and most recently by Ladd et al. (1993). It is now unambiguously clear that IRS5 is one of the most luminous sources, with an output of $1.7\,10^5\ L_\odot$ radiated primarily in the far-infrared. Submillimeter continuum studies (Richardson et al. 1989; Oldham et al. 1994; Ladd et al. 1993) show that the mass of the GMC is concentrated in the core and divided about equally among IRS5, IRS4 and a source 20″ south of IRS4. The nature of the last source is somewhat enigmatic since it is not associated with any of the near-IR sources, and it will not be discussed further.

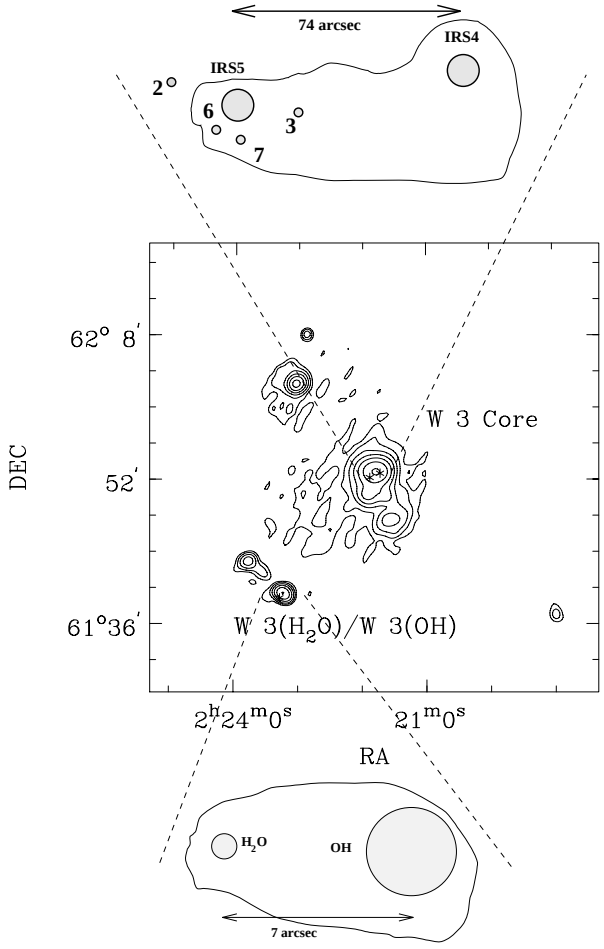

Fig. 1. Middle: a high resolution 25 μm IRAS map (prepared by P. Roelfsema, SRON Groningen) of the W 3 region. The condensation in the center is the core of the giant molecular cloud. The condensation in the lower left corner is the interface between the W 3 and the W 4 region. The core is shown in more detail in the cartoon at the top. The near-infrared sources IRS 2 to 7 and the extent of the dense material traced in the submillimeter continuum are indicated. Below a cartoon of the second condensation is shown, with the compact H II region W 3(OH) and the "hot core" W 3(H_2O) indicated. The coordinates for the three sources studied in the survey are (B1950.0): IRS4 $02^{\rm h}21^{\rm m}43.5^{\rm s}$ $+61°52'49''$; IRS5 $02^{\rm h}21^{\rm m}53.1^{\rm s}$ $+61°52'20''$; W 3(H_2O) $02^{\rm h}23^{\rm m}17^{\rm s}3$ $+61°38'58''$

Early molecular line studies of the entire cloud (Dickel 1980; Dickel et al. 1980; Hayashi et al. 1989) showed that the extent of the GMC core is $4' \times 3'$ (2.7 pc $\times$2.0 pc). Attempts were made to derive accurate column densities from the low-J CO, CS and HCN millimeter lines, but these studies suffer from large optical depths in the lines. The small velocity gradient present over the core has been interpreted as evidence for collapse (Dickel 1980), but recent higher resolution maps in optically thin lines by Tieftrunk et al. (1995) suggest rotation of the core as a whole in the sense of Galactic differential rotation.

Another result from the molecular line mapping is that at the interface region of the W 3 and W 4 clouds the density appears to be rising. At this interface, a second site of high-mass star-formation is located, the compact H II region W 3(OH). Close to W 3(OH) ($\sim 6-7''$ E), at the place of the water masers, Turner & Welch (1984) found a strong, compact object in their millimeter interferometer data, called W 3(H_2O). Both sources are embedded in a core of warm and dense molecular material (Mauersberger et al. 1988; Wilson et al. 1991), as are the infrared sources in the main W 3 core.

3.1. W 3 IRS4

IRS4 is a luminous (near-)IR source (Ladd et al. 1993), associated with a concentration of molecular material and dust of 1500 $M_\odot$ (Oldham et al. 1994). The molecules found toward this source are simple species containing 2−4 atoms, with the exception of methanol (see Paper I), while the lines are narrow with a typical line width of 3.5 km s^{-1} around $V_{\rm LSR} = -44$ km s^{-1}. As shown in Paper I, the cloud is dense (10^6 cm^{-3}) and warm (~ 55 K). Taken together, a picture of a relatively unperturbed, somewhat warm molecular cloud emerges. This is strengthened by the fact that, in contrast with other pre-main sequence objects, no clear outflow signature has been found (e.g. Hasegawa et al. 1994, HMMT hereafter; see also Sect. 5.1). Also, the characteristic H_2O or OH masers seen in other sites of star-formation are missing.

Close to the peak of the near-infrared radiation, a shell-like structure is found in the radio continuum by Colley (1980). Together with the high infrared luminosity, this has been interpreted in Paper I as a blister structure arising at the back-side of the cloud, indicating that IRS4 is a more evolved object of spectral type O9 (Colley 1980) which has already broken free from its parent cloud. This explanation is not generally accepted, since IRS4 could also be at the earliest evolutionary stages where the outflow has yet to emerge (Tieftrunk et al. 1995).

3.2. W 3 IRS5

The most luminous source in the W 3 cloud core is IRS5. Its energy output has long been thought to be due to a single, young O-star heating its environment. Recently Claussen et al. (1994) showed the existence of several small radio-blobs at the position of IRS5. Each "blob" has the ionizing radiation comparable to that of an early-B star. Near-infrared observations of Megeath et al. (1996) show that there are infrared counterparts to at least 4 of these radio sources. Moreover, they provide evidence that these sources have masses larger than 10 $M_\odot$ each. Together with these high-mass stars, a dense cluster of less massive stars has been detected in the IRS5 clump, giving a star-formation efficiency of more than 20%.

The activity in this region was traced by earlier observations of molecular lines. The CO, CS and HCN lines (Dickel 1980; Dickel et al. 1980; Hayashi et al. 1989; Mitchell et al. 1991, 1992; Choi et al. 1993, HMMT) all show broad wings characteristic of outflowing gas. This gas was also detected in the ro-vibrational CO lines seen in absorption toward IRS5 at near-infrared wavelengths by Mitchell et al. (1990, 1991). However, whereas the (sub-)millimeter emission lines are all centered at $V_{\rm LSR} = -39$ km s^{-1}, the infrared lines show absorption ranging from -100 to -39 km s^{-1}. Mitchell et al. were able to derive temperatures and column densities for the absorbing components (see HMMT for the most recent values). In Paper I the outflowing gas was tentatively linked to the high temperature SO_2 emission found toward IRS5. At the place where the outflow runs into the ambient medium the temperature is expected to rise. Subsequent high-temperature chemistry efficiently converts sulfur into sulfur dioxide.

The majority of the gas is, however, at lower temperatures (~ 100 K, Paper I) than the SO_2 and at the same density as IRS4. It is this gas that is expected to be traced by most other molecular lines. In general, lines toward IRS5 have a typical width of 5 km s^{-1}, although some show wings due to the outflowing gas. Deep self-absorptions are seen in the optically thick lines of CO, indicating the presence of colder, lower density foreground gas.

3.3. W 3(H_2O)

Most earlier observations have concentrated on the very bright, compact H II region W 3(OH), mainly because the OH masers provide excellent tools to study kinematics (see Bloemhof et al. 1992 for an overview). Subsequent work at high spatial resolution showed that the source of the H_2O masers 7″E is much stronger in lines of molecules such as HCN, NH_3 and CH_3CN (Wink et al. 1994; Mauersberger et al. 1988; Turner & Welch 1984). The line widths are typically 5.5 km s^{-1}, although the outflow can be seen in the CO lines. Using millimeter aperture synthesis, it was shown by Turner et al. (1994) and Wilner et al. (1995) that there is a very compact core ($< 1''$) of line and continuum radiation, which most likely hosts an early B-star. Turner & Welch already argued that the heating of the W 3(H_2O) clump cannot be provided by W 3(OH), so that it must be a site of star-formation itself. This is confirmed by measurements of the spatial and kinematical changes in the H_2O maser positions by Alcolea et al. (1992) and Reid et al. (1995). Reid et al. also showed that synchrotron emission is coming from this clump and that it is likely that the jets, producing the synchrotron emission, drive the outflow from this source.

Three components of molecular gas can be distinguished in the direction of W 3(H_2O). The first is the warm and dense core in which both W 3(H_2O) and

W 3(OH) reside. On the basis of submillimeter continuum maps (Sandell 1995, private communication) the size of this core is estimated to be $\sim 1'$, larger than our JCMT beam. The second are the $5 - 10''$ condensations seen in the interferometer map of HCO^+ by Wink et al. (1994), and the third is the very dense clump of $\sim 1''$ seen in CH_3CN by Wink et al. and in the continuum by Wilner et al. (1995). In general the emission lines occur at a V_{LSR} of -47 km s^{-1}. Absorbing gas is found only in the direction of W 3(OH) but at a velocity of -44 km s^{-1}, indicating the presence of a less dense envelope surrounding the core. We will argue that most of our observed single-dish emission comes from the dense core surrounding W 3(H_2O) and W 3(OH), and from condensations within it.

3.4. Evolutionary stages

Although the three sources originate from the same parent molecular cloud, they have very different chemical characteristics (Paper I), and the question arises if this can be explained by different evolutionary stages.

Toward IRS5, there are clear signs of large amounts of molecular material frozen on the grains, and the overall kinetic temperature may still be rising with time. Toward W 3(H_2O), the large abundance of methanol provides evidence for a "hot core" chemistry, in which species like methanol and formaldehyde have recently evaporated from the grains and drive a complex organic chemistry. Toward IRS4, a quiescent chemistry with simple molecules was found. This is in agreement with the current scenarios of the evolution of gas and dust in high-mass star-forming regions. We therefore interpreted the phenomena seen in Paper I with an evolutionary sequence in which IRS5 is the youngest, IRS4 is the oldest and W 3(H_2O) is somewhere in between. This hypothesis will be further investigated through the more detailed, complete set of observations presented here and through quantitative chemical models by Helmich et al. (1997).

4. Analysis

4.1. Line identification and profile fits

In the $334 - 365$ GHz range ~ 28 GHz was scanned for the three W 3 sources, compared with ~ 23 GHz in the $216 - 263$ GHz range. In total 100 lines of 14 different molecules (24 including isotopic species) were detected in W 3 IRS4, 187 of 18 molecules (31 isotopes) in IRS5, and 354 of 22 molecules (41 isotopes) in W 3(H_2O). After calibration, base line subtraction, smoothing and line identification, the lines were fit with single Gaussians using the IRAM CLASS software. The line frequencies were obtained mainly from the JPL[2] (Pickett 1991) and Lovas catalog (see Groesbeck 1994). A detailed list with frequencies for methanol, methyl formate and dimethyl ether is given in Anderson et al. (1990, and by Herbst (private communication). A complete list of $^{34}SO_2$ lines in this frequency range became available at the end of 1994, while some frequencies for ^{33}SO were taken from Sutton et al. (1991, 1995). Most of this information was incorporated into the SIMCAT software at the California Institute of Technology (Groesbeck 1994), and was heavily used during this study. The results can be found in Tables 7-12. Only a handful of lines remain unidentified, which are summarized in Table 4 at the end of the paper.

Although in general good single Gaussian fits were readily obtained, the widths of the lines were found to vary considerably. Explanations for this behavior can be blending with other lines; blending with a line in the other sideband; outflowing gas (e.g., CO); saturation of the line (e.g., SO), blending of hyper-fine components; and in some cases problems in the determination of the base line (some CH_3OCH_3 and CH_3OCHO lines). In cases where the line widths varied substantially this is indicated in the discussion per molecule. In Tables 7-12 the listed values are generally those from the Gaussian fits, but in a few complicated cases the integrals over the line are given. Footnotes indicate blending, absorption, or problems encountered. No attempt has been made to disentangle the individual contributions to the integrated line strength in case of blended components. In the subsequent analysis, error bars on high S/N lines are taken to be 30%, whereas 60% is adopted for marginal cases. If upper limits are used in the analysis their integrated line strength was calculated using the 2σ noise temperature together with the characteristic velocity width of the source given in Sect. 3.

As discussed in Paper I, not only emission from W 3(H_2O) is picked up by our 15 and $21''$ beams, but also from the compact H II region W 3(OH). In the analysis of the data it turned out that this confusion is very small and that most emission is indeed from W 3(H_2O). This is strengthened by interferometric observations (Wink et al. 1994; Wilner et al. 1995; Turner & Welch 1984) which show that compact line emission is concentrated at W 3(H_2O) (the Turner-Welch object), whereas W 3(OH) dominates the continuum maps. Most of the extended emission stems from the core surrounding the two objects.

4.2. Excitation analysis

As was done in Paper I, rotation diagrams were constructed for those species for which a sufficient number of lines are available. The rotation diagram method (e.g., Blake et al. 1987; Sutton et al. 1985; Turner 1991; Sutton et al. 1995) is a powerful tool to determine the rotational excitation temperature and the beam-averaged column density. It requires the lines to be optically thin and the level populations to be thermalised, but even deviations provide very useful information about optical

[2] http://spec.jpl.nasa.gov/

thickness and/or non-thermal excitation (cf. Blake et al. 1994; Sutton et al. 1995). The method only works well, however, if a sufficient number of lines of the same molecule have been detected. Especially linear molecules often have only two or three transitions in the scanned frequency range, which limits the usefulness of the derived rotational temperature. An exception is OCS, which is heavy enough that several lines are covered in the survey and detected toward W 3(H_2O). On the other hand, asymmetric rotors, like SO_2 and CH_3OH, have a large number of transitions in the scanned frequency range which are easily observed. Other species for which rotation diagrams could be constructed are CH_3CN, CH_3OCH_3, CH_3OCHO and CH_3C_2H. They are shown in Fig. 2. It should be noted that these organics are found primarily toward W 3(H_2O).

A better method to analyze the data is through statistical equilibrium calculations. This has not been done with earlier survey data (e.g. Blake et al. 1995; Schilke et al. 1996), but provides direct constraints on the physical parameters, in particular kinetic temperature and density. The adopted method, described in detail in Jansen et al. (1994), van Dishoeck et al. (1993b) and Jansen (1995), solves the level populations of a molecule by balancing the collisional and radiative upward and downward rates. The necessary decoupling of radiative transfer and level populations is done by means of an escape probability formalism. The adopted collisional rate coefficients are summarized in Jansen et al. (1994) and Jansen (1995). Linear rotors are particularly useful in determining the density, whereas (near-) symmetric rotors like H_2CO also have transitions which are very sensitive to the kinetic temperature. In Paper I, the densities were constrained to be $\sim 1\ 10^6$, $1\ 10^6$ and $2\ 10^6$ cm^{-3} for IRS4, IRS5 and W 3(H_2O), respectively, and the temperatures 55^{+20}_{-10}, 100^{+40}_{-20} and 220 ± 40 K from the ratios of H_2CO lines. These values will be adopted in this work for those molecules that do not provide constraints themselves (e.g. single lines).

The statistical equilibrium calculations have been applied mostly to the optically thin (isotopomer) lines present in the survey, although the code can handle moderately optically thick transitions as well. The optically thick lines are useful for a different purpose: once their excitation temperature has been obtained from the isotopomers, they give valuable information about the area-filling factor of the beam, or equivalently, about the source size. Two different methods have been used. For species for which rotation diagrams have been constructed, the inferred excitation temperature for the optically thin isotope has been used in conjunction with the observed main beam temperature of the most optically thick line observed. For other molecules, excitation calculations have been performed using the physical conditions and column density derived from the optically thin isotope. The predicted radiation temperature of the main species has then been compared with the observed value to derive the area-filling factor. Although the results are not very accurate, they give a useful indication of the distribution of the species in the source. The main uncertainty in the first method is caused by the fact that often the main lines have optical depths of $\sim 0.5 - 3$, i.e., somewhat optically thick but not very thick.

For consistency, it is assumed *throughout* this paper in the excitation analysis that the emission fills the beams, thereby implying that the inferred beam-averaged column densities are lower limits to the "true" column densities (see Sect. 4.3). The beam-averaged column densities refer to the $\sim 15''$ 345 GHz beam, unless otherwise stated.

4.3. Discussion of uncertainties

As mentioned in Sect. 2, the absolute calibration of submillimeter lines is accurate to about 30%. The rotation diagram method gives a formal error in rotation temperature and column density, but optical depth and non-LTE conditions can introduce additional uncertainty. In particular, if the lines are optically thick, this will lead to an overestimate of the rotational temperature. Subthermal excitation, on the other hand, implies that the rotational temperature is an underestimate of the kinetic temperature. These effects are better taken into account in the statistical equilibrium calculations, but these depend on the relative and absolute accuracy of the collisional rate coefficients, which can vary from species to species. Altogether, we estimate that the *beam-averaged* column densities obtained in this study are accurate to better than a factor of two.

A much larger uncertainty in the eventual chemical analysis is introduced by the unknown coupling between telescope beam and source. It is difficult to estimate this influence, since it will vary from molecule to molecule, or even from line to line. A source size of $10''$ implies that lines in the 345 GHz window are diluted by a factor of 3, and lines in the 230 GHz window by a factor of 5. For source sizes of $1 - 2''$, as may apply to some species in W 3(H_2O) (Wink et al. 1994), the correction to the column density can be more than two orders of magnitude.

The analysis of the physical parameters is much less affected by the unknown source size. The ratio of a 230 and a 345 GHz line intensity is off by at most a factor of two, if the emission comes from a point source. The excitation effects are often much larger than a factor of two over a narrow density range (cf. Jansen 1995), so that the physical parameters can still be determined quite accurately. For small source sizes, the density will tend to be overestimated, and the beam-averaged column densities underestimated.

In order to determine abundances which can be compared directly with chemical models, information on the H_2 column density is needed. In this study the total column density is determined from observations of an optically thin $C^{17}O$ line. The uncertainty in the

$C^{17}O/H_2$ abundance introduces a factor of 2–3 uncertainty in derived H_2 column density. This value is again beam-averaged; because CO may be more broadly distributed than some other molecules, the correction factors for source structure are not necessarily the same. Thus, local abundances may differ considerably from the beam-averaged integrated abundances along the line of sight presented here.

4.4. Isotopic abundances

The determination of column densities from optically thin lines of isotopic species requires information on the overall isotopic abundances. As a convention, the main isotopomer is given without atomic weight numbers throughout this paper. Thus CO stands for $^{12}C^{16}O$, whereas the ^{13}C isotopomer is written ^{13}CO etc. The following solar abundance ratios are used (Wilson & Rood 1994): $[^{12}C]/[^{13}C] = 60$; $[^{16}O]/[^{18}O] = 500$; $[^{16}O]/[^{17}O] = 2600$; $[^{14}N]/[^{15}N] = 270$; $[^{32}S]/[^{34}S] = 22$; $[^{32}S]/[^{33}S] = 127$ and $[^{28}Si]/[^{29}Si] = 20$. For deuterium no ratio is given, since deuterium fractionation is highly variable in dense molecular clouds.

5. Results

The spectra obtained in the line survey are presented in order of increasing frequency in Fig. 4. Tables 7 to 12 summarize the resulting fits to the line profiles, whereas Table 3 contains the beam-averaged column densities. In the following, the results will be discussed per molecule, describing first the data for IRS4, then for IRS5 and finally for W 3(H_2O).

5.1. CO

The most recent CO maps of W 3 include those by Hasegawa et al. (1994) in ^{12}CO and ^{13}CO $3-2$ and $6-5$ lines and by Oldham et al. (1994) in $C^{18}O$ $2-1$. The data obtained here on additional isotopic species at just a few positions form a complement to this study, since mapping is beyond the scope of this work.

The CO $3-2$ line toward W 3 IRS4 is strong with $T_{\rm MB} \approx 60$ K, but the CO profiles decrease sharply on the red side, which was already noted by Mitchell et al. (1991) and HMMT. In some of the spectra shown here the profile is further affected by emission at the off-position, seen as an extra "absorption". No other molecule or CO isotopomer shows a similar line shape. The profile can be affected by absorption by cold foreground material, but it also bears some resemblance to shocked profiles like those found in IC 443 (van Dishoeck et al. 1993). In the case of IRS4, such a shock could be generated at the interface region where the ionization front runs into the cloud. Because IRS4 is at the back, the shock would be coming toward us, consistent with the blue wing. HMMT also find evidence for moving gas associated with IRS4 from pedestal features in the spectra, which they interpret either as outflow or due to the expansion of the H II region. The main beam temperature of ~ 60 K is close to the kinetic temperature of 55 K found from the formaldehyde lines. Because the line is heavily optically thick, it suggests that the warm gas fills most of the beam, and that the kinetic temperature is likely somewhat higher than 55 K.

The CO $3-2$ spectrum toward W 3 IRS5 shows strong wings, caused by the massive outflow known from other studies (e.g., Mitchell et al. 1991, 1992; Choi et al. 1993, HMMT). Another interesting feature is the strong self-reversal of the $2-1$ and $3-2$ profiles toward IRS5. Even in the $3-2$ line, the absorption is very strong, implying a large amount of cold material in front of IRS5. Our absorption is deeper than that found in HMMT, which may be partly due to lower spectral resolution in the HMMT data. Also, a slight pointing offset from the IRS5 position results in a less strong absorption and a less symmetric profile, as is well illustrated by Figs. 1 and 2 of HMMT. HMMT estimate an excitation temperature of 26 K for the foreground gas at the IRS5 position, and find that this temperature is rather constant over the cloud. Note that this value is similar to that found from the ro-vibrational absorption line spectroscopy toward IRS5 (HMMT; Mitchell et al. 1990). The depth of the absorption in our data suggests that even colder or lower excitation material is present along the line of sight.

At least three Gaussian components are needed to fit the central line, its wings and the self-absorption, making the fit somewhat uncertain. It is, however, difficult to obtain any fit for the central emission with $T_{\rm MB}$ smaller than 100 K, which again is close to the kinetic temperature found from the H_2CO lines (see Paper I), indicating that this gas fills a significant fraction of the beam. Additional evidence for these high temperatures stems from high-J CO $9-8$, $12-11$, $14-13$ and $16-15$ measurements (Boreiko & Betz 1991; Betz & Boreiko 1995). On the other hand, no good fit can be obtained for $T_{\rm MB}$ larger than 200 K. Thus, the hotter gas with $T_{\rm kin} \approx 200-270$ K visible in the ro-vibrational CO absorption lines (Mitchell et al. 1990); HMMT) must originate in a volume which is smaller than the $15''$ beam.

The self-reversal of the CO $3-2$ line toward W 3(H_2O) is less strong than that toward IRS5. Several absorption components appear to be present, although their appearance is again affected by the small beam-switch of $+180''$. The $3-2$ line profile also shows strong wings. Although no map of the red and blue components has yet been made, the movement of the water masers (Alcolea et al. 1992; Reid et al. 1995) suggests that an outflow is present at the H_2O position. However, the close proximity of the compact H II region W 3(OH) and its unknown contribution to the line profiles can complicate the picture. The fit to the central component is even more difficult and no reliable upper limit can be given. A lower limit to the main-beam

temperature is again 100 K, which is probably close to the kinetic temperature of the warm core surrounding both W 3(OH) and W 3(H_2O). Higher temperatures ($\sim$ 220 K) may be present, but are not observed, because the emission from the core is already optically thick.

The data on the CO isotopomers for the three sources are much easier to analyze, since they do not show self-absorption and are almost Gaussian in shape. For all three sources, even the ^{13}CO lines are still optically thick. Only the C^{17}O emission is surely optically thin. CO column densities have been derived using the physical parameters found in Paper I and the isotope ratios of Sect. 4.4. The H_2 column densities are subsequently determined using $[CO]/[H_2] = 2.7\,10^{-4}$, as found for the warm star-forming region NGC 2024 by Lacy et al. (1994). The resulting beam-averaged total CO and H_2 column densities are summarized in Table 2. Note that the H_2 column densities are a factor of 3 lower than those listed in Paper I because of the higher adopted CO abundance.

As discussed in Sect. 3, the C^{18}O $1-0$ line has been mapped interferometrically in the direction of W 3(OH)/W 3(H_2O). The emission is concentrated in a $\sim 5''$ clump toward W 3(H_2O). However, most of the single dish emission ($\sim$ 80%) is resolved out, suggesting that indeed the emission observed at the JCMT largely fills the beam.

5.2. Linear nitrogen-bearing molecules

The molecules in this section are all linear nitrogen-bearing molecules. Due to the non-zero nuclear spin of the nitrogen atom, these molecules show hyperfine splitting of the lower rotational lines, but in the higher lines the splitting is generally smaller than the line widths, so that these blended components are treated as a single line.

5.2.1. CN

CN is one of the few molecules which is more prominent in the direction of W 3 IRS4 than in the other two sources, as can be seen in several spectra around 337 and 340 GHz. Some satellite lines well separated from the main lines can be detected, but do not allow an accurate determination of the optical depth. A complication in determining the CN rotational excitation is that the lines in the 230 and 345 GHz windows stem essentially from just two energy upper levels, both lower than 40 K. The column density derived from the rotation diagram method is therefore very uncertain. Excitation calculations have been performed for this molecule, using a more extended set of collision rates of Bergman (1995, private communication). The $3\frac{5}{2}\frac{7}{2} - 2\frac{3}{2}\frac{5}{2}/\ 2\frac{3}{2}\frac{5}{2} - 1\frac{3}{2}\frac{5}{2}$ ratio has been used to restrict the gas density to $\sim 1\,10^6$ cm^{-3} toward IRS4, assuming $T = 55$ K. Note that the 345 GHz main lines become slightly optically thick ($\tau \approx 0.55$).

For IRS5 the observed line ratio is the same as that found for IRS4, implying a similar density of $1\,10^6$ cm^{-3}, even for the slightly higher kinetic temperature of 100 K. The beam-averaged column density is a factor 2 lower than in IRS4. For W 3(H_2O), the column density is $1.1\,10^{14}$ cm^{-2}, similar to IRS5.

5.2.2. HCN

Early interferometer measurements by Wright et al. (1995) and single-dish observations of Dickel et al. (1980) and Hayashi et al. (1989) have shown that there is a large concentration of HCN south of IRS4, and a lack toward IRS5. With the current improved receiver technology, not only HCN but also the ^{13}C and ^{15}N isotopomers have been detected toward all three sources, implying high optical depths in the lines of the main isotope. The best candidates for statistical equilibrium calculations are therefore the H^{13}CN $4-3$ and $3-2$ lines, but unfortunately the $4-3$ line is severely blended with SO_2, even in the case of IRS4 where little SO_2 present. Therefore the physical parameters derived in Paper I were used to fit the measured strength of the H^{13}CN $3-2$ line.

The corresponding H^{13}CN beam-averaged ($20''$) column density for IRS4 is $1.1\,10^{13}$ cm^{-2}, whereas the ^{15}N isotopomer N(HC^{15}N) gives $3.1\,10^{12}$ cm^{-2}, resulting in N(HCN) $= 6.6\,10^{14}$ cm^{-2} and $8.4\,10^{14}$ cm^{-2}, respectively. The difference between the two numbers is well within the error bars. The excitation temperature inferred from the statistical equilibrium calculations is 26 K. The fact that the optically thick main isotopomer line ($J = 4-3$) has a main beam temperature of 5.6 K implies a source size of more than $9.5''$.

For IRS5 the same procedure was followed giving N(H^{13}CN) $= 5.9\,10^{12}$ cm^{-2} and N(HC^{15}N) $= 2.1\,10^{12}$ cm^{-2}, which correspond to N(HCN) $= 3.5$ and $5.3\,10^{14}$ cm^{-2} respectively. Again, the strength of the optically thick line suggests that the emission is beam filling. The failure of Wright et al. (1995) to detect HCN emission in this direction may thus also stem from the fact that the emission is not very concentrated and therefore filtered out by the interferometer.

For W 3(H_2O) the beam-averaged column densities are N(H^{13}CN) $= 1.1\,10^{13}$ cm^{-2} and N(HC^{15}N) $= 6.6\,10^{12}$ cm^{-2}, resulting in N(HCN) $= 6.6$ and $12\,10^{14}$ cm^{-2}. The large difference suggests that even H^{13}CN emission is still somewhat optically thick. If the emission comes from a small source, the inferred column densities are much higher and only the HC^{15}N lines stay optically thin. A small HCN source ($\sim 1.2''$) is consistent with the interferometer observations of Turner & Welch (1984). However, some of the emission must also come from the more extended surrounding envelope, since the excitation temperature combined with the observed main beam temperature of the optically thick HCN indicates a source of $\sim 11''$.

Table 2. $C^{17}O$ $3-2$ fit parameters and beam-averaged column densities

Source	T_{MB} (K)	ΔV (km s^{-1})	W (K km s^{-1})	T_{kin} (K)	$n(H_2)$ (cm^{-3})	$N(C^{17}O)$ (cm^{-2})	$N(CO)$ (cm^{-2})	$N(H_2)^a$ (cm^{-2})
W 3 IRS4	3.73	3.6	14.3	55	$1\,10^6$	$7.3\,10^{15}$	$1.9\,10^{19}$	$7.0\,10^{22}$
W 3 IRS5	4.47	4.1	19.5	100	$1\,10^6$	$1.3\,10^{16}$	$3.3\,10^{19}$	$1.3\,10^{23}$
W 3(H_2O)	3.23	4.4	15.1	100	$2\,10^6$	$1.0\,10^{16}$	$2.6\,10^{19}$	$9.6\,10^{22}$

[a] Using $[CO]/[H_2] = 2.7\ 10^{-4}$ determined by Lacy et al. (1994) for NGC 2024.

5.2.3. HNC

HNC is of interest for comparison with HCN since the HNC/HCN abundance ratio has been found to differ significantly between cold dark clouds, where it is close to unity, and warm clouds, where HCN can be more abundant by up to two orders of magnitude (Irvine et al. 1987; Goldsmith et al. 1986; Schilke et al. 1992). In W 3, HCN is also observed to be more prominent than HNC. Lines of HNC and $HN^{13}C$ were detected toward all three sources, while there is a detection of one $H^{15}NC$ line toward W 3(H_2O). The lines of the main isotopomer are most likely optically thick, thereby necessitating the use of the ^{13}C isotopomer for statistical equilibrium calculations. The density can in principle be derived from the $4-3/3-2$ ratio, but the $HN^{13}C$ lines are weak and the signal-to-noise ratio is poor. Also, the $3-2$ line can be affected by a blend with SO_2, especially toward IRS5. Nevertheless, the line ratios of order unity indicate high densities, consistent with or perhaps even somewhat larger than those derived in Paper I from H_2CO.

If the physical parameters of Paper I are used to fit the $4-3$ line, $N(HN^{13}C) = 3.3\,10^{12}$ cm^{-2} toward IRS4 and thus $N(HNC) = 2.0\,10^{14}$ cm^{-2}. The source size is found to be $\sim 10''$. For IRS5, $N(HN^{13}C)$ is found to be $3.2\,10^{12}$ cm^{-2} and thus the beam-averaged HNC column density is $1.9\,10^{14}$ cm^{-2}. The (uncertain) source size is $\sim 5''$, smaller than that found for HCN. Toward W 3(H_2O), $N(HN^{13}C) = 1.5\,10^{12}$ cm^{-2} and thus $N(HNC) = 9.0\,10^{13}$ cm^{-2}. Using these parameters the inferred source size is $9''$. The corresponding HCN/HNC column density ratios for the three sources are ~ 4, ~ 3, and ~ 13, respectively.

5.2.4. HC_3N

Although HC_3N is a common molecule in the Orion and Taurus clouds, it is still undetected in the W 3 GMC core. The non-detections toward IRS4 and IRS5 may have several reasons. The most important one is that the lines available in the 230 and 345 GHz windows originate from levels that are rather high up in energy ($\sim 120-300$ K), making it difficult to populate these levels in gas with temperatures below 100 K. Moreover, the molecule has a large dipole moment, so that the critical densities are large ($> 10^6$ cm^{-3}). The upper limits on the lines still provide useful limits on the beam-averaged column density, if the temperature and density from Paper I are adopted. For IRS4 the best upper limit comes from the $24-23$ line and is $N(HC_3N) < 2.5\,10^{13}$ cm^{-2}. For IRS5 the same line gives $N(HC_3N) < 9.8\,10^{12}$ cm^{-2}. The HC_3N column densities are an order of magnitude less than those of HCN toward the two sources.

HC_3N is detected toward W 3(H_2O), and is one of the few more complex unsaturated molecules identified here. Although one of the detected lines is blended, it still gives an upper limit on density ($< 2\,10^8$ cm^{-3}) and on temperature (≤ 300 K). These limits are not very stringent, because an error of 30% can already bring these values down to the physical parameters of Paper I. Using the Paper I values gives a beam-averaged column density of $1.5\,10^{13}$ cm^{-2}.

5.2.5. HNCO

HNCO is not detected toward IRS4, but is marginally present toward IRS5 and clearly toward W 3(H_2O). Care has to be taken in analyzing its excitation, since it is well known from observations of the Galactic Center that infrared pumping can affect the populations (Churchwell et al. 1986). Since only a few lines have been detected in this survey, a study like that of Churchwell et al. is not possible, even though intense far-infrared radiation is present toward these two sources and pumping is likely. An alternative is the rotation diagram method, which gives $T_{rot} = 53 \pm 9$ K and $N = 4.8 \pm 1.8\,10^{14}$ cm^{-2} toward W 3(H_2O).

Toward IRS5, the rotation temperature was assumed equal to the kinetic temperature from Paper I, because only two weak lines have been observed. The fit of the strength of the 351.633 GHz line results in a (highly uncertain) beam-averaged column density of $4.4\,10^{13}$ cm^{-2}. If $T_{rot} = T_{kin}$ is assumed for IRS4, the non-detections give an upper limit $N(HNCO) < 2.8\,10^{13}$ cm^{-2}.

5.3. Unsaturated organic molecules

5.3.1. CCH

CCH is a linear molecule with strong doublet lines toward IRS4. The measurements allow determination of the density from the $4-3/3-2$ line ratio, and the results are consistent with those found in Paper I. Using these values, the beam-averaged column density is $1.9\,10^{14}$ cm^{-2}. Toward IRS5, the molecule is also detected and the line ratio indicates a similar density as found from formaldehyde. The corresponding column density is $1.2\,10^{14}$ cm^{-2}.

Toward W 3(H_2O), the 349 GHz lines of CCH are blended with the CH_3CN 19_K-18_K lines, but the CH_3CN contribution can be estimated rather well so that this does not pose a problem but only increases the error bars. The density derived from the line ratio is again consistent with that found in Paper I and implies $N(\mathrm{CCH}) = 1.3\,10^{14}$ cm^{-2}.

5.3.2. CH_3C_2H

CH_3C_2H is a non-saturated molecule, which can be made quite easily through pure gas-phase chemistry. Three lines have been detected toward IRS4, but the corresponding rotation temperature is uncertain since one of the lines is on the edge of the spectrum. The results are $T_{\rm rot} = 25 \pm 12$ K and $N(\mathrm{CH_3C_2H}) \approx 8\,10^{14}$ cm^{-2} with an uncertainty of a factor of two (see Fig. 2). CH_3C_2H is not detected toward IRS5, but an upper limit of $1\,10^{14}$ cm^{-2} is found if an excitation temperature of 50 K is assumed.

Many lines are detected toward W 3(H_2O), allowing a more accurate rotation diagram than for IRS4. The inferred parameters are $T_{\rm rot} = 63 \pm 8$ K and $N(\mathrm{CH_3C_2H}) = 6.1 \pm 2.3\,10^{14}$ cm^{-2}. The rotational temperature seems to indicate that the CH_3C_2H resides in the same gas as the CO ($\sim$ 100 K), and not in the compact "hot core" with a much higher temperature, since no lines were detected from very high energy levels (e.g. like methanol, see Paper I).

5.4. Complex organics

Formaldehyde and methanol are two particularly useful organic molecules, which can provide a large amount of information about the physical and chemical characteristics of the gas they reside in. Other (saturated) organics like CH_3CN, CH_3OCH_3 and CH_3OCHO are typical for "hot-core" type regions and are only detected toward W 3(H_2O). Ethanol (C_2H_5OH) also belongs in this category but has not been detected in this survey.

5.4.1. H_2CO

The results of Paper I for IRS4 and IRS5 have not changed, but more information on the ^{13}C isotopomer has been obtained toward W 3(H_2O). The $3_{12}-2_{11}$ line has been detected in two independent sets of observations and indicates that the $H_2CO/H_2^{13}CO$ ratio of integrated intensities lies in between 10 and 40. The column density for ortho-$H_2^{13}CO$ is $3.8\,10^{12}$ cm^{-2}, which implies $N(\mathrm{H_2CO}) \approx 3\ 10^{14}$ cm^{-2} for an ortho/para ratio of 3. This value is consistent with $N(\mathrm{H_2CO}) \approx 4\ 10^{14}$ cm^{-2} derived in Paper I.

The source size determined from the (slightly) optically thick $H_2CO 3_{12}-2_{11}$ line is larger than the 220 GHz beam, suggesting that the emission comes largely from the warm core surrounding W 3(H_2O) and W 3(OH). Some H_2CO is likely to be present as well in the compact "hot core", but observations of higher excitation lines and/or ^{13}C isotopomer are needed to probe this region.

5.4.2. CH_3OH

Methanol was discussed extensively in Paper I, and the results remain valid except for small corrections based on more extensive data. See Table 3 for beam-averaged column densities and rotational temperatures. It should be noted that the values for IRS5 are still uncertain, since the detections have large error bars. The methanol lines have been grouped in Tables 8-10. For W 3(H_2O) the lines are grouped according to the quantum number of the torsional mode ($\nu_{\rm t} = 0, 1, 2$). The different sets were fitted separately, but this did not improve the fit, nor was any systematic trend visible. Therefore, just as in Paper I, a single temperature was used and the scatter in the diagram is explained best with the methanol being subthermally excited.

5.4.3. CH_3CN

The CH_3CN lines toward W 3(H_2O) were fitted with $T_{\rm rot} = 375 \pm 210$ K and $N(\mathrm{CH_3CN}) \approx 6\,10^{13}$ cm^{-2} with large uncertainties. Especially the two lines coming from levels with energies higher than 300 K seem to deviate from the fit. If these two lines are left out, the rotational temperature becomes 81 ± 20 K and the column density $3.2 \pm 2.1\,10^{13}$ cm^{-2}. Thus, the column density is fairly robust, whereas the rotational temperature is not. The first estimate is favoured since there is no good reason to delete the two detected lines. The scatter can come from subthermal excitation such as found for methanol, but perhaps infrared pumping and optical depth effects can play a rôle as well.

Statistical equilibrium calculations have been performed and show that the kinetic temperature must be higher than 120 K and the density of order $4\,10^6$ cm^{-3}. The ortho and para column densities are 1.0 and $1.7\,10^{13}$ cm^{-2} respectively. The ortho-para ratio is close to unity, as expected for a warm region.

The above analysis assumed that the CH_3CN emission fills the 230 and 345 GHz beams. However, the interferometer data of Wink et al. (1994) show that the

CH_3CN emission comes from an unresolved region, with most of the single dish flux recovered in the interferometer. Assuming a source size of $1''$, they derive a column density $8\,10^{16}$ cm^{-2} and an excitation temperature of 105 K. If the size is indeed as small as $\sim 1''$, our inferred column density would increase to $\sim 6\ 10^{15}$ cm^{-2} if the lines remain optically thin. For such high column densities, however, optical depth effects start to become important and the column density may well be an order of magnitude larger. Recent $C^{17}O$ interferometer observations by Wyrowsky & Walmsley (1996, private communication) suggest an H_2 column density a factor ~ 6 larger than that listed in Table 2 in a ~ 1 region. The corresponding CH_3CN abundance is $\sim 7\,10^{-8}$ compared with the beam-averaged value of $1.4\,10^{-10}$ found here.

5.4.4. Dimethyl ether and methyl formate

Dimethyl ether, CH_3OCH_3, was detected toward W 3(H_2O) through a number of lines, which is however only a small subset of the transitions available to this molecule. Since no collisional rates are available, a rotation diagram was constructed (Fig. 2). This resulted in a rotational temperature of 193 ± 25 K and a beam-averaged column density of $2.0 \pm 0.5\,10^{15}$ cm^{-2}. Just as for CH_3CN, two outlying points at high energies affect the fit. Although these appear to be clear detections, a fit has also been made without them, giving $T_{\rm rot} = 66 \pm 6$ K and $N(CH_3OCH_3) = 1.0 \pm 0.2\,10^{15}$ cm^{-2}.

The same approach was used for methyl formate, and gives $T_{\rm rot} = 140 \pm 23$ K and $N(CH_3OCHO) = 6.7 \pm 2.5\,10^{14}$ cm^{-2}. Note that these column densities are only about one order of magnitude less than found for methanol. They could be increased considerably if most of the emission originates from a source size as small as that of CH_3CN.

5.5. Sulfur-bearing molecules

The chemistry of sulfur-bearing molecules, especially SO_2, is still poorly understood. In this work, a large number of species containing sulfur have been detected, especially toward IRS5.

5.5.1. CS

Carbon monosulfide is well known as a tracer of the densest parts of molecular clouds and indeed CS and 3 of its isotopomers are found toward the three sources in several lines. Tieftrunk et al. (1995) show in their $C^{34}S$ $3-2$ map of the W 3 core that the emission is strongest toward IRS4 and southward, but that there is relatively little $J = 3-2$ emission in the direction of IRS5 and the rest of the core. This trend is also found in the higher excitation lines.

Although blending is seldom a problem toward IRS4, it happens that the $C^{34}S$ $5-4$ line is blended with a (weak) methanol line. The integrated line strength can, however,

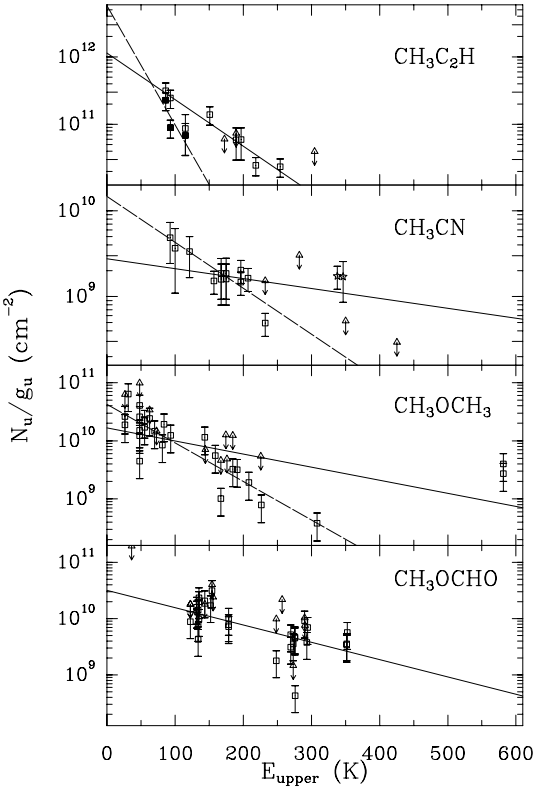

Fig. 2. Rotation diagram for CH_3C_2H (upper panel) toward W 3 IRS4 (solid symbols, dashed line) and W 3(H_2O) (open symbols, solid line). The panels for CH_3CN, CH_3OCH_3 and CH_3OCHO are for W 3(H_2O) only. Squares represent detected lines, while triangles denote upper limits. For an explanation of the stars and the two fits in the CH_3CN and CH_3OCH_3 rotation diagrams, see the text

be used as an upper limit. Together with the measured $7-6$ line, the ratio has been employed to constrain the density to $\sim 1\,10^6$ cm^{-3}, similar to that indicated by H_2CO. A confirmation of this value comes from the $C^{33}S$ $5-4$ line and the upper limit on its $7-6$ line. From the absolute strengths of the lines, the column densities are determined and listed in Table 3. Using the cosmic abundance ratios, $N(CS) = 4\,10^{14}$ cm^{-2}. The different isotopomers give values which agree within a factor two, indicating that only CS is optically thick. Note that this column density is in excellent agreement with the results of Tieftrunk et al. (1995). The source size was estimated from the optically thick CS $7-6$ line and was found to be beam-filling, in agreement with the map of Tieftrunk et al. (1995).

The density found from the CS isotopes toward IRS5 is also in excellent agreement with the H_2CO results. The column densities were derived using a kinetic temperature of 100 K, and are listed in Table 3. From the rare isotopomers, $N(CS) = 2\,10^{14}$ cm^{-2}, somewhat lower than toward IRS4. The emission was again found to fill the beam. The column density is accurate to better than a factor of two, but it is six times lower than the value given

by Tieftrunk et al. (1995). The reason is unclear since our column densities can explain their measurements of the $C^{34}S$ $5-4$ and $3-2$ lines well for the inferred physical parameters.

For W 3(H_2O) the density found from the $7-6/5-4$ lines is also in excellent agreement with the formaldehyde results of Paper I. The column densities for the different isotopomers are listed in Table 3, and give $N(CS) = 1\,10^{15}$ cm^{-2}. The source size was found to be approximately $10''$.

Using the H_2 column densities listed in Table 2, our CS abundances are larger by up to an order of magnitude than the values given by Tieftrunk et al. (1995) for IRS4 and IRS5, and Wilson et al. (1991) for W 3(H_2O).

5.5.2. SO

Several isotopomers of SO have been detected toward our sources, including ^{34}SO, ^{33}SO and $S^{18}O$. Like CS, the SO itself is optically thick, as is also implied by the large line width of the main lines, although outflowing gas could play a rôle. Although there are many lines available to construct a rotation diagram, it proved difficult to do so: the SO lines suffer from optical depth effects, whereas the ^{34}SO lines often turn out to be blended.

The excitation of SO can be studied through statistical equilibrium calculations using the recent collisional cross sections of Green (1994). For IRS4, the observed SO line ratios are not very sensitive to density and temperature, but the values agree with the parameters derived from H_2CO, although somewhat higher temperature and density are favoured. The beam-averaged column density is $1.4\,10^{14}$ cm^{-2}, when a temperature of 80 K and a density of $2\,10^6$ cm^{-3} are used.

Toward IRS5 not only ^{34}SO and ^{33}SO lines have been detected but also some $S^{18}O$, indicating that the main SO lines are very optically thick, $\tau > 10$. For example, the ratio of the 6_6-5_5 lines of SO and $S^{18}O$ is only 50 instead of the cosmic ratio $[^{16}O]/[^{18}O] = 500$. Even the ^{34}SO lines are still somewhat optically thick. Statistical equilibrium calculations were performed for the $S^{18}O$ lines, resulting in $T_{\rm kin} > 100$ K and $n(H_2) > 2\,10^6$ cm^{-3}. Assuming that the SO, just like SO_2 (see Paper I and below), originates in hotter (~ 200 K) and denser ($1\,10^7$ cm^{-3}) gas than H_2CO, the $S^{18}O$ column density was calculated to be $1\,10^{13}$ cm^{-2}, implying $N(SO) = 5\,10^{15}$ cm^{-2}. From the excitation calculations, the source size is estimated to be $\sim 5''$. Again, this number is somewhat uncertain, but it shows that the SO likely comes from a compact, warm and dense region.

The SO emission from W 3(H_2O) is very intense, just as that from IRS5, but no $S^{18}O$ lines are detected and only one ^{33}SO line. The statistical equilibrium calculations were therefore performed for ^{34}SO. The density and temperature can be constrained to $T_{\rm kin} > 100$ K and $n(H_2) > 2\,10^6$ cm^{-3}. Using the temperature and density derived from H_2CO, $N(^{34}SO) = 5.6\,10^{13}$ cm^{-2} is found, resulting in $N(SO) = 1.3\,10^{15}$ cm^{-2}. This beam-averaged column density is fairly robust since it does not change by more than 10% if the density is increased to 10^7 cm^{-3}. The source size was calculated to be large, $\sim 11''$.

5.5.3. SO_2

SO_2 is one of the most interesting molecules found in the W 3 region. In Paper I, its abundance was found to differ greatly between the three sources, with IRS5 showing the strongest SO_2 emission. Indeed, the SO_2 abundance has been found to be highly variable in other sources as well (Groesbeck 1994; McMullin et al. 1994). In some cases such as Orion/KL and Sgr-B2(N), the SO_2 lines are so overwhelmingly strong that it can be one of the major coolants in the 345 GHz range. The SO_2 excitation temperature was also found to be surprisingly high toward IRS5. With the extended data set presented here, a high temperature has been found toward IRS4 as well. Another big improvement compared with Paper I stems from the recent completion of the catalogue of $^{34}SO_2$ lines.

Toward IRS4, several additional SO_2 lines have been detected, mainly because of the better DAS backend. The inclusion of these lines in the rotation diagram (Fig. 3) results in $T_{\rm rot} = 102 \pm 15$ K and $N(SO_2) = 1.5 \pm 0.4\,10^{14}$ cm^{-2}. No lines from $^{34}SO_2$ have been detected. The column density is, within the errors, consistent with Paper I, but the rotational temperature is increased. The higher temperature is no longer consistent with the kinetic temperature derived from the formaldehyde lines. This could, as for IRS5, be due to optical depth effects, but the upper limits on the $^{34}SO_2$ column density are not stringent enough to provide clues to the optical depth since $SO_2/^{34}SO_2$ is > 3.4. More likely, the SO_2 emission comes from a somewhat warmer region in the direction of IRS4. This possibility is discussed further in Sect. 6.

For IRS5, the complete data set gives $T_{\rm rot} = 234 \pm 10$ K and $N(SO_2) = 3.0 \pm 0.3\,10^{15}$ cm^{-2}, which is within the errors consistent with Paper I. For the optically thin $^{34}SO_2$ the following parameters are found: $T_{\rm rot} = 147 \pm 25$ K and $N(^{34}SO_2) = 3.0 \pm 0.8\,10^{14}$ cm^{-2}. From these values it is clear that the ratio of the beam-averaged column densities is not equal to the solar abundance ratio of 22. This was already found in Paper I, where it was attributed to optical depth effects. Since the $\Delta J = -1$ lines have the lowest intrinsic line strengths and thus the lowest optical depth, a separate rotation diagram has been made for these lines. The results are $T_{\rm rot} = 154 \pm 14$ K and $N(SO_2) = 5.3 \pm 1.2\,10^{15}$ cm^{-2}. This rotational temperature matches very well with the $^{34}SO_2$ results, and the beam-averaged column densities are consistent if the cosmic $[^{32}S]/[^{34}S]$ ratio of 22 is used. The fact that the rotational temperatures are somewhat lower than found in Paper I is thus explained by the high optical depths which flatten the slope of the fit.

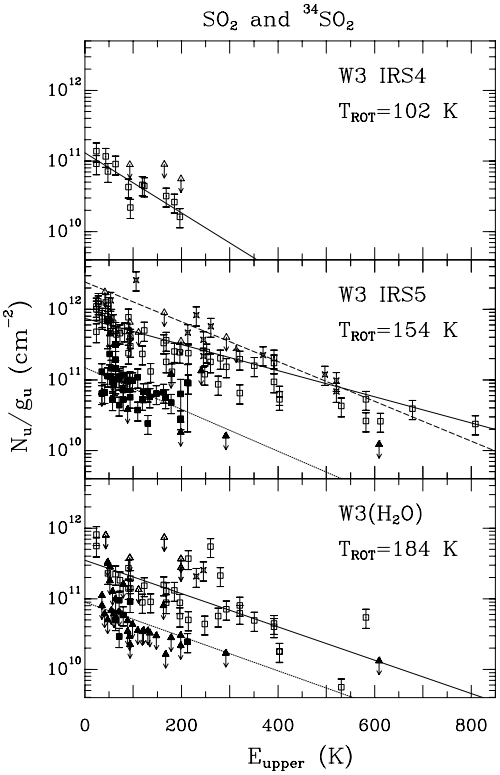

Fig. 3. Rotation diagram for SO_2 (open symbols) and $^{34}SO_2$ (filled symbols) in the three sources. Squares indicate lines that have been detected; triangles denote upper limits; stars are detected lines with $\Delta J = -1$, see text. The solid lines represent the least-squares fits using all detected transitions. The dashed line indicates the fit through the $\Delta J = -1$ lines only. The dotted lines represent the least-squares fits using all detected $^{34}SO_2$ transitions. The rotation temperatures are those derived from all detected SO_2 transitions (IRS4 and W 3(H_2O)) or from the $\Delta J = -1$ transitions only (IRS5)

In Paper I it was also argued that the lower rotational temperature of $^{34}SO_2$ may be caused by lack of data at higher energies. Since then, the catalog has been completed, and this lower temperature still persists. At the same time, our list of detected $SO_2 \Delta J = -1$ lines has increased and this more complete data set now nicely confirms the $^{34}SO_2$ results, giving more weight to the optical depth argument. The SO_2 rotational temperature of ~ 150 K is no longer consistent with the rotational temperature of ~ 270 K of the outflowing CO (Mitchell et al. 1991). However, a recent re-analysis of the CO excitation by HMMT shows that there may be multiple components with $T = 100 - 200$ K. Furthermore a kinetic temperature of more than 200 K can still result in a rotational temperature of ~ 150 K if the SO_2 is subthermally excited. Since the densities toward W 3 appear to be lower than those toward the Orion Plateau region and since SO_2 has a large number of (optically thin) lines to radiate through, subthermal excitation cannot be excluded. The optically thick lines lead to a crude determination of the source size. For $T_{\rm rot} = 150$ K, the most optically thick line gives a source size of $\sim 2''$ if the optical depth were very high. However, the $SO_2/^{34}SO_2$ ratio suggests that the optical depth is still less than unity, so that a larger source size of $\sim 6''$, similar to that found for SO, is more likely.

The results for W 3(H_2O) from the rotation diagram are $T_{\rm rot} = 184 \pm 12$ K and $N(SO_2) = 1.0 \pm 0.1\, 10^{15}$ cm^{-2}. The $^{34}SO_2$ lines give 179 ± 75 K and $2.4 \pm 1.6\, 10^{14}$ cm^{-2} respectively. Only few lines with $\Delta J = -1$ have been identified at low signal to noise, but the same trend was found as in IRS5, implying that the main lines are somewhat optically thick. The inferred source size is $\sim 5''$.

5.5.4. H_2CS

H_2CS, like H_2CO, is a near-prolate rotor with transitions that can be used to determine both density and kinetic temperature (see Fig. 9 of Blake et al. 1994). Toward IRS4, two ortho and two para lines have been detected, and good upper limits on several other lines have been obtained. The corresponding temperature range is $T_{\rm kin} = 50 - 120$ K and density interval $n(H_2) = 1 - 2\, 10^6$ cm^{-2}. Using 80 K and $2\, 10^6$ cm^{-3} as the best parameters, $N(\mathrm{o} - H_2CS) = 2.5\, 10^{13}$ cm^{-2} and $N(\mathrm{p} - H_2CS) = 1.7\, 10^{13}$ cm^{-2}, so that the ratio differs somewhat from the theoretical high-temperature ortho/para ratio of 3. The total column density $N(H_2CS) = 4.4\, 10^{13}$ cm^{-2} is the same as found by the rotation diagram method. The rotational temperature is $T_{\rm rot} = 41 \pm 11$ K, indicating subthermal excitation.

Toward IRS5 only the $7_{16} - 6_{15}$ line has been detected, prohibiting an analysis as given for IRS4. Using the physical parameters from H_2CO, $N(\mathrm{o}-H_2CS) = 1.0\, 10^{13}$ cm^{-2} is found. Assuming an ortho/para ratio of 3, this results in $N(H_2CS) = 1.3\, 10^{13}$ cm^{-2}.

Many more lines were detected toward W 3(H_2O) allowing a rotation diagram to be constructed. The fitting parameters are $T_{\rm rot} = 75 \pm 8$ K and $N(H_2CS) = 2.0 \pm 0.6\, 10^{13}$ cm^{-2}. Statistical equilibrium calculations were performed as well, resulting in $n(H_2) = 2^{+2}_{-0.3}\, 10^6$ cm^{-3} and $T_{\rm kin} = 100^{+20}_{-30}$ K. The column densities are $N(\mathrm{o} - H_2CS) = 1.0\, 10^{14}$ and $N(\mathrm{p} - H_2CS) = 5.1\, 10^{13}$ cm^{-2}. Again, the ortho/para ratio differs from three but the sum of the two column densities is close to the rotation diagram value. Most significant however is the low temperature found from the statistical equilibrium calculations. It suggests that the H_2CS emission does not come from the compact "hot core", but from the warmer core surrounding the W 3(OH)/W 3(H_2O) clumps. This interpretation is strengthened by the fact that the emission from IRS4 comes from a similar region, which is not compact and hot, but extended and warm.

5.5.5. H_2S

H_2S has only few lines available in atmospheric windows, and is therefore not much studied. Therefore the analysis of this molecule is largely based on the single $2_{20} - 2_{11}$ line at 216 GHz. Since collisional rates for this molecule are not known and since no rotational temperature can be derived from a single line, the excitation temperature has to be assumed. Fortunately, the upper energy level of this line lies at 84 K, nicely in the temperature range of the three sources. Moreover, for excitation temperatures between 50 and 250 K, the H_2S column density changes by only a factor of three. Taking $T_{\rm rot} = T_{\rm kin}$, we obtain $N(H_2S) = 1.1\,10^{14}$; $2.0\,10^{14}$; and $1.0\,10^{15}$ cm^{-2} for IRS4, IRS5 and W 3(H_2O) respectively. The upper limits on the $H_2^{34}S$ line at 214.7 GHz indicate that the 216 GHz line is not very optically thick toward IRS5 and W 3(H_2O).

For IRS5 the analysis can be improved by using the $1_{10} - 1_{01}$ line at 168.763 GHz toward this source observed by Minh et al. (1991a) in a 35″ beam. They also measured the corresponding $H_2^{34}S$ line and found the main line to be optically thick. If the two H_2S lines are combined, $T_{\rm rot} = 34 \pm 10$ K and $N(H_2S) = 2.0 \pm 1.5\,10^{14}$ cm^{-2} is derived. While the rotational temperature is of the same order as their adopted excitation temperature, the inferred column density is more than an order of magnitude smaller than that of Minh et al. Using the lines of the rarer isotopomer (assuming the upper limit at 214.7 GHz to be a two sigma detection) gives a somewhat higher rotational temperature and a $H_2^{34}S$ column density of $4.0\,10^{13}$ cm^{-2}. Although this value is uncertain, it suggests that the H_2S column density of Minh et al. is too large. The reason for this discrepancy is unclear. Therefore the value of $2.0\,10^{14}$ cm^{-2} derived above is kept.

Minh et al. (1991a) also observed W 3(OH) in $H_2^{34}S$, and their 35″ beam included W 3(H_2O) as well. The rotation diagram for this line and the two sigma upper limit at 214.7 GHz (used as a detection) gives $T_{\rm rot} = 35 \pm 12$ K and $N(H_2^{34}S) = 3.6 \pm 2.7\,10^{13}$ cm^{-2}, corresponding to $N(H_2S) = 8\,10^{14}$ cm^{-2}. This number is highly uncertain, but does not differ much from the value adopted above.

If $T_{\rm rot}$ toward IRS4 is lowered to ~ 25 K, similar to the values found for IRS5 and W 3(H_2O), its column density would be increased to $2.2\,10^{14}$ cm^{-2}.

5.5.6. OCS

OCS has not been detected toward IRS4. The best limit on the column density comes from the $19 - 18$ line, which gives $N(\rm OCS) < 5\ 10^{13}$ cm^{-2} for the physical parameters of Paper I.

The situation for IRS5 is somewhat better, since two lines were detected which are reasonably far apart in energy. As can be seen from Fig. 11 of Jansen (1995), such transitions are extremely good density tracers. The statistical equilibrium calculations give a density as high as 10^{7-8} cm^{-3} at temperatures of more than 200 K, but the signal-to-noise ratio on the data (especially for the $19-18$ line) is poor. If this line were in error by a factor of two or if the source size were small, the density would decrease to $2\,10^6$ cm^{-3} and the temperature to $150-200$ K. These conditions are similar to those found for SO and SO_2, providing additional evidence for a separate sulfur chemistry. If the lower temperature and density are adopted, the beam-averaged column density is found to be $N(\rm OCS) \approx 9\,10^{13}$ cm^{-2}.

Toward W 3(H_2O) many OCS lines are detected and their strengths are large enough to place useful limits on the OCS/$OC^{34}S$ ratio. The non-detection of $OC^{34}S$ at the level OCS/$OC^{34}S > 5$ indicates that the OCS lines are not very optically thick. The OCS lines often turn out to be blended, but in most cases OCS is the dominant component of these blends. Therefore line ratios can again be used to determine the physical conditions. Both the $28-27/19-18$ and $29-28/19-18$ ratios point at $n(H_2) > 6\,10^5$ cm^{-3} and $T_{\rm kin} > 100$ K, consistent with the H_2CO results. The inferred $N(\rm OCS)$ is $2.3\,10^{14}$ cm^{-2}.

5.6. Silicon monoxide

Silicon monoxide is a special molecule, because of its intimate connection with shocks in the interstellar medium (Bachiller et al. 1991; Martín-Pintado et al. 1992). SiO has been detected toward all three sources, often in more than one line and in more than one isotopomer. Statistical equilibrium calculations of the $8-7/6-5$ ratio were used to constrain the densities.

Toward IRS4, the $8-7$ line is very weak. The fit of the $6-5$ line and the conditions of Paper I give a column density of $3.7\,10^{12}$ cm^{-2}.

Toward IRS5, the SiO emission is strong, but the ^{29}SiO lines are not detected, indicating that the main isotope is not very optically thick. A line has been found coincident with ^{30}SiO $8-7$, but this is probably spurious. Therefore, only the SiO lines themselves can be used. The $8-7/6-5$ ratio is large, indicating high densities. A smaller source size of $\sim 5''$, comparable to that for SO and SO_2, decreases both parameters somewhat, but they remain high, $n > 10^7$ cm^{-3} for $T_{\rm kin} = 100$ K. Only for much higher temperatures would lower densities be obtained. This is not unlike the situation close to Orion IRc2 where brightness temperatures of about 1000 K are found for the thermal SiO emission (Wright et al. 1995), indicating a very hot and dense environment. For $T = 250$ K and $n(H_2) = 1\,10^7$ cm^{-3} the inferred SiO column density is $5.3\,10^{12}$ cm^{-2} in the 15″ beam. If the physical parameters of Paper I are used together with $8-7$ line, $N(\rm SiO)$ decreases to $5.1\,10^{13}$ cm^{-2}.

W 3(H_2O) shows not only emission from the main isotopomer, but also from the rarer ones. The ^{29}SiO lines indicate a density higher than $2\,10^6$ cm^{-3} and temperatures higher than 100 K, not unlike the H_2CO results.

$N(^{29}\mathrm{SiO})$ is calculated to be $3.0\,10^{12}$ cm^{-2}, corresponding to $N(\mathrm{SiO}) = 5.9\,10^{13}$ cm^{-2}. The source size can be estimated since both optically thick and thin lines are available, resulting in $> 7''$, so that the SiO emission is relatively widespread.

Although the high densities derived above are most likely evidence for the shock scenario, there remains some uncertainty. MacKay (1995, 1996) provides an alternative explanation in which silane (SiH_4) is evaporated from icy grain mantles. The silane rapidly forms SiO in the subsequent chemistry. On basis of the survey data it is difficult to judge which scenario applies. Higher spatial resolution data are clearly needed.

5.7. Molecular ions

The observed ions toward IRS5 have been discussed in detail by de Boisanger et al. (1996) and are only briefly summarized here.

5.7.1. HCO^+

The $3-2$ and $4-3$ lines of HCO^+ and its isotopomers lie at wavelengths with good atmospheric transmission, and are readily detected toward the three sources. The main lines are optically thick and the profile is self-reversed toward W 3(H_2O). The ratio of the two lines of the more optically thin ^{13}C variety is a good density indicator.

For IRS4 it is found that the inferred density is rather high, $\sim 10^7$ cm^{-3} at 55 K. This high value can be due to optical depth effects (even for $H^{13}CO^+ \tau \sim 0.3$), to a small source size, or to calibration errors. The influence on the column density is not very large, however, and $N(HCO^+) \approx 3.8\,10^{14}$ cm^{-2} is obtained. This value is consistent with that derived from the $HC^{18}O^+$ $4-3$ line. An estimate for the source size of $17''$ is found from the optically thick HCO^+ $4-3$ line.

De Boisanger et al. (1996) found that the density indicated by the $4-3/3-2$ line ratio toward IRS5 is somewhat higher than that found from H_2CO but still consistent with the latter result within the error bars. The column density has been determined using the parameters of Paper I. No $HC^{18}O^+$ has been detected. The source size is estimated to be $18''$.

Toward W 3(H_2O) the $4-3/3-2$ ratio indicates a density of $1\,10^6$ cm^{-3} at 220 K, somewhat lower than found from H_2CO. From the $HC^{18}O^+$ $4-3$ line $N(HC^{18}O^+) = 4.3\,10^{11}$ cm^{-2} is inferred. This is consistent with $N(H^{13}CO^+) = 3.9\,10^{12}$ cm^{-2}, so that $N(HCO^+) = 2\,10^{14}$ cm^{-2}. Note that this result does not depend sensitively on temperature. Decreasing the temperature to 100 K increases the column density by only 15%. The source size was calculated from the optically thick $4-3$ line. The peak temperature is found to be more than 15 K, from fits obtained by putting a mask around the self-absorption. This results in a source size of $\lesssim 8''$. The interferometer map of Wink et al. (1994) shows that some fraction of the emission indeed comes from a compact clump of size $\sim 5''$, but that most of the emission originates in the more extended core surrounding W 3(H_2O) and W 3(OH).

5.7.2. HCS^+

Much less information is available on HCS^+. There has been an intensive search for this ion toward IRS5 (see de Boisanger et al. 1996), and the $8-7$ line has been detected in the survey toward W 3(H_2O).

Assuming that the HCS^+ stems from the same region as H_2CO toward IRS4, the upper limit on the $8-7$ line implies $N(HCS^+) < 2.0\,10^{13}$ cm^{-2}. If the high density found for HCO^+ is taken, the column density decreases to $7.5\,10^{12}$ cm^{-2}.

Toward IRS5, the lines are very weak, but certainly present. It is interesting that their widths are very small, just as found for the CS isotopomers. The $8-7/6-5$ ratio implies an (uncertain) density of $2\,10^6$ cm^{-3}, comparable to that found from the H_2CO. The column density is $N(HCS^+) = 6.3\,10^{11}$ cm^{-2}.

The HCS^+ $8-7$ line was detected toward W 3(H_2O), but is unfortunately blended with a methyl formate line. If the methyl formate excitation is in LTE at $T_{\rm rot} = 141$ K, the line is not expected to be very strong, but subthermal excitation may enhance its contribution. If we assume that HCS^+ is the dominant component and use the physical parameters from Paper I, $N(HCS^+) \leq 1.7\,10^{13}$ cm^{-2} is obtained.

5.7.3. $HOCO^+$ and $HCNH^+$

$HOCO^+$ is interesting because its abundance provides an indirect determination of that of CO_2, which cannot be observed at (sub-)millimeter wavelengths. $HOCO^+$ has been detected toward the Galactic Center in its $4_{0,4}-3_{0,3}$ line (Minh et al. 1991b). In this work, the $16_{0,16}-15_{0,15}$ line was searched toward IRS5, which lies at an energy $E_{\rm u} = 138$ K. The non-detection implies an upper limit on the column density of $2\ 10^{12}$ cm^{-2}, using a line strength $\mu^2 S = 63.98$ Db^2 and assuming an excitation temperature of 50 K.

In the search for ions (de Boisanger et al. 1996), a deep integration on the $HCNH^+$ $3-2$ line at 222 GHz was made toward IRS5, but the line was not detected, giving an upper limit on the column density in a $20''$ beam of $1.5\,10^{13}$ cm^{-2}.

5.7.4. SO^+

SO^+ has been detected toward IRS4 and IRS5 by Turner (1994) in 4 lines, who derived a column density of $1.1\,10^{13}$ and $1.5\,10^{13}$ cm^{-2} for IRS4 and IRS5 respectively, assuming a source size of $30''$. In this survey the

347740.0 MHz line is detected toward IRS5, and absent toward W 3(H_2O). The 348115.2 MHz line is unfortunately blended with $^{34}SO_2$, and is thus of limited use. Therefore we adopt the column densities of Turner (1994).

5.7.5. H_3O^+

H_3O^+ has been searched for toward all three sources by Phillips et al. (1992) through observations of three lines The detection toward IRS5 is confirmed in this survey by the 364 GHz line. The total H_3O^+ column density is calculated assuming a high temperature ortho/para ratio of unity. Using the standard physical parameters, $N(\mathrm{p-H_3O^+}) = 1.5\,10^{14}$ cm^{-2} toward IRS5, neglecting radiative excitation. However, the 396/364 line ratios observed by Phillips et al. (1992) indicate that higher densities ($\gtrsim 5\,10^6$ cm^{-3}) are more appropriate. This results in $N(\mathrm{p-H_3O^+}) = 6.0\,10^{13}$ cm^{-2}, close to the value calculated by de Boisanger et al. (1996). The fact that the 364 GHz line is a factor of 2 stronger in the 15″ JCMT beam than in the 20″ CSO beam implies a small source size of a few ″.

The non-detection towards IRS4 implies $N(\mathrm{p-H_3O^+})$ less than $2.3\,10^{13}$ cm^{-2}.

In the case of W 3(H_2O) a marginal feature at 364 GHz is present, with a width much smaller than expected from other lines in this survey and the data for the 396 GHz line of Phillips et al. (1992). Using the main beam temperature and the data of Phillips et al. (1992) the uncertain p − H_3O^+ column density is $5.0\,10^{13}$ cm^{-2}.

5.7.6. Electron fraction

De Boisanger et al. (1996) have determined the electron fraction toward IRS5 to be $x_\mathrm{e} = n(\mathrm{e})/n(\mathrm{H_2}) = (0.5 - 1.1)\,10^{-8}$, using many lines and specialized models. For the other two W 3 sources such detailed information is not available, prohibiting a thorough study of the electron abundance toward IRS4 and W 3(H_2O). Nevertheless, a lower limit is easily estimated by adding the abundances of the observed molecular ions, which is primarily HCO^+. For IRS4 this results in an abundance $x_\mathrm{e} > 5\ 10^{-9}$ and for W 3(H_2O) $x_\mathrm{e} > 2\ 10^{-9}$.

5.8. Deuterated molecules

Only few deuterated molecules have been detected toward the three sources. One of the most prominent is DCN, which has been seen toward W 3(H_2O). Unfortunately the $5-4$ line is blended with $^{34}SO_2$, but it is estimated that $^{34}SO_2$ contributes less than 30% of the integrated line flux. Assuming standard physical parameters, $N(\mathrm{DCN}) = 9\,10^{12}$ cm^{-2} is obtained, giving $[\mathrm{DCN}]/[\mathrm{HCN}] = 7.5\,10^{-3}$ with a factor of four uncertainty. Toward the other two sources, DCN has not been detected. The amount of deuteration, $[\mathrm{DCN}]/[\mathrm{HCN}] < 4.3\,10^{-3}$ and $< 4.9\,10^{-3}$, appears less than for W 3(H_2O), but can still be the same within the uncertainties.

From the upper limits on the DNC $3-2$ line the following upper limits on N(DNC) are derived: $< 1.4\,10^{12}$ and $< 7.7\,10^{11}$ cm^{-2} toward IRS4 and IRS5 respectively. Toward W 3(H_2O) the DNC 3–2 line has been marginally detected and using the standard physical conditions a column density N(DNC) of $4.3\ 10^{11}$ cm^{-2} (in a 20″ beam) is inferred. The [DNC]/HNC] is $< 7.1\,10^{-3}$, $< 4.2\,10^{-3}$, and $4.8\,10^{-3}$ respectively, similar to the [DCN]/[HCN].

DCO^+ is commonly found in star-forming regions (Wootten et al. 1982). Toward IRS4 the DCO^+ $5-4$ line is blended with HCO^+ $4-3$ and thus no column density could be derived. Toward IRS5, the $5-4$ line was observed sepearately by de Boisanger et al. (1996). Standard physical parameters give $N(\mathrm{DCO^+}) = 4.8\,10^{11}$ cm^{-2}. In the same way, the beam-averaged column density toward W 3(H_2O) was found to be $9.5\,10^{11}$ cm^{-2}. This implies $[\mathrm{DCO^+}]/[\mathrm{HCO^+}]$ ratios of $2.5\,10^{-3}$ and $4.1\,10^{-3}$ respectively, again close to the deuteration values for HCN and HNC.

The high beam-averaged H_2S column densities found toward the three sources make an inspection of the HDS upper limits of some interest. If the same approach is used as for H_2S, i.e., if $T_\mathrm{rot} = T_\mathrm{kin}$ is assumed, the following HDS upper limits are found from the $2_{1,1} - 2_{0,2}$ line for IRS4, IRS5 and W 3(H_2O) respectively: $< 1.0\,10^{13}$; $< 2.7\,10^{13}$; and $< 8.1\,10^{13}$ cm^{-2} and $[\mathrm{HDS}]/[\mathrm{H_2S}] < 9.1\,10^{-2}$; < 0.14 and $< 8.1\,10^{-2}$ respectively. Unfortunately, these values provide no useful limits on the deuteration of H_2S. If the lower excitation temperature of $T_\mathrm{rot} = 20$ K is adopted (see Sect. 5.5.5), the limits for IRS5 and W 3(H_2O) both become $< 1.4\,10^{13}$ cm^{-2} but the ratio $[\mathrm{H_2S}]/[\mathrm{HDS}]$ still does not give useful information.

Another deuterated ion is N_2D^+ for which only upper limits on the $3-2$ line were obtained, although a hint of the line is present toward IRS5 (de Boisanger et al. 1996). Taking the standard physical parameters, the limits on the column densities are $< 3.1\,10^{11}$; $< 3.3\,10^{11}$; and $< 2.7\,10^{11}$ cm^{-2} for IRS4, IRS5 and W 3(H_2O) respectively.

Several lines of HDO have been detected toward both W 3(H_2O) and W 3(OH). The excitation and abundance of this species are described in a separate paper (Helmich et al. 1996). The inferred $[\mathrm{HDO}]/[\mathrm{H_2O}]$ ratio of $(2-6)\,10^{-4}$ is lower than that of other species.

Using $T_\mathrm{rot} = T_\mathrm{kin}$ the upper limits on the HDCO column density for IRS4, IRS5 and W 3(H_2O) are $< 3\,10^{12}$; $< 4\,10^{12}$ and $< 1\,10^{13}$ cm^{-2} respectively. The $[\mathrm{HDCO}]/[\mathrm{H_2CO}]$ ratios are $< 3.7\,10^{-3}$; $< 5.0\,10^{-2}$ and $< 2.5\,10^{-2}$ respectively. The same method yields $3\,10^{13}$; $4\,10^{13}$ and $1\,10^{14}$ cm^{-2} for the CH_3OD column densities of IRS4, IRS5 and W 3(H_2O) respectively. The $[\mathrm{CH_3OD}]/[\mathrm{CH_3OH}]$ ratios are $< 7.1\,10^{-2}$; < 0.25 and $< 1.1\,10^{-2}$.

Table 3. Beam-averaged column densities and adopted physical parameters

X	W 3 IRS4			W 3 IRS5			W 3(H_2O)		
	T_{kin} (K)	$n(H_2)$ (10^6 cm^{-3})	N(X) (cm^{-2})	T_{kin} (K)	$n(H_2)$ (10^6 cm^{-3})	N(X) (cm^{-2})	T_{kin} (K)	$n(H_2)$ (10^6 cm^{-3})	N(X) (cm^{-2})
H_2	–	–	7.0(22)	–	–	1.3(23)	–	–	9.6(22)
$C^{17}O$	55	1.0	7.3(15)	100	1.0	1.3(16)	100	2.0	1.0(16)
$C^{18}O$	55	1.0	2.3(16)	100	1.0	3.7(16)	100	2.0	5.3(16)
^{13}CO	–	–	–	–	–	–	100	2.0	1.1(17)
CO	–	–	1.9(19)[3]	–	–	3.3(19)[3]	–	–	2.6(19)[3]
CN	55	1.0	3.3(14)	100	1.0	1.8(14)	220	2.0	1.1(14)
$HC^{15}N$	55	1.0	3.1(12)	100	1.0	2.1(12)	220	2.0	6.6(12)
$H^{13}CN$	55	1.0	1.1(13)	100	1.0	5.9(12)	220	2.0	1.1(13)
HCN	–	–	8.4(14)[3]	–	–	5.3(14)[3]	–	–	1.2(15)[3]
$HN^{13}C$	55	1.0	3.3(12)	100	1.0	3.2(12)	220	2.0	1.5(12)
HNC	–	–	2.0(14)[3]	–	–	1.9(14)[3]	–	–	9.0(13)[3]
HC_3N	55	1.0	<2.5(13)	100	1.0	<9.8(12)	220	2.0	1.5(13)
HNCO	55[1]	–	<2.8(13)	100[1]	–	4.4(13)	53[1]	–	4.8(14)
CCH	55	1.0	1.9(14)	100	1.0	1.2(14)	220	2.0	1.3(14)
CH_3C_2H	25[1]	–	7.7(14)	50[1]	–	<1.0(14)	63[1]	–	6.1(14)
$H_2^{13}CO$	–	–	–	–	–	–	220	2.0	5.1(12)
H_2CO	55	1.0	8.0(13)	100	1.0	8.0(13)	220	2.0	4.0(14)
CH_3OH	28[1]	–	4.2(14)	47[1]	–	1.6(14)	265[1]	–	8.8(15)
CH_3CN	55	1.0	<1.2(13)	100	1.0	<9.4(12)	120	4.0	2.7(13)
CH_3OCH_3	–	–	–	–	–	–	193[1]	–	2.0(15)
CH_3OCHO	–	–	–	–	–	–	141[1]	–	6.7(14)
$C^{33}S$	55	1.0	6.4(12)	100	1.0	1.4(12)	220	2.0	1.5(13)
^{13}CS	55	1.0	6.6(12)	100	1.0	2.5(12)	220	2.0	2.0(13)
$C^{34}S$	55	1.0	1.9(13)	100	1.0	1.0(13)	220	2.0	4.3(13)
CS	–	–	4.0(14)[3]	–	–	2.0(14)[3]	–	–	1.0(15)[3]
$S^{18}O$	–	–	–	200	10	1.0(13)	–	–	–
^{33}SO	–	–	–	200	10	5.3(13)	220	2.0	4.3(13)
^{34}SO	–	–	–	200	10	8.0(13)	220	2.0	5.6(13)
SO	80	2.0	1.4(14)	–	–	5.0(15)[3]	–	–	1.3(15)[3]
$^{34}SO_2$	102[1]	–	<4.4(13)	147[1]	–	3.0(14)	179[1]	–	2.4(14)
SO_2	102[1]	–	1.5(14)	154[1,2]	–	5.3(15)	184[1]	–	1.0(15)
H_2CS	80	2.0	4.4(13)	100	1.0	1.3(13)	100	2.0	1.5(14)
H_2S	55[1]	–	1.1(14)	100[1]	–	2.0(14)	220[1]	–	1.0(15)
OCS	55	1.0	<5.0(13)	150	2.0	8.9(13)	220	2.0	2.3(14)
^{29}SiO	–	–	–	–	–	–	220	2.0	3.0(12)
SiO	55	1.0	3.7(12)	250	10	5.3(12)	–	–	5.9(13)[3]
$HC^{18}O^+$	55	10	6.7(11)	–	–	–	220	2.0	4.3(11)
$H^{13}CO^+$	55	10	6.3(12)	100	1.0	3.3(12)	220	2.0	3.9(12)
HCO^+	–	–	3.8(14)[3]	–	–	1.9(14)[3]	–	–	2.3(14)[3]
HCS^+	55	1.0	<2.0(13)	100	1.0	6.3(11)	220	2.0	≤1.7(13)
$HOCO^+$	–	–	–	50[1]	–	<2.0(12)	–	–	–
$HCNH^+$	–	–	–	100	1.0	<1.5(13)	–	–	–
H_3O^+	55	1.0	<4.6(13)	100	5.0	1.2(14)	220	2.0	1.0(14)
DCN	55	1.0	<3.6(12)	100	1.0	<2.6(12)	220	2.0	9.0(12)
DNC	55	1.0	<1.4(12)	100	1.0	<7.7(11)	220	2.0	4.3(11)
DCO^+	–	–	–	100	1.0	4.8(11)	220	2.0	9.5(11)
HDS	55[1]	–	<1.0(13)	100[1]	–	<2.7(13)	220[1]	–	<8.1(13)
N_2D^+	55	1.0	<3.1(11)	100	1.0	<3.3(11)	220	2.0	<2.7(11)
HDCO	55[1]	–	<3(12)	100[1]	–	<4(12)	220[1]	–	<1(13)
CH_3OD	55[1]	–	<3(13)	100[1]	–	<4(13)	220[1]	–	<1(14)

$a(b)$ denotes $a \cdot 10^b$; see text for derived physical parameters from observed line ratios of each molecule.
[1] Inferred rotational temperature rather than kinetic temperature. The rotation diagram method has been used to determine the listed column densities for these species.
[2] Value derived from $\Delta J = -1$ lines, see text.
[3] Column density of main isotopomer determined from optically thin isotopomers.

5.9. Vibrationally excited molecules

Apart from the torsional modes of CH_3OH, several other lines originating in vibrationally-excited levels were found in the W 3 survey. Two $J = 4 - 3$ lines within the first vibrational level of the bending mode υ_2 of HCN were detected toward W 3(H_2O). This mode lies at much higher energies, approximately 1000 K, than the torsional modes of CH_3OH, so that the levels are unaccessible in most molecular cloud environments. Vibrationally excited HCN was first detected by Ziurys & Turner (1986) in Orion. In principle there are two ways to populate such high states. The first interpretation, favoured by Ziurys & Turner, is through absorption of 14 μm photons into the $\upsilon_2 = 1$ bending mode. In the case of W 3(H_2O), these photons can be provided by the embedded late O/early B star which heats the dust in the inner part of the envelope and the compact clump surrounding the star. Depending on the actual physical conditions and geometry, the rotational level populations in the ground vibrational state can also be controlled by this infrared pumping (see e.g., Hauschildt et al. 1993). Note that the continuum from W 3(OH) is not able to pump the HCN around W 3(H_2O), as Turner & Welch (1984) already concluded.

The second mechanism for populating the vibrationally excited levels is through collisions at sufficiently high densities and temperatures. Wink et al. (1994) estimate a density of $6\,10^8$ cm^{-3} on a $1''$ scale, whereas Wilner et al. (1995) obtain $\sim 10^9$ cm^{-3} within $0.5''$. Although the optically thick dust emission prevents any submillimeter lines from $< 1''$ to be observed, the density in a $1 - 2''$ region is obviously very high and close to the critical density for excitation. More detailed modeling is needed to assess which process dominates in the case of W 3(H_2O).

The $J = 7 - 6$ line within the $\upsilon = 1$ level of CS was detected in three independent spectra toward W 3(H_2O). This vibrational level lies at approximately 1900 K (7.9 μm) and is thus even more difficult to populate than that of HCN. This suggests that close to W 3(H_2O), either the dust must be very hot or the conditions quite extreme (see also Helmich et al. 1996).

CCH has its lowest vibrational level at 370 cm^{-1} or 27 μm (Hsu et al. 1993; Kanamori & Hirota 1988). At these wavelengths the infrared radiation is intense enough to pump this vibrational level. Black (private communication) predicts the lines within the 345 GHz window to lie at 346248, 346929, 348974 and 349650 MHz. However, no CCH lines within this vibrational level are found in the survey. This suggests that the CCH abundance in the inner region is lower than those of HCN and CS. CCH is also unique in that it has its first electronic state at low energies (< 1 eV).

5.10. Unidentified lines

As in other surveys, some lines remain unidentified, but the fraction is small. The U-lines are generally quite weak, but are thought to be true detections. Because the data are taken in double side-band mode, there are two possible frequencies listed, unless the U-line turns up in more than one spectrum with different local oscillator settings. In those cases, a definite determination of the frequency can be made and only one value is given. Most of the U-lines (7) are found toward IRS5.

Table 4. U-lines Gaussian fit parameters

ν (MHz)	$T_{\rm MB}$ (K)	ΔV (km s^{-1})	W (K km s^{-1})
	W 3 IRS4		
342794	0.37	5.96	2.35
342803	0.58	3.97	2.43
	W 3 IRS5		
338855/342255	0.23	5.21	1.25
338966/342106	0.083	9.47	0.84
339098/342012	0.11	10.7	1.24
339209/341901	0.079	4.01	0.34
339220/341890	0.073	4.19	0.33
342794	0.48	4.12	2.09
342803	0.49	4.17	2.19
	W 3(H_2O)		
362098	0.24	6.53	1.67
231310/233990	0.093	7.27	0.72
336497/339897	0.22	2.76	0.65

The fact that the three sources have different chemical characteristics provides hints on the identity of the carriers of the lines. Small, non-saturated molecules are mostly found toward IRS4, so there is a large probability of identifying the two U-lines toward this source with a simple molecule. Since the same U-lines are also found toward IRS5, the molecule may involve sulfur. Indeed, the other U-lines toward IRS5, which are not found toward the other sources, most likely contain sulfur or silicon. The U-lines toward W 3(H_2O) can be due to any species, but most likely originate from some complex organic molecule.

The U-lines were compared with those found in surveys for other sources but there are no U-lines in common with either the Orion surveys of Sutton et al. (1995) and Schilke et al. (1996), the Sgr-B2 survey of Sutton et al. (1991) or the IRAS 16293–2422 survey of Blake et al. (1994).

6. Discussion

In the previous section, a detailed description of the observations and analysis for each individual species has been given. We discuss here the results in general, both for

the physical structure and the chemical state of the three sources.

6.1. Physical structure

In Paper I, the physical parameters were derived primarily from the observed H_2CO excitation under the assumption that a single physical component is present within the 15″ beam (0.16 pc). We have analyzed here the excitation of many more species and can compare the results with those found from H_2CO. At the same time, it provides information on the question of multiple components within the beam. In this respect, it is useful to compare the observed scale in W 3 with that of structures found in the more nearby Orion giant molecular cloud, which is at 450 rather than 2300 pc. From observations of the extended Orion ridge component, it appears that variations in physical and chemical parameters occur on scales of a few arcmin, corresponding to $\sim 0.2 - 0.3$ pc (Ungerechts et al. 1995; Schilke et al. 1992). Thus, for the surrounding, more quiescent molecular cloud material, the linear scales probed in W 3 are comparable and the assumption of a single component may be reasonable. However, in the Orion/KL region around the massive young stellar object IRc2, significant changes occur on scales of $< 10''$, corresponding to < 0.02 pc. Structures of similar linear size in the W 3 region will be strongly diluted in the 15″ beam.

6.1.1. W 3 IRS4

For IRS4, the deviations from the picture of a single extended, quiescent warm cloud are the smallest. The cloud seems to be well described by a density $n(H_2) = 1.0^{+1}_{-0.4}\,10^6$ cm^{-3} and $T_{\rm kin} = 55^{+20}_{-10}$ K, as derived from H_2CO. The excitation of other species such as CS, CN, CCH and HNC results in similar parameters. However, there is some evidence that warmer material is present in the beam. Weak evidence comes from the fact that the CO main beam brightness temperatures and the H_2CS line ratios indicate temperatures of order $70 - 80$ K. The strongest case is formed by the SO_2 rotational temperature $T_{\rm rot} = 102 \pm 15$ K. Sulfur-bearing molecules have also been found in other regions to be associated with elevated temperatures and shocks (Ziurys 1991).

There are several ways to create elevated temperatures in the IRS4 region. The most likely are through shocks or through heating by ultraviolet radiation. In star-forming regions shocks are often associated with outflowing material, but IRS4 does not show any clear sign of an outflow in its line profiles (see Sect. 5.1). Recently, "hyper-compact" objects (e.g. Claussen et al. 1994) have been discovered in giant molecular clouds. These are small ($< 1''$) clumps of ionized material seen in VLA measurements. The ionization presumably originates from embedded B-stars, but is kept to small scales due to very high densities close to the star. Therefore it will only have an impact on very small scales within the molecular cloud. In Paper I, we postulated the picture that IRS4 is located on the far side of the molecular cloud and has already broken free on one side, illuminating the cloud from behind. In this scenario, the ultraviolet radiation from the newly formed star can heat the gas and set up a photon-dominated region (PDR) on the back side. In addition, it will drive an ionization front into the dense material. At the interface between the expanding ionization front and the molecular cloud, a shock will be present, which can also heat the gas and return grain mantle material. The shocked gas can be quite extended, since the H II region itself already has a size of several arcsec ($\sim 6''$) (Colley 1980). The PDR will extend over similar scales or larger. This interpretation can be distinguished from the hyper-compacts scenario through interferometer observations of species like SO_2.

6.1.2. W 3 IRS5

In the case of IRS5, more than one physical component is certainly present in the beam, since it is well known that the source has a strong outflow (see HMMT 1994 for the most recent results). In addition, the extremely deep self-absorption in the CO profiles shows that there must be a temperature and density gradient or stratification. The depth of the absorption in the lower-J lines indicates that low temperature (< 30 K) and/or low density gas is present on the outside. The fact that the $6 - 5$ line still shows self-absorption (HMMT 1994), but not the $9-8$ line (Boreiko & Betz 1991), suggests that a range of conditions is present. The latter authors give an upper limit on the temperature of the absorbing gas of 80 K, whereas HMMT find an excitation temperature of 26 K. From the smaller self-absorption in the ^{13}CO $3 - 2$ line and its absence in the $C^{18}O$ lines, the column density of the absorbing gas is limited to $N(CO) < 5\ 10^{18}$ cm^{-2}. Since this is a factor of 6 smaller than the column density of the emitting gas and since our submillimeter observations are biased toward the warmer and denser gas, our results are not expected to refer to the cold component.

Although gradients are likely to be present, the excitation analysis shows that most molecules (including CS, HCO^+, HCN) are located in fairly extended gas with $n(H_2) = 1\ 10^6$ cm^{-3} and $T_{\rm kin} = 100^{+40}_{-20}$ K. Part of this agreement stems from the fact that most lines in the 230 and 345 GHz windows have critical densities of order a few $10^5 - 10^6$ cm^{-3}, so that it is no surprise that most detected species give a similar result. Observations of higher excitation lines are needed to determine whether the density is fairly homogeneous, or whether a gradient or power law distribution is present, as would be expected for a collapsing cloud core.

A physically distinct region appears to be probed by the sulfur-bearing molecules, at least by those containing oxygen. In Paper I, it was already found that the SO_2 emission comes from a warmer region, which was

tentatively connected with the outflow. The rotational temperature has been better constrained in this work, but the same conclusion remains (see Sect. 5.5.3). In addition, it was found from the strengths of the optically thick lines of SO and SO_2 that the source size is $\sim 5''$. Just as in IRS4, the chemical composition of this material seems disjunct from that of the bulk of the gas. In Orion IRc2, SO_2 turned out to be a major coolant of the gas in this frequency range (Groesbeck 1994). This is not the case for IRS5. Not only is the column density much lower than that toward IRc2, but the line width is smaller as well. A crude estimate shows that the total SO_2 emission in the 345 GHz range is less than half of that of CO, putting IRS5 somewhere in between IRc2 and the Orion-S source in this respect (Groesbeck 1994). H_3O^+ may be formed from the large amount of H_2O in the same gas.

The region probed by SiO appears to be even denser with $n(H_2) = 10^8 - 10^9$ cm^{-3}. Similarly high densities and even higher temperatures have been found for SiO toward Orion IRc2, which has brightness temperatures in interferometer observations of ~ 1000 K (Wright et al. 1995). This suggests disruption of grains by strong shocks and rapid formation of SiO in the warm post-shock gas. Note, however, that in contrast with Orion/KL, the SiO and SO_2 lines are not noticeably broader toward IRS5 than those of other species. Also, the SiO is not kinematically displaced in contrast with L 1448 (Guilloteau et al. 1992) and NGC 1333 IRAS4 (Blake et al. 1995). Interferometric observations of both SiO and SO_2 are needed to properly investigate these hot and dense regions.

The fact that no rotational lines within the first vibrational levels of HCN, CS and/or CCH have been detected toward IRS5 implies that the hot and dense gas does not contain large quantities of these molecules.

6.1.3. W 3(H_2O)

At least two different components are observed toward W 3(H_2O) within the $15''$ JCMT beam. For many species, a significant fraction of the emission comes from the warm $T_{\rm kin} \approx 100$ K and dense ($\sim 10^6$ cm^{-3}) core ($> 20''$) in which both W 3(H_2O) and W 3(OH) are located.

The second component is the more compact "hot core" type region, which is warmer ($T_{\rm kin} \approx 220$ K) and denser ($\sim 5\ 10^6$ cm^{-3}) than the surrounding envelope. The saturated organic molecules such as CH_3CN (Wink et al. 1994), part of the H_2CO and CH_3OH, and probably most of the dimethyl ether and methyl formate are found here as well, based on their rotational temperatures. The unresolved continuum source of $< 1''$ (Wilner et al. 1995) is too diluted in our beam to result in detectable emission. In addition, at submillimeter wavelengths the continuum is optically thick, so that the line emission must originate from a larger region. This strong continuum radiation can, however, affect the excitation of molecules such as HNCO and HDO (Helmich et al. 1996), and lead to large populations in vibrationally excited levels of molecules such as HCN and CS.

The SO_2, SO and SiO lines again indicate high temperature and densities. Most likely, these species are located in the outflow traced by the H_2O masers (Alcolea et al. 1992). This region probably contains the H_3O^+ found by Phillips et al. (1992).

6.2. Chemical characteristics

Surveys like the one presented here are ideal tools to establish the beam-averaged composition of the gas, since the excitation effects can largely be taken out. As discussed in Sect. 4.3, it is more difficult to make the final step toward abundances, which can be directly compared with models. The beam-averaged H_2 column densities are obtained from $C^{17}O$, but this refers to the cloud as a whole whereas some molecules may be more localized. The excitation analysis only gives an estimate of the local H_2 number density, not of its column density. For some species such as SO_2 in IRS5 or CH_3CN in W 3(H_2O), the local abundances may be more than two orders of magnitude higher than the beam averaged values listed in Table 5 (see Sect. 5.4.3). These abundances should therefore be interpreted with care.

The resulting abundances are listed in Table 5. They reinforce the main conclusion from Paper I that there are large chemical differences between the three sources which cannot be ascribed to excitation effects. Toward IRS4, mostly simple molecules are found. The abundances of these species are low toward IRS5, except those of sulfur- and silicon-containing species. Toward W 3(H_2O), the abundances of complex organic species such as CH_3OH, CH_3CN, dimethyl ether and methyl formate are at least $1-2$ orders of magnitude larger than those found toward the other two sources. For comparison, the abundances found by Sutton et al. (1995) for the Orion extended ridge and the compact ridge scaled to the same CO abundances are included. In the following, some aspects of the chemistry in the three sources will be discussed in more detail.

Toward IRS4 the abundances of most molecules listed in Table 5 are expected to be reliable, since their emission fills the 230 and 345 GHz beams to first order. Moreover, there seems to be no indication of a density gradient for these species. Only the SO, SO_2 and perhaps SiO pose some problems, if they arise in a more localized, hotter (shocked) region. Their listed abundances should be regarded as lower limits.

The abundances of unsaturated radicals and molecules like CN, C_2H and CH_3C_2H are large toward IRS4, suggesting that these molecules are present mostly in the quiescent gas and avoid the shock or "hot core" type conditions. This is consistent with observations of the low mass young stellar object IRAS 16293–2422, where CN and C_2H were also found to trace the colder, more quiescent outer part of the circumbinary envelope (van Dishoeck et al. 1995).

Table 5. Abundances[1]

	W 3 IRS4	W 3 IRS5	W 3 (H_2O)	Extended Ridge[2]	Compact Ridge[2]
H_2	0.5	0.5	0.5	0.5	0.5
CO	1.35(–4)	1.35(–4)	1.35(–4)	1.35(–4)	1.35(–4)
CN	2.4(–9)	6.9(–10)	5.7(–10)	1.0(–8)	1.9(–9)
HCN	6.0(–9)	2.0(–9)	6.3(–9)		
HNC	1.4(–9)	7.3(–10)	4.7(–10)		
HC_3N	<1.3(–10)	<3.8(–11)	7.8(–11)		1.5(–8)
HNCO	<2.0(–10)	1.7(–10)	2.5(–9)		
CCH	1.4(–9)	4.6(–10)	6.8(–10)		
CH_3C_2H	5.5(–9)	<3.9(–10)	3.2(–9)	2.3(–8)	3.1(–9)
H_2CO	5.7(–10)	3.1(–10)	2.1(–9)	<2.6(–8)	9.1(–8)
CH_3OH	3.0(–9)	6.2(–10)	4.6(–8)	1.9(–8)	9.4(–7)
CH_3CN	<1.4(–10)	<7.2(–11)	1.4(–10)		1.2(–8)
CH_3OCH_3	–	–	1.0(–8)	<5.6(–9)	4.7(–8)
CH_3OCHO	–	–	3.5(–9)	<1.1(–8)	7.8(–8)
CS	2.9(–9)	7.7(–10)	5.2(–9)	3.3(–8)	2.5(–8)
SO	1.0(–9)	1.9(–8)	6.8(–9)	1.1(–8)	6.3(–7)
SO_2	1.1(–9)	2.0(–8)	5.2(–9)	4.6(–9)	4.1(–7)
H_2CS	3.1(–10)	5.0(–11)	7.8(–10)	3.4(–9)	3.1(–9)
H_2S	7.9(–10)	7.7(–10)	5.2(–9)		
OCS	3.6(–10)	3.4(–10)	1.2(–9)	<1.0(–8)	6.9(–9)
SiO	2.6(–11)	2.0(–11)	3.1(–10)	<1.5(–9)	1.9(–8)
HCO^+	2.7(–9)	7.3(–10)	1.2(–9)	1.1(–8)	2.4(–9)
HCS^+	<1.4(–10)	2.4(–12)	≤8.9(–11)	5.9(–10)	1.0(–10)
$HOCO^+$	–	<7.7(–12)	–		
$HNCH^+$	–	<5.8(–11)	–		
H_3O^+	<3.3(–10)	4.6(–10)	5.2(–10)		

[1] Abundances are calculated using $x(\mathrm{X}) = N(\mathrm{X})/2N(\mathrm{H_2})$; $a(b)$ denotes $a \cdot 10^b$.
[2] Column densities taken from Sutton et al. (1995). Their CO column density was translated into $N(\mathrm{H_2})$ by taking $\mathrm{CO/H_2} = 2.7\,10^{-4}$ as for the three W 3 sources.

CN and C_2H are known to be prominent in the outer zones of photon-dominated regions (PDR) such as the Orion Bar (Jansen et al. 1995; Sternberg & Dalgarno 1995; Simon et al. 1995; Fuente et al. 1995). Indeed, the observed abundances of simple molecules in IRS4 are very similar to those found in the Orion Bar (see Helmich et al. 1997). The extended ridge in Orion also shows enhancements in these species. The ultraviolet radiation from IRS4 (and any other stars in the W 3 region) could create a PDR at the back of the cloud, resulting in large abundances of these species.

The abundances toward IRS5 are more difficult to interpret since there certainly is some stratification of material in the beam. Nevertheless, there is no doubt that the (beam-averaged) abundances of SO_2 and SiO in this source are larger by at least an order of magnitude compared with IRS4. Surprisingly, however, the abundances of sulfur-bearing molecules containing carbon (CS, H_2CS) appear lower than those found toward IRS4. Their line widths are also narrower, suggesting that these species are located in the outer, more quiescent part of the envelope. The proposed connection of SO_2 and SiO with the outflow in IRS5 needs to be tested further through interferometer observations of these species. If the column density derived by Mitchell et al. (1991) for the outflow is used, the abundances are increased by up to two orders of magnitude.

Although IRS5 has a powerful outflow and emits copious infrared photons, apparently only a small fraction of the envelope has been affected, since the abundances of many species, including HCN and CH_3OH, are lower compared with IRS4 and W 3(H_2O). In Paper I, we suggested that at least some of these molecules are still present in the ice mantles on the grains. This case is particularly strong for CH_3OH, where the amount of solid CH_3OH as measured by Allamandola et al. (1992) is 4 orders of magnitude larger than that of gas phase CH_3OH. The amount of depletion for many other molecules is still unknown, however, although most of the CO is certainly located in the gas phase (Tielens et al. 1991). Observations with the Infrared Space Observatory (ISO) will provide a complete inventory of the ice-mantle composition, which

together with this work can be used to determine the relative amounts present in the gas and on the grains (cf. van Dishoeck et al. 1996).

Toward W 3(H_2O) the largest complication is formed by the fact that the relative abundances of the molecules in the more extended core and in the compact clump are poorly determined. Nevertheless, the high temperature, the high methanol abundance, and the large column densities of methyl formate, dimethyl ether and OCS are clear signs of a "hot core" chemistry within the beam, in which molecules such as CH_3OH are released from the grains and drive a rapid gas-phase chemistry leading to complex organic molecules. This chemistry has been modelled e.g. by Charnley et al. (1992), and from their work it is obvious that at least 10^3 yr must have passed since the onset of methanol release. The amount of methanol relative to methyl formate and dimethyl ether is small, an order of magnitude smaller than found in e.g. the Orion compact ridge (see Table 5), and therefore difficult to account for in chemical models. The situation is worse in G34.3 (Millar private communication) where the methanol column density equals the dimethyl ether and methyl formate column densities. High optical depths can influence the methanol abundance severely, but as shown above it is not very likely to be significant here. More detailed chemical modeling will be presented in a later paper (Helmich et al. 1997).

The HCN over HNC ratio has been used to determine time scales for the chemical evolution (Goldsmith et al. 1986; Irvine et al. 1987; Schilke et al. 1992). It is beyond the scope of this work to perform a similar analysis here for the W 3 sources, but it is worthwhile to note that the values for the three W 3 sources lie somewhere between those of Orion IRc2 and the Ridge.

Only few deuterated species have been found in this work. The simplest molecules like DCO^+, DCN and DNC have been detected and these show indeed signs of some deuterium fractionation suggesting that the cloud had lower temperatures in its past. On the other hand, the observed amount of deuteration is less than the values of $0.01 - 0.1$ found in cold clouds such as TMC-1, and more comparable to that found in other warm clouds (see e.g. Table 2 of van Dishoeck et al. 1993a for an overview). It is also much lower than found in the low-mass star-forming region IRAS 16293–2422 (van Dishoeck et al. 1995). Together with the relatively low deuteration for HDO (Helmich et al. 1996) this can be interpreted as an indication that the cloud never went through a very cold ($T < 50$ K) phase. The limits on most other species such as HDCO and CH_3OD are not very stringent.

Table 6. Deuteration

Ratio	W 3 IRS4	W 3 IRS5	W 3(H_2O)
DCN/HCN	$< 4.3\,10^{-3}$	$< 5.0\,10^{-3}$	$7.7\,10^{-3}$
DNC/HNC	$< 7.1\,10^{-3}$	$< 4.2\,10^{-3}$	$4.8\,10^{-3}$
DCO^+/HCO^+	–	$2.5\,10^{-3}$	$4.2\,10^{-3}$
HDS/H_2S	$< 9.1\,10^{-2}$	< 0.14	$< 8.3\,10^{-2}$
$HDCO/H_2CO$	$< 3.8\,10^{-2}$	$< 5.0\,10^{-2}$	$< 2.5\,10^{-2}$
CH_3OD/CH_3OH	$< 7.1\,10^{-2}$	< 0.25	$< 1.1\,10^{-2}$
HDO/H_2O	–	–	$5\,10^{-4\,a}$

[a] Helmich et al. (1996).

7. Conclusions

A molecular line survey in the 345 GHz window has been performed toward three sources in the W 3 Giant Molecular Cloud with the James Clerk Maxwell Telescope. The analysis not only uses the rotation diagram method, but also statistical equilibrium calculations to determine beam-averaged column densities and physical parameters such as kinetic temperature and density. The column densities are accurate within a factor of two, but the abundances are much more uncertain, however. Clear physical and chemical differences between the three sources have been found.

W 3 IRS4 is the simplest of the three lines of sight studied in this work. The region is well characterised by a temperature of about 55 K and a density of $1\,10^6$ cm^{-3}. Only the sulfur-bearing molecules seem to favour slightly higher temperatures and densities. It is proposed that the star has already broken free of the molecular cloud and has created a PDR on the back side. In addition, a shock, perhaps connected with the penetration of the ionization front into the dense cloud, may be responsible for the creation of the sulfur-bearing molecules and for the elevated temperature and density.

W 3 IRS5 is more complicated, since several physical components are present in the beam. The bulk of the gas is well characterised by a temperature of approximately 100 K and a density of $1\,10^6$ cm^{-3}, but gradients are present. Again the sulfur-bearing molecules seem to trace the denser and hotter gas, which are proposed to be formed in the shock connected with the very powerful outflow. The hottest region is traced by SiO emission. Since this emission is expected to be very compact, interferometer measurements are needed to properly study this component.

Multiple components are also present toward W 3(H_2O), with the molecular emission arising partly from the extended core surrounding both W 3(H_2O) and W 3(OH), and partly from the compact clump near W 3(H_2O). The latter gas is warm (220 K) and dense ($\geq 2\,10^6$ cm^{-3}) and contains complex organic molecules.

This survey has provided an unique view on three star-forming clumps within the same parent cloud. Chemical modeling will be the natural next step. In addition, further constraints on the physical structure of the IRS5 region must be obtained through a multi-component excitation

analysis of both low- and high excitation lines. Mapping and interferometer data at subarcsec resolution, together with infrared absorption line data, are urgently needed to complete the picture of this high-mass star-forming cloud.

Acknowledgements. The authors are indebted to Fred Baas, Remo Tilanus, David Jansen and the JCMT staff for assistance with the observing runs, and to Todd Groesbeck, Peter Schilke and Eric Herbst for help with updating the line catalogs. They thank Geoff Blake, Lee Mundy, Tom Wilson and Malcolm Walmsley for useful discussions, David Jansen for his efforts in setting up the excitation calculations, and Per Bergman for providing them with his $CN - H_2$ collisional rate coefficients. This research was supported by the Netherlands Organisation for Scientific Research (NWO) through a PIONIER grant, and by the Space Research Organisation Netherlands (SRON).

References

Alcolea J., Menten K.M., Moran J.M., Reid M.J., 1992, in: "Astrophysical Masers", Clegg A.W. & Nedoluha G.E. (eds.). Springer Verlag, Berlin, p. 225
Allamandola L.J., Sandford S.A., Tielens A.G.G.M., Herbst T.M., 1992, ApJ 399, 134
Anderson T., de Lucia F.C., Herbst E., 1990, ApJS 72, 797
Bachiller R., Martín-Pintado J., Fuente A., 1991, A&A 243, L21
Betz A.L., Boreiko R.T., 1995, in: "Airborne Astronomy Symposium on the Galactic Ecosystem", Haas M.R., Davidson J.A., Erickson E.F. (eds.) p. 41
Blake G.A., Sutton E.C., Masson C.R., et al., 1984, ApJ 286, 586
Blake G.A., Sutton E.C., Masson C.R., Phillips T.G., 1986, ApJS 60, 357
Blake G.A., Sutton E.C., Masson C.R., Phillips T.G., 1987, ApJ 315, 621
Blake G.A., van Dishoeck E.F., Jansen D.J., Groesbeck T.D., Mundy L.G., 1994, ApJ 428, 680
Blake G.A., Sandell G., van Dishoeck E.F., 1995, ApJ 441, 689
Bloemhof E.E., Reid M.J., Moran J.M., 1992, ApJ 397, 500
Boreiko R.T., Betz A.L., 1991, ApJ 369, 382
Caselli P., Hasegawa T.I., Herbst E., 1993, ApJ 408, 548
Charnley S.B., Tielens A.G.G.M., Millar T.J., 1992, ApJ 399, L71
Choi M.H., Evans N.J., Jaffe D.T., 1993, ApJ 417, 624
Churchwell E., Wood D., Myers P.C., Myers R.V., 1986, ApJ 305, 405
Claussen M.J., Gaume R.A., Johnston K.J., Wilson T.L., 1994, ApJ 424, L41
Colley D., 1980, MNRAS 193, 495
Cummins S.E., Linke R.A., Thaddeus P., 1986, ApJS 60, 819
Cunningham C.T., Hayward R.H., Wade J.D., et al., 1992, Int. J. Infrared Millim. Waves 13, 1827
Davies S.R., Cunningham C.T., Little L.T., Matheson D.N., 1992, Int. J. Infrared Millim. Waves 13, 647
de Boisanger C., Helmich F.P., van Dishoeck E.F., 1996, A&A (in press)
Dickel H.R., 1980, ApJ 238, 829
Dickel H.R., Dickel J.R., Wilson W.J., Werner M.W., 1980, ApJ 237, 711
Fuente A., Martín-Pintado J., Gaume R., 1995, ApJ 442, L33
Georgelin Y.M., Georgelin Y.P., 1976, A&A 49, 57
Goldsmith P.F., Irvine W.M., Hjalmarson Å., Elldér J., 1986, ApJ 358, L49
Greaves J.S., White G.J., 1991, A&AS 91, 237
Green S., 1994, ApJ 434, 188
Groesbeck T.D., 1994, Ph.D. thesis California Institute of Technology
Guilloteau S., Bachiller R., Fuente A., Lucas R., 1992, A&A 265, L49
Harris S., Wynn-Williams C.G., 1976, MNRAS 174, 649
Hasegawa T.I., Mitchell G.F., Matthews H.E., Tacconi L., 1994, ApJ 426, 215 (HMMT)
Hauschildt H., Güsten R., Phillips T.G., Serabyn E., Walker C.K., 1993, A&A 273, L23
Hayashi M., Kobayashi H., Hasegawa T., 1989, ApJ 340, 298
Helmich F.P., Jansen D.J., de Graauw Th., Groesbeck T.D., van Dishoeck E.F., 1994, A&A 283, 626 (Paper I)
Helmich F.P., van Dishoeck E.F., Jansen D.J., 1996 (in press)
Helmich F.P., Millar T.J., van Dishoeck E.F., 1997, A&A (submitted)
Hjalmarson Å., Bergman P., 1992, in: "Chemistry and Spectroscopy of Interstellar Molecules", Bohme D.K., Herbst E., Kaifu N., Saito S. (eds.). University of Tokio Press, p. 41
Hsu Y.-C., Min-Lin Jr. J., Papoušek D., Tsai J.-J., 1993, J. Chem. Phys. 98, 6690
Irvine W.M., Goldsmith P.F., Hjalmarson Å., 1987, in: "Interstellar Processes", D.J. Hollenbach, H.A. Thronson (eds.). Kluwer, Dordrecht, p. 561
Jaffe D.T., Davidson J.A., Dragovan M., Hildebrand R.H., 1984, ApJ 284, 637
Jansen D.J., van Dishoeck E.F., Black J.H., 1994, A&A 282, 605
Jansen D.J., 1995, Ph.D. thesis University of Leiden
Jansen D.J., Spaans M., Hogerheijde M.R., van Dishoeck E.F., 1995, A&A 303, 541
Jewell P.R., Hollis J.M., Lovas F.J., Snyder L.E., 1989, ApJS 70, 833
Kanamori H., Hirota E., 1988, J. Chem. Phys. 89, 3962
Kutner M.L., Ulich B.L., 1981, ApJ 250, 341
Lacy J.H., Knacke R., Geballe T.R., Tokunaga A.T., 1994, ApJ 428, L69
Ladd E.F., Deane J.R., Sanders D.B., Wynn-Williams C.G., 1993, ApJ 419, 186
Macdonald G.H., Gibb A.G., Habing R.J., Millar T.J., 1996, A&A (in press)
MacKay D.S.S., 1995, MNRAS 274, 694
MacKay D.S.S., 1996, MNRAS 278, 62
Martín-Pintado J., Bachiller R., Fuente A., 1992, A&A 254, 315
Mauersberger R., Wilson T.L., Henkel C., 1988, A&A 201, 123
Mcmullin J.P., Mundy L.G., Wilking B.A., Hezel T., Blake G.A., 1994, ApJ 424, 222
Megeath S.T., Herter T., Beichman C., et al., 1996, A&A (in press)
Millar T.J., Rawlings J.M.C., Bennett A., Brown P.D., Charnley S.B., 1991, A&AS 87, 585
Minh Y.C., Ziurys L.M., Irvine W.M., McGonagle D., 1991a, ApJ 366, 192
Minh Y.C., Brewer M.K., Irvine W.M., Friberg P., Johansson L.E.B., 1991b, A&A 244, 470

Mitchell G.F., Maillard J.-P., Allen M., Beer R., Belcourt K., 1990, ApJ 363, 554
Mitchell G.F., Maillard J.-P., Hasegawa T.I., 1991, ApJ 371, 342
Mitchell G.F., Hasegawa T.I., Schella J., 1992, ApJ 386, 604
Oldham P.G., Griffin M.J., Richardson K.J., Sandell G., 1994, A&A 284, 559
Pickett H.M., 1991, J. Molec. Spectrosc. 148, 371
Reid M.J., Argon A.L, Masson C.R., Menten K.M., Moran J.M., 1995, ApJ 443, 238
Richardson K.J., Sandell G., White G.J., Duncan W.D., Krisciunas K., 1989, A&A 221, 95
Shalabiea O.M., Greenberg J.M., 1994, A&A 290, 266
Schilke P., Walmsley C.M., Pineau des Forêts G., et al., 1992, A&A 256, 595
Schilke P., Groesbeck T.D., Blake G.A., Phillips T.G., 1996, ApJSS (in press)
Simon R., Saleck A.H., Schneider N., Jacobs K., Vowinkel B., Winnewisser G., 1995, in: "The Physics and Chemistry of Interstellar Molecular Clouds", G. Winnewisser & G.C. Pelz (eds.). Springer Verlag, Berlin, p. 252
Sternberg A., Dalgarno A., 1995, ApJS 99, 565
Sutton E.C., Blake G.A., Masson C.R., Phillips T.G., 1985, ApJS 58, 341
Sutton E.C., Jaminet P.A., Danchi W.C., Blake G.A., 1991, ApJS 77, 255
Sutton E.C., Peng R., Danchi W.C., Jaminet P.A., Sandell G., Russell A.P.G., 1995, ApJS 97, 455
Tieftrunk A.R., Wilson T.L., Steppe H., Gaume R.A., Johnston K.J., Claussen M.J., 1995, A&A 303, 901
Tielens A.G.G.M., Tokunaga A.T., Geballe T.R., Baas F., 1991, ApJ 381, 181
Turner B.E., 1991, ApJS 76, 617
Turner B.E., 1994, ApJ 430, 727
Turner J.L., Welch W.J., 1984, ApJ 287, L81
Ungerechts H., Bergin E.A., Goldsmith P.F., Irvine W.M., Schloerb F.P., Snell R.L., 1995, in: "The Physics and Chemistry of Interstellar Molecular Clouds", Winnewisser G. & Pelz G.C. (eds.). Springer Verlag, Berlin, p. 258
van Dishoeck E.F., Blake G.A., Draine B.T., Lunine J.I., 1993a, in: Protostars and Planets III, E.H. Levy and J.I. Lunine (eds.). University of Arizona Press, Tucson, p. 163
van Dishoeck E.F., Jansen D.J., Phillips T.G., 1993b, A&A 279, 541
van Dishoeck E.F., Blake G.A., Jansen D.J., Groesbeck T.D., 1995, ApJ 447, 760
van Dishoeck E.F., Helmich F.P., de Graauw Th., et al., 1996, A&A (in press)
Werner M.W., Becklin E.E., Gatley I., et al., 1980, ApJ 242, 601
Westerhout G., 1958, BAN 14, 215
Willner S.P., Gillett F.C., Herter T.L., et al., 1982, ApJ 253, 174
Wilner D.J., Welch W.J., Forster J.R., 1995, ApJ 449, L73
Wilson T.L., Rood R.T., 1994, ARA&A 32, 191
Wilson T.L., Johnston K.J., Mauersberger R., 1991, A&A 251, 220
Wink J.E., Duvert G., Guilloteau S., et al., 1994, A&A 281, 505
Wootten A., Loren R.B., Snell R.L., 1982, ApJ 255, 160
Wright M.C.H., Dickel H.R., Ho P.T.P, 1984, ApJ 281, L71
Wright M.C.H., Plambeck R.L., Mundy L.G., Looney L.W., 1995, ApJ 455, L185
Wynn-Williams C.G., 1971, MNRAS 151, 397
Wynn-Williams C.G., Becklin E.E., Neugebauer G., 1972, MNRAS 160, 1
Ziurys L.M., Turner B.E., 1986, ApJ 300, L19
Ziurys L.M., 1991, ApJ 379, 260
Ziurys L.M., McGonagle D., 1993, ApJS 89, 155

Table 7. Gaussian fit parameters

Species	ν (MHz)	J	W3 IRS4 $T_{\rm MB}$ (K)	W3 IRS4 ΔV (km/s)	W3 IRS4 W (K km/s)	W3 IRS5 $T_{\rm MB}$ (K)	W3 IRS5 ΔV (km/s)	W3 IRS5 W (K km/s)	W3(H_2O) $T_{\rm MB}$ (K)	W3(H_2O) ΔV (km/s)	W3(H_2O) W (K km/s)
CO	230538.0	2–1	–[1]	–	333	–[1]	–	894	–	–	–
CO	345796.0	3–2	–[1]	–	536	–[1]	–	701	–[1]	–	341
^{13}CO	220398.7	2–1	–	–	–	–	–	–	17.1	6.10	111
C^{18}O	219560.3	2–1	9.41	4.25	42.8	8.91	4.71	44.4	11.4	5.35	64.9
C^{17}O	224714.4	2–1	1.04	5.42	6.00	–	–	–	–	–	–
C^{17}O	337061.1	3–2	3.73	3.67	14.3	4.47	4.09	19.5	3.23	4.40	15.1
CN	226341.9	$2_{\frac{3}{2}\frac{5}{2}} - 1_{\frac{3}{2}\frac{3}{2}}$	<0.11	–	–	0.42	1.51	0.28	0.51	3.82	2.06
CN	226359.9	$2_{\frac{3}{2}\frac{5}{2}} - 1_{\frac{3}{2}\frac{5}{2}}$	0.81	3.94	3.39	0.42	4.95	2.24	0.50	3.56	1.84
CN	339493.3	$3_{\frac{5}{2}\frac{7}{2}} - 2_{\frac{5}{2}\frac{7}{2}}$	<0.14	–	–	<0.087	–	–	0.33[a]	6.89	2.45
CN	339516.7	$3_{\frac{5}{2}\frac{5}{2}} - 2_{\frac{5}{2}\frac{5}{2}}$	0.27	5.52	0.91	<0.087	–	–	<0.098	–	–
CN	339992.3	$3_{\frac{5}{2}\frac{3}{2}} - 2_{\frac{3}{2}\frac{5}{2}}$	0.85	2.15	1.94	<0.17	–	–	2.23[b]	5.03	11.9
CN	340008.1	$3_{\frac{5}{2}\frac{5}{2}} - 2_{\frac{3}{2}\frac{5}{2}}$	0.24	2.06	0.53	0.45	2.70	1.30	0.23	2.25	0.57
CN	340019.6	$3_{\frac{5}{2}\frac{3}{2}} - 2_{\frac{3}{2}\frac{3}{2}}$	0.66	3.06	2.15	0.35	5.11	1.90	0.20	4.00	0.87
CN	340031.5	$3_{\frac{5}{2}\frac{7}{2}} - 2_{\frac{3}{2}\frac{5}{2}}$	3.32	3.50	12.4	2.57	3.50	9.58	2.24	4.00	9.54
CN	340035.4	$3_{\frac{5}{2}\frac{3/5}{2}} - 2_{\frac{3}{2}\frac{1/3}{2}}$	3.04	3.28	10.6	2.35	3.43	8.58	1.14	4.0[4]	4.83
CN	340248	$3_{\frac{7}{2}\frac{7/9/5}{2}} - 2_{\frac{5}{2}\frac{5/7/3}{2}}$	9.83	4.24	44.3	5.84	5.44	33.8	5.70	4.72	28.7
CN	340261.8	$3_{\frac{7}{2}\frac{5}{2}} - 2_{\frac{5}{2}\frac{5}{2}}$	0.59	2.29	1.43	0.52	3.15	1.74	0.64	5.20	3.53
CN	340265.0	$3_{\frac{7}{2}\frac{7}{2}} - 2_{\frac{5}{2}\frac{7}{2}}$	0.97	2.80	2.89	0.51	5.84	3.15	0.66	5.08	3.58
HCN	354505.5	4–3	5.62	5.32	31.8	–[1]	–	72.8	–[1]	–	104
H^{13}CN	259011.8	3–2	1.62	3.78	6.49	1.06	4.30	4.87	2.00	6.50	13.9
H^{13}CN[c]	345339.8	4–3	1.29	3.07	4.22	2.71	6.32	18.2	2.62	6.77	18.9
HC^{15}N	258157.1	3–2	0.51	3.29	1.79	0.40	3.40	1.47	1.22[d]	7.38	9.57
HC^{15}N	344200.5	4–3	<0.085	–	–	0.54	3.43	1.98	0.58	7.65	4.74
HNC	362629.9	4–3	2.38	3.23	8.18	1.85	3.22	6.33	3.55[e]	5.83	22.0
HN^{13}C	261263.3	3–2	0.18	4.89	0.93	0.49[f]	5.42	2.83	0.14	4.27	0.63
HN^{13}C	348340.3	4–3	0.18	6.16	1.20	0.32	5.12	1.75	0.27	4.37	1.23
H^{15}NC	355439.5	4–3	<0.053	–	–	<0.063	–	–	1.39[g]	9.19	13.6
HC_3N	218324.7	24–23	<0.086	–	–	<0.060	–	–	0.61	5.63	3.67
HC_3N	227419.0	25–24	<0.14	–	–	<0.15	–	–	0.70	5.12	3.83
HC_3N	336521.0	37–36	<0.16	–	–	<0.089	–	–	<0.11	–	–
HC_3N	345610.1	38–37	<0.14	–	–	<0.12	–	–	<0.14	–	–
HC_3N	354698.7	39–38	<0.27	–	–	<0.32	–	–	–[h]	–	–
HNCO	219798.3	$10_{010} - 9_{09}$	<0.10	–	–	<0.092	–	–	0.44	6.00	2.81
HNCO	240875.9	$11_{111} - 10_{110}$	<0.062	–	–	<0.062	–	–	–[i]	–	–
HNCO	241708.4	$11_{29} - 10_{28}$	<0.064	–	–	<0.068	–	–	<0.11	–	–
HNCO	241774.1	$11_{011} - 10_{010}$	<0.064	–	–	0.24	2.56	0.64	0.47	7.75	3.92
HNCO	242639.8	$11_{110} - 10_{19}$	<0.064	–	–	<0.059	–	–	<0.068	–	–
HNCO	351633.5	$16_{016} - 15_{015}$	<0.14	–	–	0.27	5.91	1.71	0.29	5.75	1.80
CCH	262005	$3, \frac{7}{2}, 4/3 - 2, \frac{5}{2}, 3/2$	2.30	5.94	14.5	1.31	7.23	10.1	1.70	5.70	10.3
CCH	262066	$3, \frac{5}{2}, 3/2 - 2\frac{3}{2}, 2/1$	1.49	6.52	10.3	0.92	7.58	7.44	1.14	5.64	6.84
CCH	349338	$4, \frac{9}{2}, 4 - 3\frac{7}{2}, 3$	4.66	4.02	20.0	2.25	5.53	13.2	2.08	4.77	10.5
CCH	349399	$4, \frac{7}{2}, 4/3 - 3\frac{5}{2}, 3/2$	3.70	4.17	16.4	1.85	5.01	9.89	1.58	6.10	10.2
CH_3CCH	239211.2	$14_3 - 13_3$	–[5]	–	–	–[5]	–	–	0.77	3.67	3.00
CH_3CCH	239234.0	$14_2 - 13_2$	0.12[5]	6.03	0.76	<0.080	–	–	0.33[5]	2.74	0.96
CH_3CCH	239247.7	$14_1 - 13_1$	0.38	2.47	1.00	<0.080	–	–	0.78	3.33	2.76

Table 7. continued

Species	ν (MHz)	J	$T_{\rm MB}$ (K)	ΔV (km/s)	W (K km/s)	$T_{\rm MB}$ (K)	ΔV (km/s)	W (K km/s)	$T_{\rm MB}$ (K)	ΔV (km/s)	W (K km/s)
CH_3CCH	239252.3	$14_0 - 13_0$	0.51	4.67	2.56	<0.080	–	–	0.89	3.75	3.54
CH_3CCH	341741.1	$20_0 - 19_0$	<0.049	–	–	<0.14	–	–	<0.12	–	–
CH_3CCH	358708.9	$21_4 - 20_4$	<0.078	–	–	<0.075	–	–	<0.083	–	–
CH_3CCH	358756.6	$21_3 - 20_3$	<0.078	–	–	<0.075	–	–	0.20	5.59	1.17
CH_3CCH	358790.8	$21_2 - 20_2$	<0.078	–	–	<0.075	–	–	0.15	3.70	0.62
CH_3CCH	358811.2	$21_1 - 20_1$	<0.078	–	–	<0.075	–	–	0.29[j]	9.59	3.00
CH_3CCH	358818.0	$21_0 - 20_0$	<0.078	–	–	<0.075	–	–	0.29[j]	9.59	3.00
H_2CO	218222.2	$3_{03} - 2_{02}$	2.13	3.91	8.86	1.25	5.60	7.45	3.07	5.94	19.4
H_2CO	218475.6	$3_{22} - 2_{21}$	0.52	5.19	2.85	0.53	6.05	3.37	1.28	4.69	6.39
H_2CO	225697.8	$3_{12} - 2_{11}$	4.54	4.58	23.0	2.98	5.92	18.7	5.09	7.00	38.0
H_2CO	351768.7	$5_{15} - 4_{14}$	0.28	3.69	10.8	2.92	4.52	14.0	5.87	5.99	37.3
H_2CO	362735.9	$5_{05} - 4_{04}$	1.33	3.37	1.62	1.33	4.25	6.02	4.80	6.06	31.0
H_2CO	363945.9	$5_{24} - 4_{23}$	0.53	2.86	4.78	0.64	4.67	3.18	2.80	6.06	18.2
H_2CO	364102.8	$5_{42} - 4_{41}$	<0.052	–	–	0.10[k]	4.92	0.55	1.04[l]	8.87	9.83
H_2CO	364103.0	$5_{40} - 4_{40}$	<0.052	–	–	0.10[k]	4.92	0.55	1.04[l]	8.87	9.83
H_2CO	364275.2	$5_{33} - 4_{32}$	0.79	2.98	2.50	0.74	3.84	3.00	3.60	5.92	22.7
H_2CO	364289.0	$5_{32} - 4_{31}$	0.90	3.00	2.87	0.92	3.11	3.05	4.55[m]	6.42	31.2
$H_2^{13}CO$	219908.5	$3_{12} - 2_{11}$	<0.094	–	–	<0.099	–	–	0.22	4.39	1.03
$H_2^{13}CO$	343325.5	$5_{15} - 4_{14}$	<0.10	–	–	<0.16	–	–	1.20[n]	7.86	10.0
$H_2^{13}CO$	353811.8	$5_{05} - 4_{04}$	<0.14	–	–	<0.10	–	–	<0.13	–	–
$H_2^{13}CO$	354898.5	$5_{24} - 4_{23}$	<0.19	–	–	0.97[o]	6.61	6.82	<0.22	–	–
$H_2^{13}CO$	355028.7	$5_{42/1} - 4_{41/0}$	<0.19	–	–	<0.20	–	–	<0.22	–	–
$H_2^{13}CO$	355041.4	$12_{111} - 11_{112}$	<0.19	–	–	2.29[p]	6.67	16.3	0.67[p]	6.52	4.67
$H_2^{13}CO$	355190.9	$5_{33} - 4_{32}$	<0.19	–	–	<0.19	–	–	<0.22	–	–
$H_2^{13}CO$	355202.6	$5_{32} - 4_{31}$	<0.077	–	–	<0.077	–	–	<0.078	–	–
$H_2^{13}CO$	356176.1	$5_{23} - 4_{22}$	<0.081	–	–	<0.076	–	–	<0.081	–	–
CH_3CN	238972.4	$13_6 - 12_6$	<0.060	–	–	<0.060	–	–	0.41	5.40	2.33
CH_3CN	257349.2	$14_6 - 13_6$	<0.060	–	–	<0.066	–	–	<0.072	–	–
CH_3CN	257448.1	$14_4 - 13_4$	<0.060	–	–	<0.066	–	–	0.28	5.0[4]	1.49
CH_3CN	257482.8	$14_3 - 13_3$	<0.066	–	–	<0.066	–	–	0.54	5.0[4]	2.88
CH_3CN	257507.5	$14_2 - 13_2$	<0.066	–	–	<0.066	–	–	0.61[q]	5.0[4]	3.24
CH_3CN	257522.4	$14_1 - 13_1$	<0.066	–	–	<0.066	–	–	0.68[q,r]	5.0[4]	3.60
CH_3CN	257527.3	$14_0 - 13_0$	<0.066	–	–	<0.066	–	–	0.90[q]	5.0[4]	4.82
CH_3CN	349212.1	$19_6 - 18_6$	<0.12	–	–	<0.10	–	–	<0.083	–	–
CH_3CN	349285.8	$19_5 - 18_5$	<0.11	–	–	<0.10	–	–	0.33[6]	8.23	2.92
CH_3CN	349346.1	$19_4 - 18_4$	–[s]	–	–	_[6,s]	–	–	0.91[s]	5.5[4]	5.32
CH_3CN	349393.0	$19_3 - 18_3$	<0.14	–	–	<0.12	–	–	0.26	6.37	1.75
CH_3CN	349426.6	$19_2 - 18_2$	<0.14	–	–	<0.12	–	–	0.41	6.16	2.68
CH_3CN	349446.7	$19_1 - 18_1$	<0.14	–	–	<0.12	–	–	0.55[t]	9.92	5.84
CH_3CN	349453.4	$19_0 - 18_0$	<0.14	–	–	<0.12	–	–	0.55[t]	9.92	5.84
CS	342883.0	7–6	9.77	3.85	40.0	6.18	4.21	27.6	12.4	6.61	87.0
$C^{34}S$	241016.2	5–4	1.19[u]	4.74	5.98	1.14	2.91	3.54	3.04	6.48	21.0
$C^{34}S$	337396.7	7–6	0.46	2.84	1.40	0.74	1.96	1.55	3.17	5.98	20.2
^{13}CS	231220.8	5–4	0.41	3.73	1.64	0.35	2.77	1.04	1.43	4.67	7.13
$C^{33}S$	242913.7	5–4	0.42	4.64	2.08	0.19	2.84	0.58	1.13	4.93	5.92
$C^{33}S$	340052.7	7–6	<0.092	–	–	0.59	1.35	0.85	1.15	5.49	6.74
SO	219949.4	56–45	2.89	4.28	13.7	3.65	6.18	24.0	5.44	5.99	34.7
SO	258255.8	66–55	6.93	4.37	7.79	6.50[3]	–	–	5.56	6.25	37.0
SO	261843.7	67–56	1.56	4.95	8.24	3.65	6.46	25.1	3.67	5.89	23.0

Table 7. continued

Species	ν (MHz)	J	$T_{\rm MB}$ (K)	ΔV (km/s)	W (K km/s)	$T_{\rm MB}$ (K)	ΔV (km/s)	W (K km/s)	$T_{\rm MB}$ (K)	ΔV (km/s)	W (K km/s)
SO	340714.2	87–76	1.49	3.73	5.90	7.71	6.48	53.2	8.68	5.98	55.1
SO	344310.6	88–77	0.55	5.36	3.12	8.18[3]	–	–	4.88	6.24	32.4
SO	345704.6	32–12	<0.11	–	–	<0.12	–	–	<0.19	–	–
SO^{v}	346528.5	89–78	2.39	4.47	11.3	10.3[3]	–	–	7.71	6.96	57.1
^{34}SO	253208.0	66–55	–	–	–	0.80	5.84	4.96	–	–	–
^{34}SO	256877.5	67–56	<0.074	–	–	1.27	5.72	7.70	0.72	4.94	3.76
^{34}SO	337582.2	88–77	0.17[w]	6.25	1.16	3.00	5.93	18.9	1.37[w]	7.22	10.5
^{34}SO	339857.6	89–78	<0.10	–	–	1.12	5.00	5.90	0.84	6.30	5.60
^{34}SO^{x}	356887.4	76–67	<0.28	–	–	<0.12	–	–	<0.18	–	–
^{33}SO^{y}	337198.5	87–76	<0.16	–	–	0.42	5.66	2.52	0.39	8.39	3.49
^{33}SO	343088.0	89–78	0.22	6.91	1.60	0.66	5.77	4.07	–	–	–
^{33}SO	340838.5	88–77	–	–	–	–	–	–	0.27	4.23	1.23
S^{18}O	228272.3	98–88	–	–	–	–	–	–	<0.30	–	–
S^{18}O	239128.7	66–55	<0.084	–	–	0.13	4.36	0.59	–[z]	–	–
S^{18}O	243039.9	67–56	<0.076	–	–	0.19	6.30	1.30	<0.066	–	–
S^{18}O	355573.6	98–87	< 0.57	–	–	0.24	5.08	1.32	< 0.97	–	–
S^{18}O	358648.8	99–88	<0.11	–	–	0.21	4.30	0.96	<0.11	–	–
SO_2	216643.3	$22_{220} - 22_{121}$	<0.057	–	–	0.76	6.80	5.52	0.22	8.63	2.00
SO_2	222869.1	$36_{333} - 37_{236}$	–	–	–	–	–	–	5.69[aa]	5.63	34.1
SO_2	226300.0	$14_{311} - 14_{212}$	0.23	5.91	1.43	0.95	7.13	7.23	0.39	6.75	2.77
SO_2	227335.8	$32_{923} - 33_{826}$	<0.15	–	–	<0.15	–	–	<0.18	–	–
SO_2	230965.2	$37_{1028} - 38_{929}$	<0.035	–	–	<0.035	–	–	<0.022	–	–
SO_2	234187.1	$28_{325} - 28_{226}$	<0.035	–	–	0.70	6.50	4.81	0.28	4.71	1.39
SO_2	234421.6	$16_{610} - 17_{513}$	–	–	–	0.53	5.98	3.39	–[5]	–	–
SO_2	237068.9	$12_{39} - 12_{210}$	–	–	–	1.24	7.91	10.4	0.46	7.45	3.66
SO_2	238992.5	$21_{715} - 22_{616}$	<0.070	–	–	<0.056	–	–	<0.16	–	–
SO_2	239832.5	$15_{313} - 16_{016}$	<0.078	–	–	<0.078	–	–	<0.073	–	–
SO_2	240942.8	$18_{117} - 18_{018}$	<0.067	–	–	1.23	5.86	7.67	0.38	8.97	3.61
SO_2	241615.8	$5_{24} - 4_{13}$	0.24	4.45	1.13	1.42	5.40	8.18	0.89	4.83	4.59
SO_2	242997.8	$19_{317} - 20_{020}$	<0.078	–	–	<0.078	–	–	<0.073	–	–
SO_2	243087.6	$5_{42} - 6_{33}$	<0.078	–	–	0.25	5.00	1.31	<0.073	–	–
SO_2	243245.4	$26_{818} - 27_{721}$	<0.077	–	–	<0.078	–	–	<0.010	–	–
SO_2	244254.2	$14_{014} - 13_{113}$	0..38	2.27	0.90	2.05	5.60	12.2	1.24	5.98	7.91
SO_2	245339.2	$26_{323} - 25_{422}$	–	–	–	0.58	4.93	3.03	0.098	8.97	0.94
SO_2	245563.4	$10_{37} - 10_{28}$	–	–	–	1.64	5.63	9.80	0.80	4.58	3.91
SO_2	248436.9	$13_{311} - 14_{014}$	–	–	–	0.12	6.24	0.76	<0.058	–	–
SO_2	251199.7	$13_{113} - 12_{012}$	–	–	–	2.56	7.00	19.0	–	–	–
SO_2	251210.6	$8_{35} - 8_{26}$	–	–	–	1.81	6.64	12.7	–	–	–
SO_2	254280.5	$6_{33} - 6_{24}$	–	–	–	2.09[ab]	9.31	20.8	–	–	–
SO_2	254283.3	$24_{222} - 24_{123}$	–	–	–	2.09[ab]	9.31	20.8	–	–	–
SO_2	255958.0	$3_{31} - 3_{22}$	–	–	–	0.83	5.34	4.70	–	–	–
SO_2	256246.9	$5_{33} - 5_{24}$	–	–	–	1.01	6.39	6.85	–	–	–
SO_2	257100.0	$7_{35} - 7_{26}$	0.18	5.24	1.01	1.43	6.73	10.2	0.60	5.08	3.27
SO_2	258388.7	$32_{428} - 32_{329}$	<0.051	–	–	0.61	6.91	4.48	0.11	5.17	0.59
SO_2	258667.0	$20_{713} - 21_{616}$	<0.061	–	–	0.49[f]	5.42	2.83	0.25[ac]	7.39	2.02
SO_2	258942.2	$9_{37} - 9_{28}$	0.24	6.77	1.73	1.47	6.09	9.56	0.63	6.93	4.29
SO_2	261091.2	$27_{424} - 28_{127}$	<0.049	–	–	<0.049	–	–	<0.059	–	–
SO_2	317250.4	$17_{711} - 18_{612}$	–	–	–	0.71	7.02	5.33	–	–	–
SO_2	334673.3	$8_{26} - 7_{17}$	0.27	3.97	1.15	1.69	6.86	12.3	1.00[z]	7.47	7.92
SO_2	335773.2	$29_{525} - 30_{228}$	<0.11	–	–	0.28	4.27	1.30	2.28[ad]	8.00	19.4
SO_2	336089.2	$23_{321} - 23_{222}$	<0.12	–	–	0.78	6.00	4.96	0.32	9.58	3.25
SO_2	336669.6	$16_{79} - 17_{612}$	0.30	7.19	2.28	0.42	7.34	3.23	0.30	7.07	2.23

Table 7. continued

Species	ν (MHz)	J	$T_{\rm MB}$ (K)	ΔV (km/s)	W (K km/s)	$T_{\rm MB}$ (K)	ΔV (km/s)	W (K km/s)	$T_{\rm MB}$ (K)	ΔV (km/s)	W (K km/s)
SO_2	338306.0	$18_{414} - 18_{315}$	0.32	2.59	0.88	1.89	6.60	13.3	0.39	7.38	3.09
SO_2^{ae}	338611.8	$20_{119} - 19_{218}$	0.33	8.61	2.95	2.30	6.52	16.0	1.79	7.67	14.6
SO_2	339149.2	$37_{434} - 38_{137}$	<0.12	–	–	0.090	9.22	0.89	<0.10	–	–
SO_2	339259.6	$39_{634} - 40_{337}$	<0.12	–	–	<0.047	–	–	<0.10	–	–
SO_2	340316.4	$28_{226} - 28_{127}$	<0.11	–	–	1.67	6.36	11.3	0.45	6.08	2.92
SO_2	341275.5	$21_{814} - 22_{715}$	<0.25	–	–	0.42	6.61	2.93	<0.12	–	–
SO_2	341403.1	$40_{436} - 40_{337}$	<0.22	–	–	0.31	10.8	3.50	<0.12	–	–
SO_2	341674.0	$36_{531} - 36_{432}$	<0.21	–	–	0.57	9.10	5.48	<0.11	–	–
SO_2	342761.6	$34_{331} - 34_{232}$	<0.090	–	–	0.39	6.67	2.73	<0.14	–	–
SO_2	345149.0	$5_{51} - 6_{42}$	0.21	4.48	0.99	<0.093	–	–	<0.098	–	–
SO_2^{c}	345338.5	$13_{212} - 12_{111}$	1.29	3.07	4.22	2.71	6.32	18.2	2.62	6.77	18.9
SO_2	345449.0	$26_{917} - 27_{820}$	<0.12	–	–	0.35	4.54	1.70	<0.11	–	–
SO_2^{v}	346523.9	$16_{412} - 16_{313}$	2.39	4.47	11.3	10.3[3]	–	–	7.71	6.96	57.1
SO_2	346652.2	$19_{119} - 18_{018}$	0.41	6.35	2.77	3.58	8.32	31.7	1.37[af]	7.74	11.3
SO_2	348387.8	$24_{222} - 23_{321}$	<0.11	–	–	0.97	5.85	6.07	0.46	5.82	2.82
SO_2	348633.3	$5_{33} - 6_{06}$	<0.16	–	–	<0.15	–	–	<0.21	–	–
SO_2	349783.3	$46_{541} - 46_{442}$	<0.092	–	–	0.25	6.14	1.66	<0.12	–	–
SO_2	350862.7	$10_{64} - 11_{57}$	–	–	–	0.52	6.14	3.35	<0.14	–	–
SO_2	351257.2	$5_{33} - 4_{22}$	<0.30	–	–	1.75	6.57	12.2	<0.25	–	–
SO_2	351873.9	$14_{410} - 14_{311}$	<0.16	–	–	0.82	6.19	5.43	0.72	4.88	3.74
SO_2	352639.0	$36_{1125} - 37_{1028}$	<0.15	–	–	<0.11	–	–	–[5]	–	–
SO_2	355045.5	$12_{48} - 12_{39}$	<0.19	–	–	2.29[p]	6.67	16.3	0.67[p]	6.52	4.67
SO_2	355155.0	$32_{230} - 33_{133}$	<0.19	–	–	<0.20	–	–	<0.22	–	–
SO_2	355186.5	$17_{414} - 18_{117}$	<0.19	–	–	<0.20	–	–	<0.22	–	–
SO_2	356040.6	$15_{79} - 16_{610}$	<0.083	–	–	0.92	6.84	6.68	0.21	7.37	1.67
SO_2	356755.2	$10_{46} - 10_{37}$	0.16	6.86	1.19	0.80	8.00	6.65	0.66	5.54	3.89
SO_2	357165.4	$13_{410} - 13_{311}$	0.24	6.72	1.70	2.25	7.95	19.2	0.58	9.54	5.85
SO_2	357892.4	$7_{44} - 7_{35}$	<0.19	–	–	1.32	6.36	7.57	<0.22	–	–
SO_2	357926.0	$6_{42} - 6_{33}$	<0.19	–	–	1.23	6.68	8.71	<0.22	–	–
SO_2	357962.9	$17_{414} - 17_{315}$	<0.19	–	–	0.98	6.52	6.82	<0.22	–	–
SO_2	358013.1	$5_{42} - 5_{43}$	<0.19	–	–	0.97[o]	6.61	6.82	<0.22	–	–
SO_2	358038.1	$4_{40} - 4_{31}$	<0.19	–	–	0.70	7.87	5.87	<0.22	–	–
SO_2	358215.6	$20_{020} - 19_{119}$	0.33	7.19	2.50	2.75	8.23	24.2	1.35	8.75	12.6
SO_2	359151.2	$25_{323} - 25_{224}$	<0.065	–	–	0.61	6.35	4.12	0.68	7.01	5.10
SO_2	359770.7	$19_{416} - 19_{317}$	<0.11	–	–	1.72	7.88	14.3	0.39	7.26	3.00
SO_2	360290.4	$34_{529} - 34_{430}$	–	–	–	0.64	5.05	3.40	–	–	–
SO_2	363159.3	$21_{418} - 21_{319}$	–	–	–	2.36	6.59	16.6	–	–	–
SO_2	363890.9	$24_{123} - 24_{024}$	<0.092	–	–	0.97	6.57	6.86	0.68[ag]	9.99	7.20
SO_2	363925.8	$23_{222} - 23_{123}$	<0.092	–	–	0.95	5.96	6.01	2.83	6.07	18.3
SO_2	364950.1	$25_{917} - 26_{818}$	<0.11	–	–	0.43	4.51	2.05	<0.13	–	–
$^{34}SO_2$	219355.7	$11_{111} - 10_{010}$	<0.12	–	–	0.68	3.19	2.30	<0.14	–	–
$^{34}SO_2$	241509.0	$16_{115} - 15_{214}$	<0.078	–	–	0.36	4.28	1.64	<0.077	–	–
$^{34}SO_2$	241985.5	$8_{35} - 8_{26}$	<0.070	–	–	0.34	6.36	2.31	<0.16	–	–
$^{34}SO_2$	243935.9	$18_{117} - 18_{018}$	<0.067	–	–	0.14	9.58	1.47	0.18[ah]	9.55	1.76
$^{34}SO_2$	244481.5	$14_{014} - 13_{113}$	<0.071	–	–	0.35	6.30	2.32	<0.079	–	–
$^{34}SO_2$	245178.7	$15_{214} - 15_{115}$	–	–	–	0.19	5.13	1.05	<0.058	–	–
$^{34}SO_2$	245302.3	$6_{33} - 6_{24}$	–	–	–	0.24	2.92	0.74	<0.058	–	–
$^{34}SO_2$	248364.8	$7_{35} - 7_{26}$	–	–	–	0.28	5.19	1.54	<0.058	–	–
$^{34}SO_2$	254278.1	$28_{424} - 28_{325}$	–	–	–	2.09[ab]	9.31	20.8	–	–	–
$^{34}SO_2$	257468.8	$29_{921} - 30_{822}$	<0.065	–	–	<0.068	–	–	0.17[ai]	6.09	1.11
$^{34}SO_2$	337872.7	$34_{529} - 34_{430}$	<0.12	–	–	<0.13	–	–	<0.14	–	–
$^{34}SO_2$	338320.4	$13_{212} - 12_{111}$	<0.076	–	–	0.43	5.71	2.62	<0.068	–	–
$^{34}SO_2$	338785.8	$14_{410} - 14_{311}$	<0.11	–	–	0.35	4.82	1.77	<0.11	–	–
$^{34}SO_2$	342208.9	$5_{33} - 4_{22}$	<0.14	–	–	0.40	4.48	1.92	<0.14	–	–

Table 7. continued

Species	ν (MHz)	J	$T_{\rm MB}$ (K)	ΔV (km/s)	W (K km/s)	$T_{\rm MB}$ (K)	ΔV (km/s)	W (K km/s)	$T_{\rm MB}$ (K)	ΔV (km/s)	W (K km/s)
$^{34}SO_2$	342231.7	$20_{119} - 19_{218}$	<0.14	–	–	0.23	6.04	1.52	<0.14	–	–
$^{34}SO_2$	342332.1	$12_{48} - 12_{39}$	<0.16	–	–	0.27	4.29	1.23	<0.10	–	–
$^{34}SO_2$	344245.4	$10_{46} - 10_{37}$	<0.21	–	–	0.44	5.40	2.52	<0.11	–	–
$^{34}SO_2$	344581.1	$19_{119} - 18_{018}$	<0.25	–	–	0.73	7.47	5.79	0.20	4.67	0.99
$^{34}SO_2$	344808.0	$13_{410} - 13_{311}$	<0.070	–	–	0.40	5.84	2.47	<0.11	–	–
$^{34}SO_2$	344987.6	$15_{412} - 15_{313}$	<0.079	–	–	0.47	5.47	2.74	<0.11	–	–
$^{34}SO_2$	344998.2	$11_{48} - 11_{39}$	<0.079	–	–	0.45	6.01	2.89	<0.11	–	–
$^{34}SO_2$	345168.8	$8_{44} - 8_{35}$	<0.10	–	–	0.35	5.42	2.04	0.26	7.00	1.90
$^{34}SO_2$	345285.7	$9_{46} - 9_{37}$	<0.16	–	–	0.33	4.81	1.67	0.28	4.63	1.37
$^{34}SO_2$	345519.8	$7_{44} - 7_{35}$	<0.12	–	–	0.45	4.95	2.38	0.15	5.25	0.83
$^{34}SO_2$	345553.2	$6_{42} - 6_{33}$	<0.12	–	–	0.18	3.55	0.68	<0.14	–	–
$^{34}SO_2$	345651.4	$5_{42} - 5_{33}$	<0.14	–	–	0.30	6.59	2.13	<0.14	–	–
$^{34}SO_2$	345678.9	$4_{40} - 4_{31}$	<0.14	–	–	0.37[aj]	8.65	3.42	<0.14	–	–
$^{34}SO_2$	345929.4	$17_{414} - 17_{315}$	<0.096	–	–	0.35	6.33	2.38	<0.12	–	–
$^{34}SO_2$	348117.6	$19_{416} - 19_{317}$	<0.090	–	–	0.79[ak]	6.14	5.19	0.17	7.81	1.40
$^{34}SO_2$	355920.2	$34_{1123} - 35_{1026}$	<0.066	–	–	0.52[al]	5.53	3.05	<0.070	–	–
$^{34}SO_2$	356222.4	$25_{323} - 25_{224}$	<0.099	–	–	0.24	5.28	1.33	<0.14	–	–
$^{34}SO_2$	357102.2	$20_{020} - 19_{119}$	<0.11	–	–	0.61	5.64	3.64	<0.11	–	–
$^{34}SO_2$	358347.3	$23_{420} - 23_{321}$	<0.068	–	–	0.25	6.03	1.62	<0.065	–	–
$^{34}SO_2$	358988.0	$15_{214} - 14_{113}$	<0.066	–	–	0.14	4.66	0.67	1.14[am]	5.23	6.32
$^{34}SO_2$	359651.8	$24_{222} - 23_{321}$	<0.099	–	–	0.30[an]	6.87	2.20	<0.14	–	–
$^{34}SO_2$	362158.2	$6_{33} - 5_{24}$	<0.11	–	–	0.31	6.77	2.25	0.23	5.38	1.31
$^{34}SO_2$	362834.2	$23_{222} - 23_{123}$	<0.10	–	–	0.16	6.09	1.04	<0.13	–	–
H_2CS	240266.3	$7_{07} - 6_{06}$	0.30	4.35	1.38	<0.080	–	–	0.92	5.65	5.62
H_2CS	240381.8	$7_{26} - 6_{25}$	<0.066	–	–	<0.060	–	–	0.33	8.10	2.86
H_2CS	240392/3	$7_{35/4} - 6_{34/3}$	<0.072	–	–	<0.060	–	–	0.69	6.14	4.52
H_2CS	240548.2	$7_{25} - 6_{24}$	<0.078	–	–	<0.068	–	–	0.33	6.59	2.35
H_2CS	244047.8	$7_{16} - 6_{15}$	0.53	5.13	2.88	0.27	2.93	0.84	2.06[i]	5.67	12.4
H_2CS	338080.8	$10_{110} - 9_{19}$	0.43	4.08	1.87	<0.081	–	–	1.45	5.92	9.15
H_2CS	342944.4	$10_{010} - 9_{09}$	<0.090	–	–	<0.10	–	–	0.97	3.89	4.03
H_2CS	342944.4	$10_{010} - 9_{09}$	0.27	4.07	1.16	<0.12	–	–	0.78	5.33	4.41
H_2CS	343308.5	$10_{47/6} - 9_{46/5}$	<0.040	–	–	<0.12	–	–	<0.10	–	–
H_2CS	343319.6	$10_{29} - 9_{28}$	<0.11	–	–	<0.12	–	–	0.41[ao]	6.36	2.75
H_2CS	343408.1	$10_{38} - 9_{37}$	<0.046	–	–	<0.11	–	–	0.83[ap]	8.82	7.82
H_2CS	343412.3	$10_{37} - 9_{36}$	<0.046	–	–	<0.11	–	–	0.83[ap]	8.82	7.82
H_2CS	343810.8	$10_{28} - 9_{27}$	–	–	–	–	–	–	0.40	2.13	0.91
H_2CS	348531.9	$10_{19} - 9_{18}$	<0.11	–	–	<0.11	–	–	1.80	4.45	8.55
H_2S	216710.4	$2_{20} - 2_{11}$	0.30	4.50	1.46	0.33	6.18	2.16	0.97	5.49	5.65
$H_2^{34}S$	214376.9	$2_{20} - 2_{11}$	–	–	–	<0.040	–	–	<0.044	–	–
OCS	231061.0	19–18	<0.057	–	–	0.18	1.52	0.29	0.97	7.22	7.45
OCS	243218.0	20–19	–	–	–	–	–	–	0.75[5]	5.50	4.40
OCS	340449.2	28–27	0.63[5]	1.86	1.25	0.21	5.45	0.92	1.29[5]	6.74	9.29
OCS	352599.6	29–28	<0.15	–	–	<0.11	–	–	0.51	4.00	2.17
OCS	364749.0	30–29	<0.11	–	–	<0.13	–	–	0.86[aq]	8.40	7.69
$OC^{34}S$	237237.6	20–19	–	–	–	<0.048	–	–	<0.071	–	–
$OC^{34}S$	260991.8	22–21	<0.049	–	–	<0.052	–	–	<0.059	–	–
$OC^{34}S$	343983.3	29–28	<0.093	–	–	<0.12	–	–	<0.13	–	–
$OC^{34}S$	355836.0	30–29	<0.075	–	–	<0.078	–	–	<0.087	–	–
SiO	260518.0	6–5	0.17	4.86	0.84	0.76	5.11	4.14	1.85[ar]	6.40	12.6

Table 7. continued

Species	ν (MHz)	J	$T_{\rm MB}$ (K)	ΔV (km/s)	W (K km/s)	$T_{\rm MB}$ (K)	ΔV (km/s)	W (K km/s)	$T_{\rm MB}$ (K)	ΔV (km/s)	W (K km/s)
SiO	347330.6	8–7	0.21	4.01	0.89	1.07	11.4	13.0	1.10	9.49	11.1
^{29}SiO	257254.2	6–5	<0.064	–	–	<0.16	–	–	0.23	9.78	2.38
^{29}SiO	342979.1	8–7	<0.088	–	–	<0.12	–	–	0.26	4.94	1.34
^{30}SiO	338929.0	8–7	–	–	–	0.15	6.92	1.11	–	–	–
HCO^+	356734.3	4–3	20.7	4.06	89.6	25.0[1]	6.28	167	–[1]	–	107
$H^{13}CO^+$	260255.5	3–2	2.16	3.25	7.50	2.02	3.94	8.50	2.34	4.66	11.6
$H^{13}CO^+$	346998.5	4–3	2.58	2.94	8.07	2.48	3.44	9.09	1.97	4.23	8.86
$HC^{18}O^+$	340633.0	4–3	0.29	4.12	1.26	<0.12	–	–	0.27	5.19	1.49
HCS^+	256027.8	6–5	–	–	–	0.16	1.49	0.26	–	–	–
HCS^+	341350.8	8–7	<0.26	–	–	0.38	0.71	0.29	0.94[as]	5.44	5.42
$HOCO^+$	342055.6	$16_{016} - 15_{015}$	–	–	–	<0.030	–	–	–	–	–
$HCNH^+$	222329.	3–2	–	–	–	<0.047	–	–	–	–	–
SO^+	347740.0	$\frac{15}{2} - \frac{13}{2}$	–	–	–	0.51	5.31	2.90	<0.060	–	–
H_3O^+	364797.4	$3_2^+ - 2_2^-$	<0.13	–	–	0.53	4.25	2.41	0.41	1.79	0.80
DCN	362046.4	5–4	<0.085	–	–	<0.082	–	–	1.14[am]	5.23	6.32
DNC	228910.4	3–2	<0.064	–	–	<0.060	–	–	0.15	3.41	0.53
DCO^+	360169.9	5–4	–	–	–	0.22	2.67	0.64	0.51[7]	4.46	2.40
HDS	244555.6	$1_{01} - 0_{00}$	<0.072	–	–	<0.072	–	–	<0.060	–	–
HDS	257781.4	$2_{11} - 2_{02}$	<0.049	–	–	<0.057	–	–	<0.063	–	–
NND^+	231321.7	3–2	<0.054	–	–	<0.050	–	–	<0.050	–	–
HDCO	259034.9	$4_{22} - 3_{21}$	<0.057	–	–	<0.057	–	–	<0.057	–	–
CH_3OD	346065.3	$8_3 - 9_2\ A^-$	<0.063	–	–	<0.063	–	–	<0.063	–	–
	357066.2	$8_1 - 7_1\ A^+$	<0.060	–	–	<0.060	–	–	<0.060	–	–
CS v_1	340398.1	7–6	<0.11	–	–	<0.083	–	–	0.68	3.40	2.45
HCN v_2	354460.5	$4_1 - 3_1$	<0.14	–	–	<0.15	–	–	0.34	3.14	1.13
HCN v_2	356255.6	$4_1 - 3_1$	<0.11	–	–	0.30[an]	6.87	2.20	0.22	7.42	1.73
$SO_2 v_2$	346591.8	$18_{414} - 18_{315}$	<0.092	–	–	0.28	5.77	1.73	<0.12	–	–

All upper limits are 2 times the rms noise in one resolution element (generally two channels).
The sums of the integrated intensities of the lines listed in Tables 7–12 except for CO and its isotopomers are 160, 330 and 850 K km s^{-1} for W 3 IRS4, W 3 IRS5 and W 3(H_2O) respectively in the 230 GHz window and 410, 920 and 1760 K km s^{-1} in the 345 GHz window. The sums of the integrated intensities of CO and its isotopomers in Table 7 are 380, 720 and 180 K km s^{-1} for W 3 IRS4, W 3 IRS5 and W 3(H_2O) respectively in the 230 GHz region and 550, 940 and 360 K km s^{-1} in the 345 GHz window.

[1] Gaussian decomposition not unique because of selfreversed profile and strong wings, only integral under line given.
[2] Distorted profile, cause unknown.
[3] Gaussian decomposition not unique because of strong wings, only peak temperature given.
[4] The ΔV is kept fixed in the Gaussian fit.
[5] On edge of spectrum.
[6] Bad base line.
[7] Line offset by 3 MHz, incorrect identification?

[a] Blended with CH_3OCH_3 339491.
[b] Blended with $C^{34}S$ 7–6.
[c] $H^{13}CN$ 4 – 3 always blended with SO_2 345338.
[d] $HC^{15}N$ 3 – 2 blended with CH_3OCH_3 260754/56/58/61.
[e] HNC 4 – 3 blended with SO_2 359770.

[f] $HN^{13}C$ $3-2$ blended with SO_2 258666.
[g] Blended with CH_3OCH_3 358447-358456.
[h] In wing SO_2 351257.
[i] H_2CS 244047 blended with HNCO 240875/6.
[j] CH_3CCH 358818 blended with CH_3CCH 358811.
[k] Uncertain, could also be a base-line ripple
[l] H_2CO $5_{42}-4_{41}$ and $5_{41}-4_{40}$ are always blended.
[m] H_2CO 364289 blended with CH_3OH 360849.
[n] Blended with H_2CS and CN.
[o] $H_2^{13}CO$ 354898 blended with SO_2 358013.
[p] $H_2^{13}CO$ 355041 blended with SO_2 355045.
[q] CH_3CN 257507/22/27 blended with CH_3OCHO 260384/392/404/415.
[r] CH_3CN 257522 blended with CH_3OCH_3 260400/1/3/5
[s] Blended with CCH 349337/8.
[t] CH_3CN 349446 blended with CH_3CN 349453.
[u] Blended with CH_3OH 243915.
[v] SO 346528 always blended with SO_2 346523.
[w] ^{34}SO 337582 blended with CH_3OH 337581.
[x] Large frequency error in line catalogues.
[y] Four hyperfine components of ^{33}SO blended with CH_3OH 337198.
[z] Blended with CH_3OH 7_K-6_K band.
[aa] SO 219949 Slightly blended with SO_2 222689.
[ab] SO_2 254280 blended with SO_2 254283 and $^{34}SO_2$ 254278.
[ac] SO_2 258667 blended with CH_3OCH_3 261245/46/48/50.
[ad] CH_3OH 338615 blended with SO_2 338611 and SO_2 335773.
[ae] CH_3OH 338615 blended with SO_2 338611.
[af] SO_2 346652 blended with CH_3OH 349845.
[ag] SO_2 363925 blended with CH_3OH 361236.
[ah] $^{34}SO_2$ 243935 blended with CH_3OCH_3 240978/82/85/89.
[ai] $^{34}SO_2$ 260327 blended with CH_3OCH_3 26027/29/31.
[aj] $^{34}SO_2$ 342231 blended with $^{34}SO_2$ 345678.
[ak] $^{34}SO_2$ 348117 blended with $^{34}SO_2$ 345519.
[al] $^{34}SO_2$ 358988 blended with $^{34}SO_2$ 355920.
[am] $^{34}SO_2$ 358988 blended with DCN 5–4 362046.
[an] HCN v_2 356255.6 blended with $^{34}SO_2$ 359651.
[ao] Blended with $H_2^{13}CO$ 343325.
[ap] H_2CS 343408 blended with H_2CS 343412.
[aq] OCS 30-29 blended with CH_3OH 364746 and CH_3OH 364757.
[ar] Blended with CH_3CN 14_5–13_5 and CH_3OH 257402.
[as] HCS^+ 8–7 blended with CH_3OCHO 344539.

Table 8. CH_3OH Gaussian fit parameters W 3 IRS4

ν (MHz)	$N\,J$	$T_{\rm MB}$ (K)	ΔV (km s^{-1})	W (K km s^{-1})
218440.0	$4_2\,E-3_1\,E$	0.64	3.30	2.24
239746.3	$5_1A^+-4_1A^+$	0.29	5.33	1.67
241700.2	5_0E-4_0E	0.47	4.53	2.28
241767.2	$5_{-1}E-4_{-1}E$	0.79	4.96	4.18
241791.4	$5_0A^+-4_0A^+$	0.74	5.71	4.52
241806.5	$5_4A^\pm-4_4A^\pm$	0.48[1]	4.32	1.14
241832.7	$5_3A^\pm-4_3A^\pm$	0.25	3.75	0.98
241879.0	5_1E-4_1E	0.25	4.10	1.11
241904.2	$5_{\pm2}E-4_{\pm2}E$	0.42	5.52	2.46
338124.5	7_0E-6_0E	0.27	3.95	1.12
338344.6	$7_{-1}E-6_{-1}E$	0.54	5.19	3.00
338408.7	$7_0A^+-6_0A^+$	0.59	5.08	3.17
338543.2	$7_3A^--6_3A^-$	0.24	2.91	0.75
338540.8	$7_3A^+-6_3A^+$	0.24	2.91	0.75
335582.0	$7_1A^+-6_1A^+$	0.32	5.62	1.94
338615.0	7_1E-6_1E	0.32	7.42	2.57
338721.6	7_2E-6_2E	0.23	4.17	1.08
338722.9	$7_{-2}E-6_{-2}E$	0.23	4.17	1.08
335582.0	$7_1A^+-6_1A^+$	0.39	4.43	1.86
355603.0	$13_0A^+-12_1A^+$	0.17[2]	6.46	1.19
358605.8	4_1E-3_0E	0.41	5.88	2.56
360848.9	11_0E-10_1E	0.42[a]	5.21	2.32

[1] On edge of spectrum
[2] Bad base line
[a] CH_3OH 360849 slightly blended with H_2CO 364289.

Table 9. CH_3OH Gaussian fit parameters W 3 IRS5

ν (MHz)	$N\,J$	$T_{\rm MB}$ (K)	ΔV (km s^{-1})	W (K km s^{-1})
218440.0	4_2E-3_1E	0.17	2.11	0.38
241700.2	5_0E-4_0E	0.21	2.99	0.68
241767.2	$5_{-1}E-4_{-1}E$	0.37	3.09	1.21
241791.4	$5_0A^+-4_0A^+$	0.34	3.48	1.26
241832.7	$5_3A^\pm-4_3A^\pm$	0.19	2.18	0.43
241904.2	$5_{\pm2}E-4_{\pm2}E$	0.29	2.61	0.80
243915.8	$5_1A^--4_1A^-$	0.29	2.09	0.64
337581.7	7_4E-6_4E	3.00[a]	5.93	18.9
338540.8	$7_3A^+-6_3A^+$	0.28[b]	5.71	1.74
338543.2	$7_3A^--6_3A^-$	0.28[b]	5.71	1.74
338615.0	7_1E-6_1E	2.30[c]	6.52	16.0
341415.6	$7_1A^--6_1A^-$	0.31	2.94	0.97
358605.8	4_1E-3_0E	0.24	3.80	0.97

[a] Blended with ^{34}SO 337582.
[b] Not a certain detection.
[c] CH_3OH 338615 blended with SO_2 338611.

Table 10. CH_3OH Gaussian fit parameters W 3(H_2O)

ν (MHz)	$N\,J$	$T_{\rm MB}$ (K)	ΔV (km s^{-1})	W (K km s^{-1})
		$\nu_t = 0$		
218440.0	$4_2E - 3_1E$	2.09	5.26	11.7
219981.1	$25_3E - 24_4E$	<0.034	–	–
219994.0	$23_5E - 22_6E$	<0.034	–	–
220078.6	$8_0E - 7_1E$	0.62	6.60	4.34
220401.8	$10_{-5}E - 11_{-4}E$	–[a]	–	–
227814.5	$16_1A^+ - 15_2A^+$	0.28[1]	11.9	3.54
231281.1	$10_2A^- - 9_3A^-$	0.44[1]	7.56	3.54
233795.8	$18_3A^- - 17_4A^-$	<0.31[2]	–	–
237129.4	$22_1E - 22_0E$	<0.081	–	–
239731.4	$16_7A^\pm - 17_6A^\pm$	<0.082	–	–
239746.3	$5_1A^+ - 4_1A^+$	2.36	5.13	12.9
240241.5	$5_3E - 6_2E$	0.28	8.28	2.43
241143.6	$22_{-6}E - 23_{-5}E$	<0.078	–	–
241590.9	$25_3A^- - 25_2A^+$	<0.087	–	–
241700.2	$5_0E - 4_0E$	3.10	5.59	18.5
241767.2	$5_{-1}E - 4_{-1}E$	7.09	4.09	31.0
241791.4	$5_0A^+ - 4_0A^+$	5.70[b]	4.69	28.4
241806.5	$5_4A^\pm - 4_4A^\pm$	1.03	3.76	4.13
241813.3	$5_{-4}E - 4_{-4}E$	0.90	5.53	5.27
241829.7	$5_4E - 4_4E$	1.54[c]	4.27	7.02
241832.7	$5_3A^\pm - 4_3A^\pm$	2.68	3.59	11.3
241843	$5_2A^- - 4_2A^- + 5_3E - 4_3E$	2.63	5.37	15.0
241852.3	$5_{-3}E - 4_{-3}E$	1.05	5.21	5.84
241879.0	$5_1E - 4_1E$	3.37	4.05	14.5
241887.7	$5_2A^+ - 4_2A^+$	1.76	4.47	8.40
241904.2	$5_{\pm2}E - 4_{\pm2}E$	4.75[d]	4.51	22.9
242446.2	$14_{-1}E - 13_{-2}E$	0.85	3.78	3.44
242491.6	$24_3A^- - 24_2A^+$	<0.062	–	–
243397.5	$18_6A^\pm - 19_5A^\pm$	<0.094	–	–
243413.5	$23_3A^- - 23_2A^+$	<0.094	–	–
243915.3	$5_1A^- - 4_1A^-$	2.32	6.02	14.8
244330.9	$22_3A^- - 22_2A^+$	0.33[e]	13.3	4.68
245223.3	$21_3A^- - 21_2A^+$	0.18	7.66	1.48
248282.5	$17_3A^- - 17_2A^+$	0.54	6.44	3.73
257402.2	$18_3A^+ - 18_2A^-$	1.86[f]	5.58	11.0
258780.4	$19_3A^+ - 19_2A^-$	0.28	7.58	2.24
260052.1	$20_{-8}E - 21_{-7}E$	<0.086	–	–
260381.6	$20_3A^+ - 20_2A^-$	0.35[g]	10.6	4.00
261061.4	$21_{-4}E - 20_{-5}E$	<0.063	–	–
261704.4	$12_6E - 13_5E$	<0.087	–	–
261805.7	$2_1E - 1_0E$	0.70	6.06	4.54
335133.5	$2_2A^- - 3_1A^-$	0.63	7.41	5.02
335582.0	$7_1A^+ - 6_1A^+$	3.21	6.41	11.6
336438.3	$14_7A^\pm - 15_6A^\pm$	<0.11	–	–
336865.1	$12_1A^- - 12_0A^+$	1.56	6.01	9.98
337135.9	$3_3E - 4_2E$	0.32[h]	2.01	0.68
337941.9	$20_{-6}E - 21_{-5}E$	0.28	2.19	0.66
338124.5	$7_0E - 6_0E$	2.26	6.51	15.6
338344.6	$7_{-1}E - 6_{-1}E$	3.02	6.22	19.6
338404.6	$7_6E - 6_6E$	0.36	7.83	3.04
338408.7	$7_0A^+ - 6_0A^+$	2.91	5.53	17.2
338430.9	$7_{-6}E - 6_{-6}E$	0.26	2.90	0.81

Table 10. continued

ν (MHz)	$N\,J$	$T_{\rm MB}$ (K)	ΔV (km s^{-1})	W (K km s^{-1})
338442.3	$7_6A^\pm - 6_6A^\pm$	0.47	6.61	3.36
338456.5	$7_{-5}E - 6_{-5}E$	0.34	3.68	1.35
338475.3	$7_5E - 6_5E$	0.67	4.17	2.98
338486.3	$7_5A^\pm - 6_5A^\pm$	0.84	9.48	8.45
338504.1	$7_{-4}E - 6_{-4}E$	0.96	4.08	4.19
338512.6	$7_4A^\pm - 6_4A^\pm + 7_2A^- - 6_2A^-$	2.04	8.06	17.5
338530.8	$7_4E - 6_4E$	0.90	6.76	6.49
338540.8	$7_3A^+ - 6_3A^+$	0.57	8.15	4.83
338543.2	$7_3A^- - 6_3A^-$	1.04	7.98	8.81
338559.9	$7_{-3}E - 6_{-3}E$	0.65	6.87	4.77
338583.2	$7_3E - 6_3E$	0.76	7.90	6.38
338615.0	$7_1E - 6_1E$	1.79[i]	7.67	14.6
338640.0	$7_2A^+ - 6_2A^+$	1.35	6.90	9.91
338722	$7_{\pm2}E - 6_{\pm2}E$	2.55	6.55	17.7
340141.2	$2_2A^+ - 3_1A^+$	1.13[j]	5.35	6.42
340394.2	$16_6A^\pm - 17_5A^\pm$	0.68	4.09	2.98
341415.6	$7_1A^- - 6_1A^-$	2.17	7.30	16.9
342729.8	$13_1A^- - 13_0A^+$	2.15	5.40	12.4
344110.4	$18_2E - 17_3E$	0.24	1.82	0.46
344444.7	$19_1A^+ - 18_2A^+$	0.23	9.50	2.33
345904.2	$16_1A^- - 15_2A^-$	0.34	8.60	3.11
345919.2	$18_{-3}E - 17_{-4}E$	<0.10	–	–
346203	$5_4A^\pm - 6_3A^\pm$	0.79	7.66	6.40
349107.0	$14_1A^- - 14_0A^+$	1.51	9.19	14.8
350687.7	$4_0E - 3_{-1}E$	1.29	2.28	9.96
350905.1	$1_1A^+ - 0_0A^+$	1.31	6.80	9.51
351236.7	$9_5E - 10_4E$	1.18	3.08	3.87
355603.0	$13_0A^+ - 12_1A^+$	1.84	6.86	13.5
356006.6	$15_1A^- - 15_0A^+$	1.11	8.53	10.1
356627.3	$23_{-4}E - 22_{-5}E$	<0.11	–	–
356864.0	$18_{-8}E - 19_{-7}E$	<0.12	–	–
358414.9	$10_6E - 11_5E$	0.49	3.92	2.03
358605.8	$4_1E - 3_0E$	4.26	5.44	24.7
360848.9	$11_0E - 10_1E$	4.55[k]	6.42	31.2
361852.3	$8_1E - 7_2E$	1.48	4.58	7.22
		$\nu_t = 1$		
240960.6	$5_1A^+ - 4_1A^+$	0.24	3.62	0.92
241267.9	$5_0A^+ - 4_0A^+$	0.22	6.78	1.57
241441.2	$5_1A^- - 4_1A^-$	0.30	6.09	1.92
244338.0	$9_1E - 8_0E$	0.33[e]	13.3	4.68
334426.6	$3_0E - 2_1E$	0.54[l]	2.91	1.68
337297.4	$7_1A^+ - 6_1A^+$	0.55[m]	4.24	2.57
337490.5	$7_{-6}E - 6_{-6}E$	0.33	3.96	1.39
337519.1	$7_3E - 6_3E$	0.46	2.71	1.33
337546.1	$7_5A^\pm - 6_5A^\pm$	0.52	6.97	3.83
337581.7	$7_4E - 6_4E$	0.57	6.10	3.67
337605.3	$7_{-2}E - 6_{-2}E$	0.98	2.89	3.00
337610.6	$7_6E - 6_6E + 7_{-3}E - 6_{-3}E$	1.59	2.97	5.02
337625.7	$7_2A^+ - 6_2A^+$	0.37	5.62	2.20
337635.7	$7_2A^- - 6_2A^-$	0.32	1.74	0.60
337643	$7_1E - 6_1E + 7_0E - 6_0E$	1.16	7.27	8.95

Table 10. continued

ν (MHz)	$N\,J$	$T_{\rm MB}$ (K)	ΔV (km s^{-1})	W (K km s^{-1})
337647	$7_{-4}E - 6_{-4}E$ + $7_{-5}E - 6_{-5}E$	0.52	5.27	2.87
337655.2	$7_3A^{\pm} - 6_3A^{\pm}$	0.60	11.4	7.25
337671.2	$7_2E - 6_2E$	0.37	15.3	6.03
337685.3	$7_5E - 6_5E$ + $7_4A^{\pm} - 6_4A^{\pm}$	0.39	8.09	3.39
337707.6	$7_{-1}E - 6_{-1}E$	0.56[n]	9.31	5.57
337748.8	$7_0A^+ - 6_0A^+$	0.45	8.45	4.00
337969.4	$7_1A^- - 6_1A^-$	0.36	4.03	1.52
349845.4	$12_7E - 11_6E$	1.37[o]	7.74	11.3
359676.9	$14_3E - 14_2E$	4.80[p]	6.06	18.2
361236.5	$3_1A^- - 4_2A^-$	0.68[q]	9.99	7.20
364508.1	$8_3E - 8_2E$	0.41[r]	5.98	2.59
364746.2	$7_3E - 7_2E$	0.86[s]	8.40	7.69
364757.4	$12_6A^{\pm} - 13_5A^{\pm}$	0.86[s]	8.40	7.69
	$\nu_t = 2$			
240916.2	$5_3A^{\pm} - 4_3A^{\pm}$	0.14	1.59	0.24
240958.8	$5_{-1}E - 4_{-1}E$	0.24	3.62	0.92
334620.7	$22_3E - 22_2E$	0.37	2.62	1.05
337135.9	$3_3E - 4_2E$	0.71	3.96	2.98
337198.5	$7_{-5}E - 6_{-5}E$	0.33[t]	8.65	3.05
337252.2	$7_3A^{\pm} - 6_3A^{\pm}$	1.05[u]	4.45	4.98
337284.3	$7_0A^+ - 6_0A^+$	0.30	2.10	0.67
337295.8	$7_3E - 6_3E$	0.55[m]	4.24	2.57
337302.6	$7_2E - 6_2E$	0.38	2.42	0.97
337312.3	$7_{-1}E - 6_{-1}E$	0.54[l]	2.91	1.68
347443.1	$19_3E - 19_2E$	0.36	8.46	3.24

All upper limits are 2 times the rms noise in one resolution element (generally two channels).

[1] Strange profile.
[2] On edge of spectrum.
[a] Blended with ^{13}CO 2 − 1.
[b] CH_3OH 241791 blended with CH_3OH 244330.
[c] CH_3OH 241829 blended with CH_3CN 239096.
[d] CH_3OH 241904 blended with CH_3CN 239022 and CH_3OCH_3 239020/1.
[e] CH_3OH 241590 blended with CH_3OH 244338 and CH_3OH 244330.
[f] CH_3OH 257402 blended with CH3CN 257403 and SiO 6−5.
[g] CH_3OH 260381 blended with CH_3OCHO 260384.
[h] CH_3OH 337135 blended with CN 340261.
[i] CH_3OH 338615 blended with SO_2 338611.
[j] CH_3OH 340141 blended with CH_3OCHO 343435/43.
[k] CH_3OH 360849 blended with H_2CO 364289.
[l] CH_3OH 334426 blended with CH_3OH 337312.
[m] CH_3OH 337295 blended with CH_3OH 337297.
[n] CH_3OH 337707 blended with CH_3OCH_3 337708/12.
[o] CH_3OH 349845 blended with SO_2 346652.
[p] CH_3OH 359676 blended with H_2CO 362735.
[q] CH_3OH 361237 blended with SO_2 363890.
[r] CH_3OH 361852 and CH_3OH 364508 blended with CH_3OCH_3 361863 and CH_3OCH_3 361871/4/7.
[s] CH_3OH 364757 blended with CH_3OH 364746 and OCS 30−29.
[t] CH_3OH 337198 blended with ^{33}SO 337198.
[u] CH_3OH 337252 blended with CH_3OH 340141.

Table 11. CH_3OCH_3 Gaussian fit parameters W 3(H_2O)

ν (MHz)	J_{k_o,k_p}	$T_{\rm MB}$ (K)	ΔV (km s^{-1})	W (K km s^{-1})
225598/9	$40_{0,40} - 40_{1,39}$	0.71	5.74	4.35
237046/48/51	$7_{2,5} - 6_{1,6}$	–	–	3.66
237260/3/5	$25_{3,22/23} - 25_{2,24}$	–	–	0.10
239020/1	$24_{5,19} - 24_{4,20}$	4.75[a]	4.51	22.9
240978/ 82/85/89	$5_{3,3} - 4_{2,2}$	0.17	9.06	1.30
241523/28/30	$5_{3,2} - 4_{2,3}$	0.30	7.32	2.36
241523/28/30	$5_{3,2} - 4_{2,3}$	0.60[b]	8.97	5.69
241635/7/8	$21_{3,18} - 20_{4,17}$	0.54[c]	1.19	0.68
241635/7/8	$21_{3,18} - 20_{4,17}$	–[2]	–	–
241946	$13_{1,13} - 12_{0,12}$	0.64	3.45	2.33
244503/08/12	$23_{2,22} - 23_{1,23}$	0.89[d]	6.98	6.65
258548/9	$14_{1,14} - 13_{0,13}$	0.56	7.71	4.60
259982/4/6	$20_{5,16} - 20_{4,17}$	0.20	1.47	0.32
260327/29/31	$19_{5,15} - 19_{4,16}$	0.17	6.20	0.57
260400/1/3/5	$16_{5,11} - 16_{4,12}$	–[e]	–	–
260725/27/30	$18_{5,14} - 18_{4,15}$	–	–	1.15
260754/ 56/58/61	$6_{3,3} - 5_{2,4}$	1.22[f]	7.38	9.57
261145/47/50	$17_{5,13} - 17_{4,14}$	0.28[g]	10.9	3.30
261245/ 46/48/50	$15_{5,10} - 15_{4,11}$	0.25[h]	7.39	2.02
261560/1/3/6	$16_{5,12} - 16_{4,13}$	0.23	6.91	1.73
337712.4	$7_{4,4} - 6_{3,3}$	<0.11	–	–
337722/3	$7_{4,4} - 6_{3,3}$	0.12	1.78	0.23
337730/1/2	$7_{4,4/3} - 6_{3,3}$	0.26	3.87	1.05
337770/ 78/79/87/90	$7_{4,4/3} - 6_{3,4}$	–	–	7.60
337778/9	$7_{4,4} - 6_{3,4}$	0.47	3.78	1.88
337787/90	$7_{4,3} - 6_{3,4}$	0.39	3.66	1.53
339491	$19_{1,18} - 18_{2,17}$	0.33[i]	6.89	2.45
340609/12/15	$10_{3,7} - 9_{2,8}$	0.45	6.37	3.08
342608.1	$19_{0,19} - 18_{1,18}$	0.51[j]	6.83	3.73
343753/4/5	$17_{2,16} - 16_{1,15}$	0.44	8.13	3.81
344357/58	$19_{1,19} - 18_{0,18}$	0.26	3.90	0.64
344512/5/8	$11_{3,9} - 10_{2,8}$	–	–	3.66
345129/32/36	$35_{4,31/32} - 35_{3,32/33}$	0.27	4.79	1.37
356567/ 75/76/82/86	$8_{4,5/4} - 7_{3,4/5}$	–	–	3.50
356705/ 12/16/23/24	$8_{4,5/4} - 7_{3,4/5}$	–[k]	–	–
359381/4/7	$12_{3,10} - 11_{2,9}$	0.45	8.19	3.88
361863	$20_{1,20} - 19_{0,19}$	0.41[l]	5.98	2.59
361871/4/7	$11_{3,8} - 10_{2,9}$	1.22[l]	8.63	11.2

[1] On edge of spectrum.
[2] Bad base line.

[a] CH_3OCH_3 239020/1 blended with CH_3OH 241904 and CH_3CN 239022.
[b] CH_3OCH_3 241523/28/30 blended with CH_3OCHO 244594.
[c] CH_3OCH_3 241635/7/8 may be AOS spike.
[d] CH_3OCH_3 244503/08/12 blended with SO_2 241615.

[e] CH_3OCH_3 260400/1/3/5 thoroughly blended with CH_3CN257522 and CH_3OCHO 260392/404.
[f] CH_3OCH_3 260754/56/58/61 blended with $HC^{15}N$ 3 − 2.
[g] CH_3OCH_3 261145/47/48/50 blended with CH_3OCHO 261148.
[h] CH_3OCH_3 261245/46/48/50 blended with SO_2 258666.
[i] CH_3OCH_3 339491 blended with CN 339493.
[j] CH_3OCH_3 342608 blended with $^{34}SO_2$ 345285.
[k] CH_3OCH_3 356705/12/16/23/24 on wing of HCO^+ 4 − 3.
[l] CH_3OCH_3 361863 and CH_3OCH_3 361871/4/7 blended with CH_3OH 361852 and CH_3OH 364508.

Table 12. CH_3OCHO Gaussian fit parameters W 3(H_2O)

ν (MHz)	J	T_{MB} (K)	ΔV (km s^{-1})	W (K km s^{-1})
222421	$18_K - 17_K$	<0.079	–	–
222438–42	$18_K - 17_K$	0.19	15.9	3.19
223119/24	$18_K - 17_K$	0.14	5.70	0.85
223135	$18_K - 17_K$	0.06	3.90	0.23
223162	$18_K - 17_K$	0.10	7.26	0.77
225855.4	$6_K - 5_K$	<0.058	–	–
225900.7	$6_K - 5_K$	0.14[a]	9.77	1.50
227559–63	$21_K - 20_K$	0.47	6.25	3.09
234112.3	$19_K - 18_K$	0.053	7.14	0.40
234124.9	$19_K - 18_K$	0.093	7.47	0.74
234134.6	$19_K - 18_K$	0.065	7.47	0.52
237309/15	$21_K - 20_K$	–	–	2.12
237344/50	$21_K - 20_K$	–	–	2.48
240021.0	$19_K - 18_K$	0.29[2]	4.15	1.26
240034.6	$19_K - 18_K$	0.15[2]	7.66	1.26
244580.3	$20_K - 19_K$	0.26	2.59	0.72
244594.0	$20_K - 19_K$	0.18	7.74	1.48
258081/9	$21_K - 20_K$	–	–	2.97
258274/77	$21_K - 20_K$	0.095	3.72	0.38
258296	$21_K - 20_K$	<0.045	–	–
258476/82/99	$21_K - 20_K$	–[b]	–	9.57
258490–523	$23_K - 22_K$	–[b]	–	9.57
260384/ 392/404/415	$21_K - 20_K$	–[c]	–	–
261148.9	$21_K - 20_K$	0.28[d]	10.9	3.30
261165.4	$21_K - 20_K$	0.25	9.83	2.59
261433/6	$21_K - 20_K$	–[b]	–	9.57
334851.0	$27_K - 26_K$	0.48[e]	8.77	4.48
334866/72	$27_K - 26_K$	0.48	4.46	2.26
334877.4	$27_K - 26_K$	0.42[f]	2.86	1.28
338338/55	$27_K - 26_K$	–[g]	–	–
338396/414	$27_K - 26_K$	–[h]	–	–
342342–75	$30_K - 39_K$	–	–	3.72
343148/52/53	$31_K - 30_K$	–	–	2.75
343435/43	$28_K - 27_K$	1.13[i]	5.35	6.42
343148/52/53	$31_K - 30_K$	0.35[j]	2.70	1.13
344322/36/47	$28_K - 27_K$	–[k]	–	–
344029	$32_K - 31_K$	0.16	2.13	0.35
344539.7	$28_K - 27_K$	0.94[l]	5.44	5.42
345068/69	$28_K - 27_K$	–[1]	–	–

Table 12. continued

ν (MHz)	J	T_{MB} (K)	ΔV (km s^{-1})	W (K km s^{-1})
345090.3	$28_K - 27_K$	–[m]	–	–
345461/66	$28_K - 27_K$	0.22	5.46	1.30
345461/66/85	$28_K - 27_K$	–[2]	–	–
345485	$28_K - 27_K$	0.19	2.05	0.41
348909/14	$28_K - 27_K$	0.45	4.05	1.93
353723/4/8	$32_K - 31_K$	–	–	6.26[2]
354608	$33_K - 32_K$	0.49	6.31	3.27
356549.0	$13_K - 12_K$	0.21	4.64	1.05
358364.3	$28_K - 27_K$	0.17	3.88	0.71
358392.3	$28_K - 27_K$	0.14	4.69	0.68
358565/76	$29_K - 28_K$	–	–	2.35
358591.6	$29_K - 28_K$	–[n]	–	–

[1] On edge of spectrum.
[2] Bad base line.

[a] CH_3OCHO 225900 in wing HDO 225896.
[b] CH_3OCHO 258476/82/99 blended with CH_3OCHO 261433/6 and CH_3OCHO 258490/496/502/508/518/523.
[c] CH_3OCHO 260384/392/404/415 thoroughly blended with CH_3CN 257507/22/27 and CH_3OCH_3 260400/1/3/5.
[d] CH_3OCHO 261148 blended with CH_3OCH_3 261145/47/48/50.
[e] CH_3OCHO 334851 blended with CH_3OH 337546.
[f] CH_3OCHO 334877 blended with CH_3OH 337519.
[g] CH_3OCHO 338338 and CH_3OCHO 338355 in wings CH_3OH 338344.
[h] CH_3OCHO 338396 and CH_3OCHO 338414 in wings CH_3OH 338404/408.
[i] CH_3OCHO 343435/43 blended with CH_3OH 340141.
[j] On wing OCS 28–27.
[k] CH_3OCHO 344322/36/47 blended with SO 344310 and $H^{13}CO^+$ 4 – 3.
[l] CH_3OCHO 344539 blended with HCS^+ 8 – 7.
[m] CH_3OCHO 345090 in wing H_2CS 348531.
[n] CH_3OCHO 358591 in wing CH_3OH 358605.

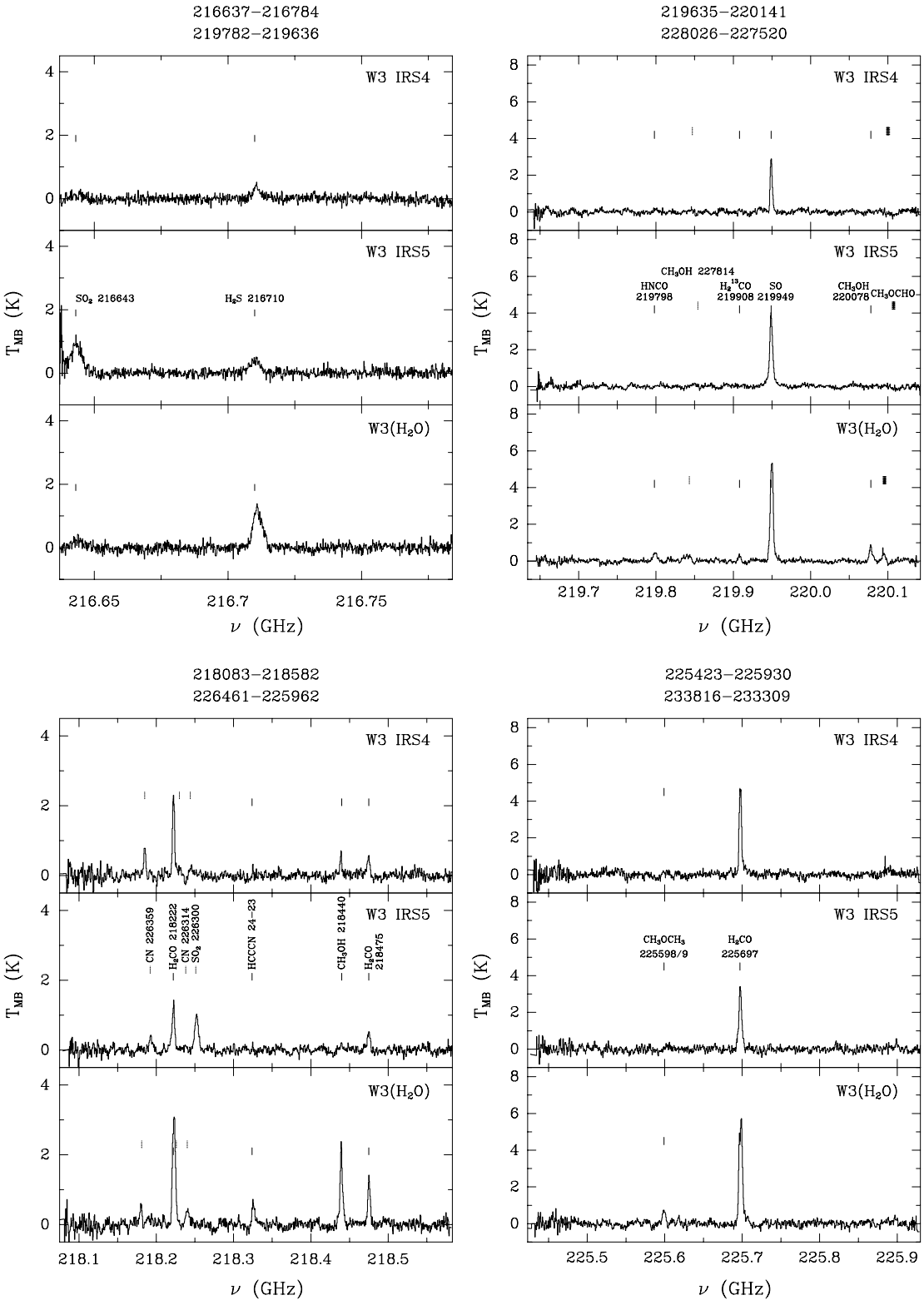

Fig. 4. Four panels containing double side band spectra for W 3 IRS4 (upper spectrum), W 3 IRS5 (middle spectrum) and W 3(H_2O) (lower spectrum). Identifications in the lower side band are given with solid tickmarks, in the upper side band with dotted tickmarks. The lower side band is chosen as the abscissa. Due to different $V_{\rm LSR}$ for the three sources the upper side bands do not line up. To ease the identification, the frequency ranges for the spectra are given at the top of each panel. The molecular identifications are only given in W 3 IRS5 but apply to all three spectra. The corresponding molecular parameters are found in Tables 7-12

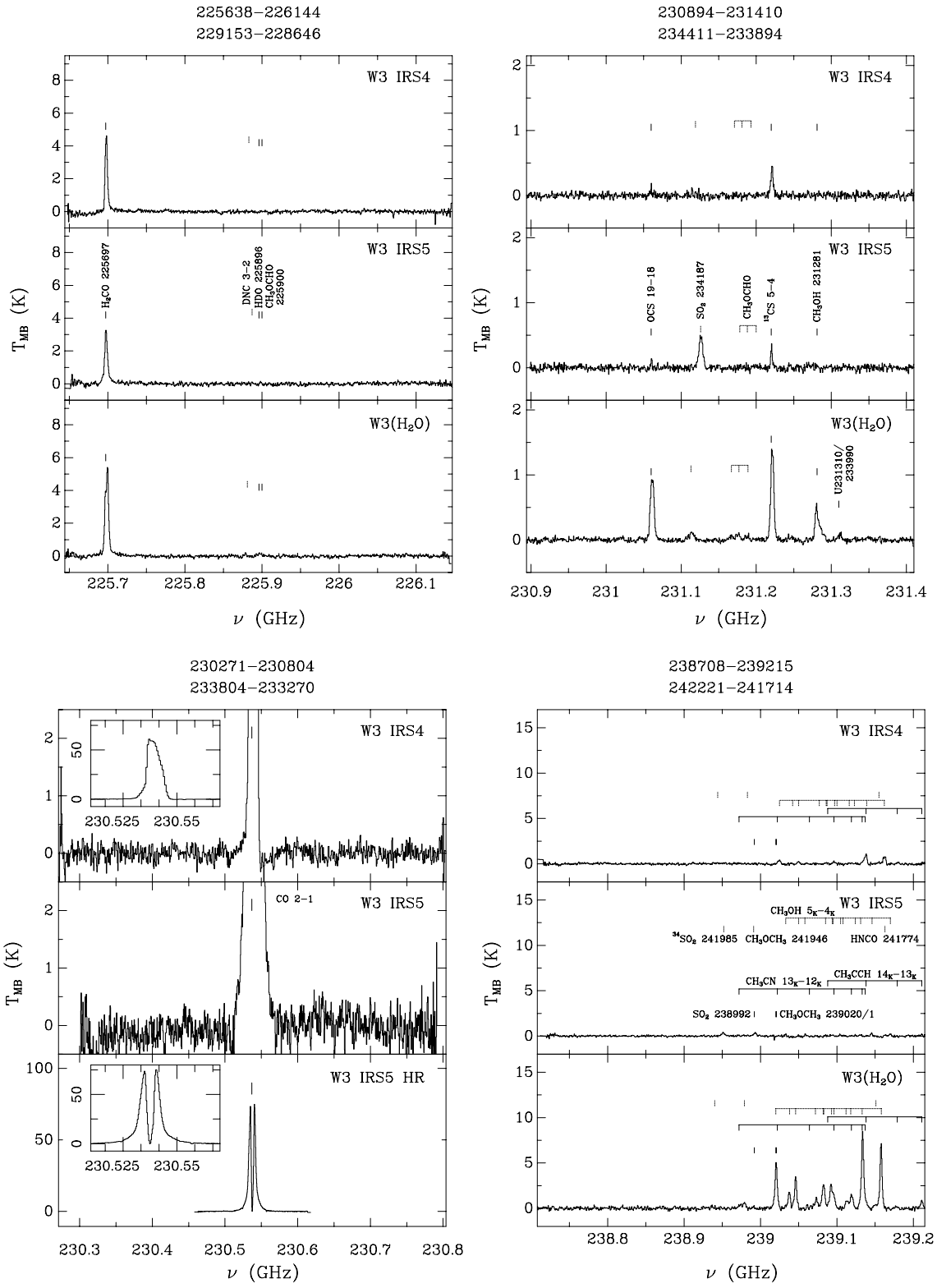

Fig. 4. continued

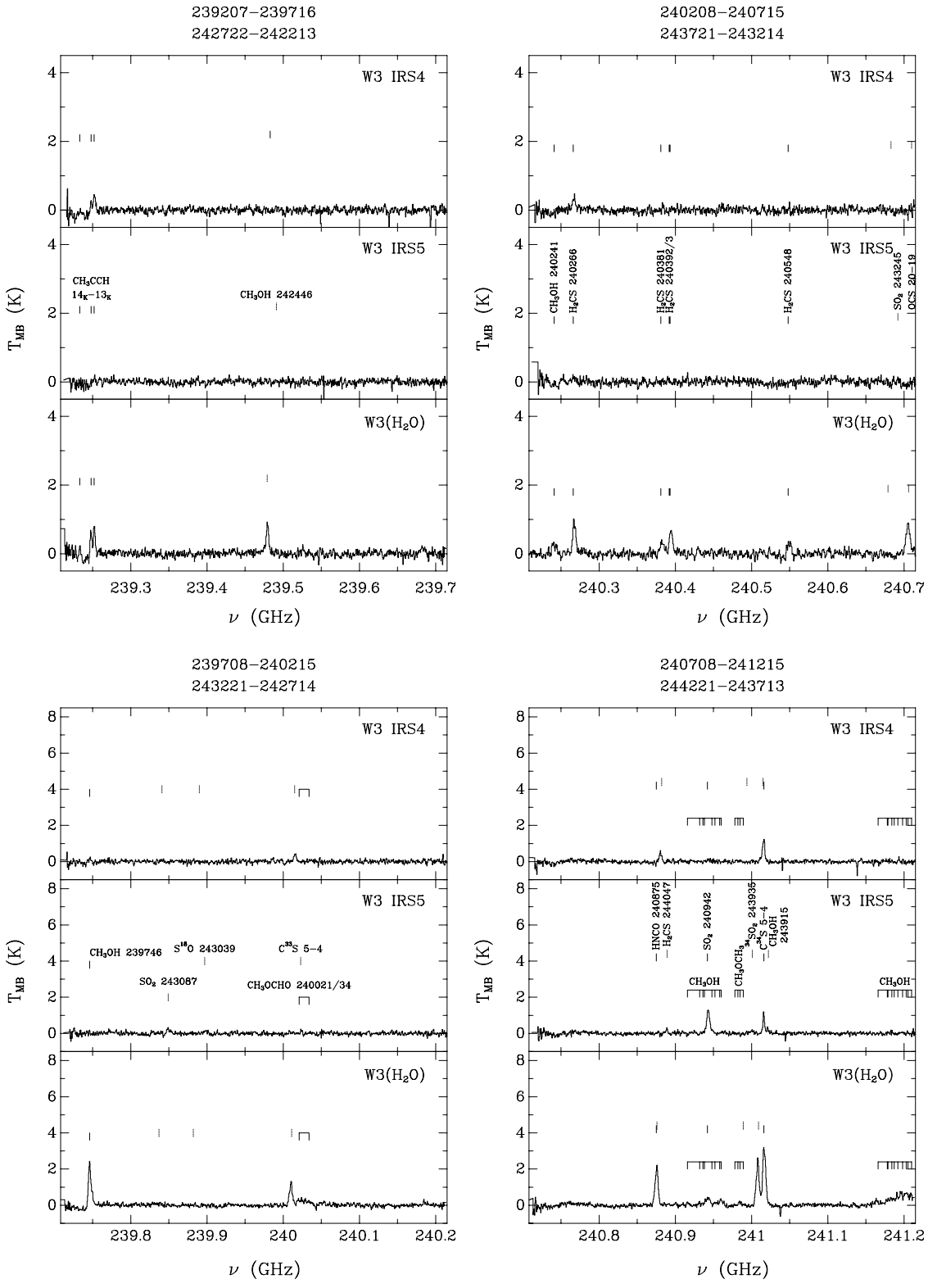

Fig. 4. continued

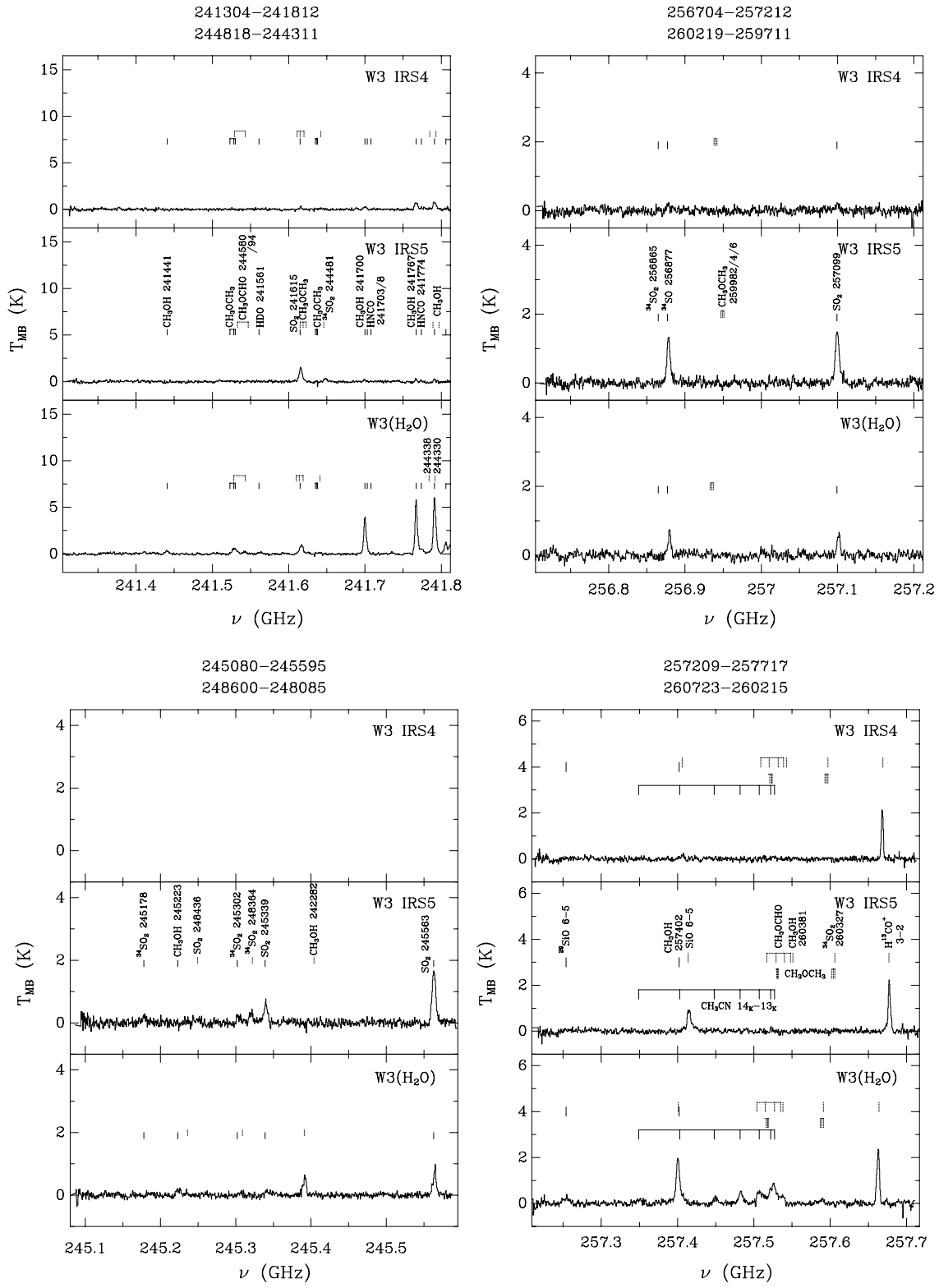

Fig. 4. continued

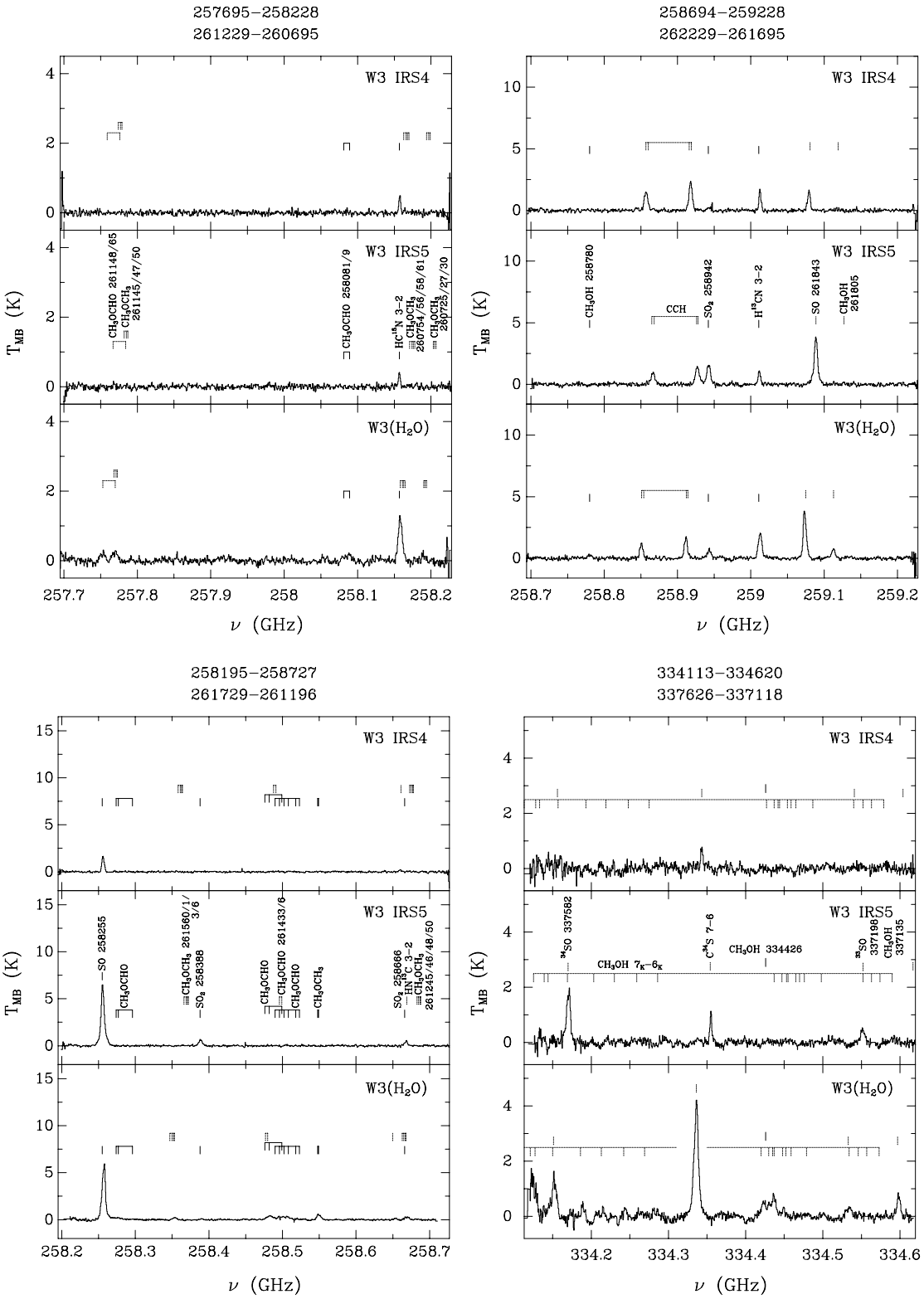

Fig. 4. continued

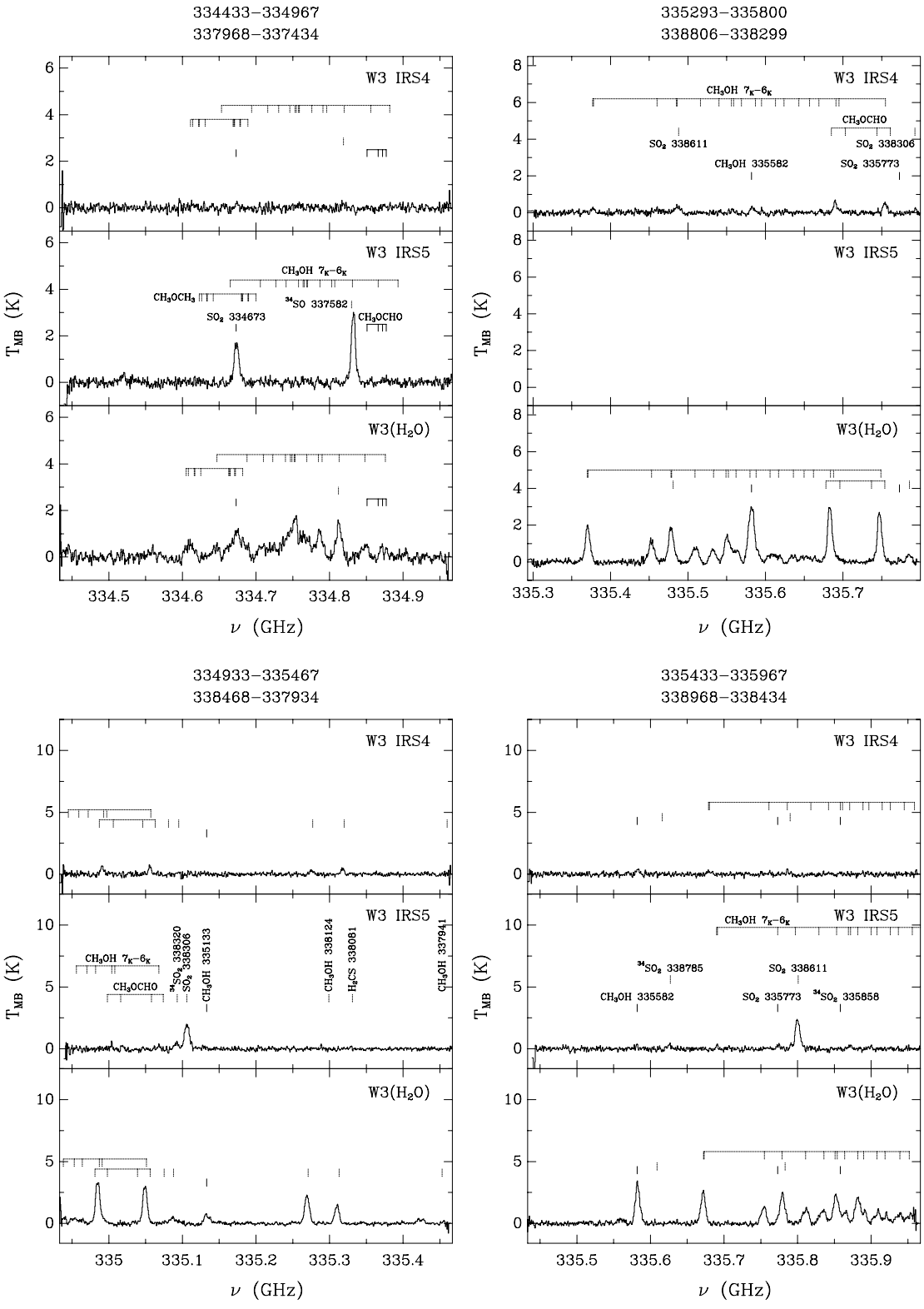

Fig. 4. continued

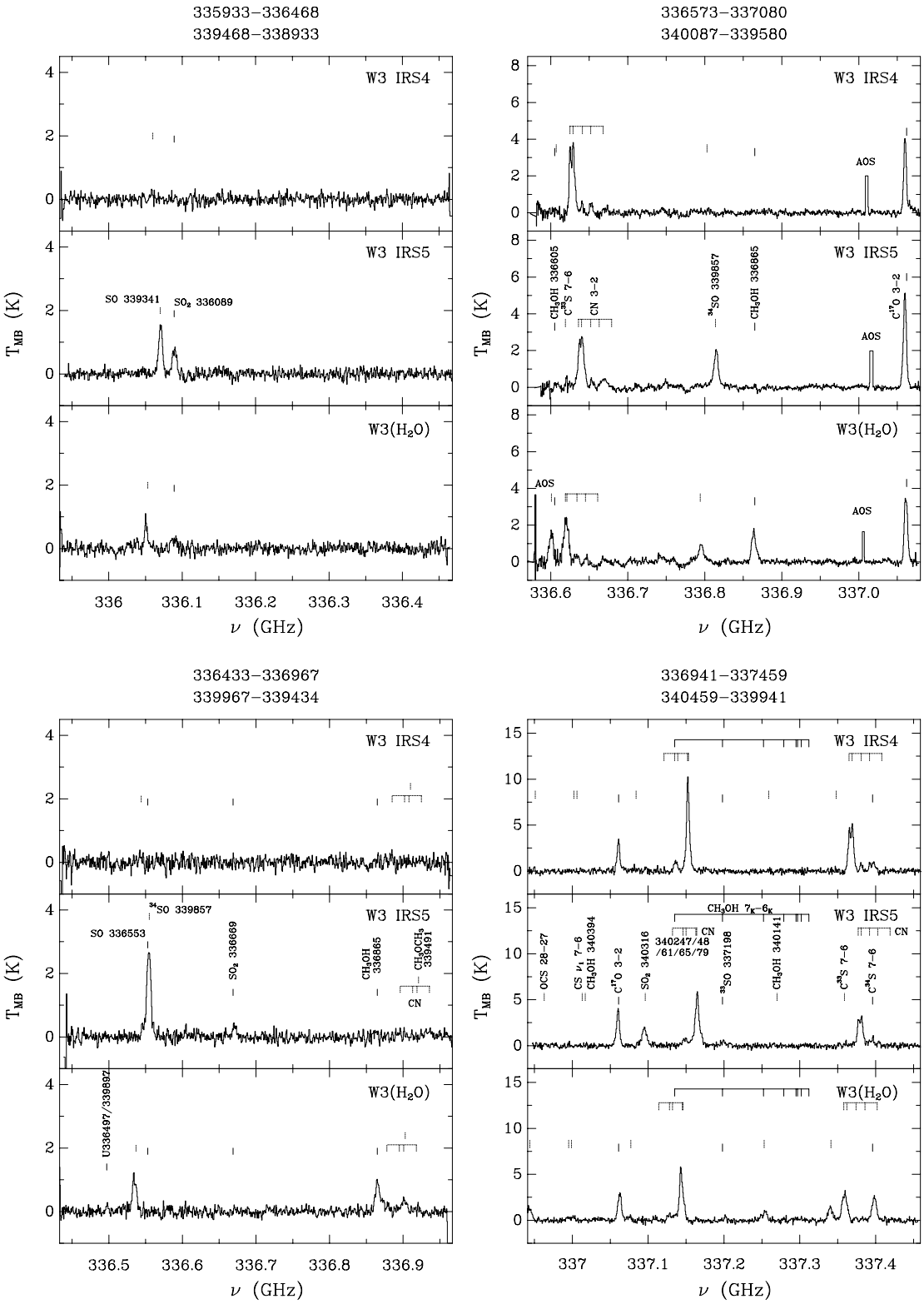

Fig. 4. continued

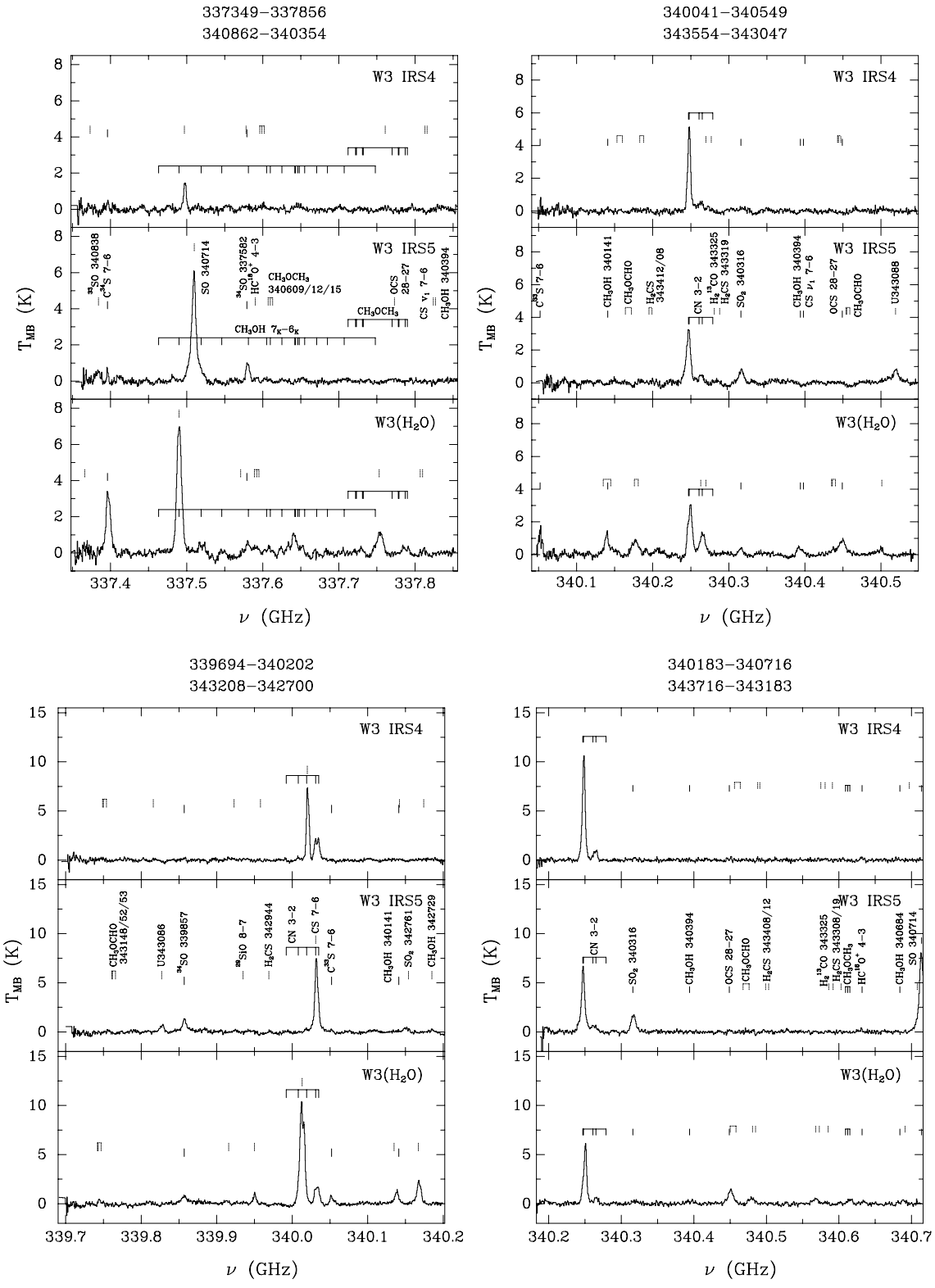

Fig. 4. continued

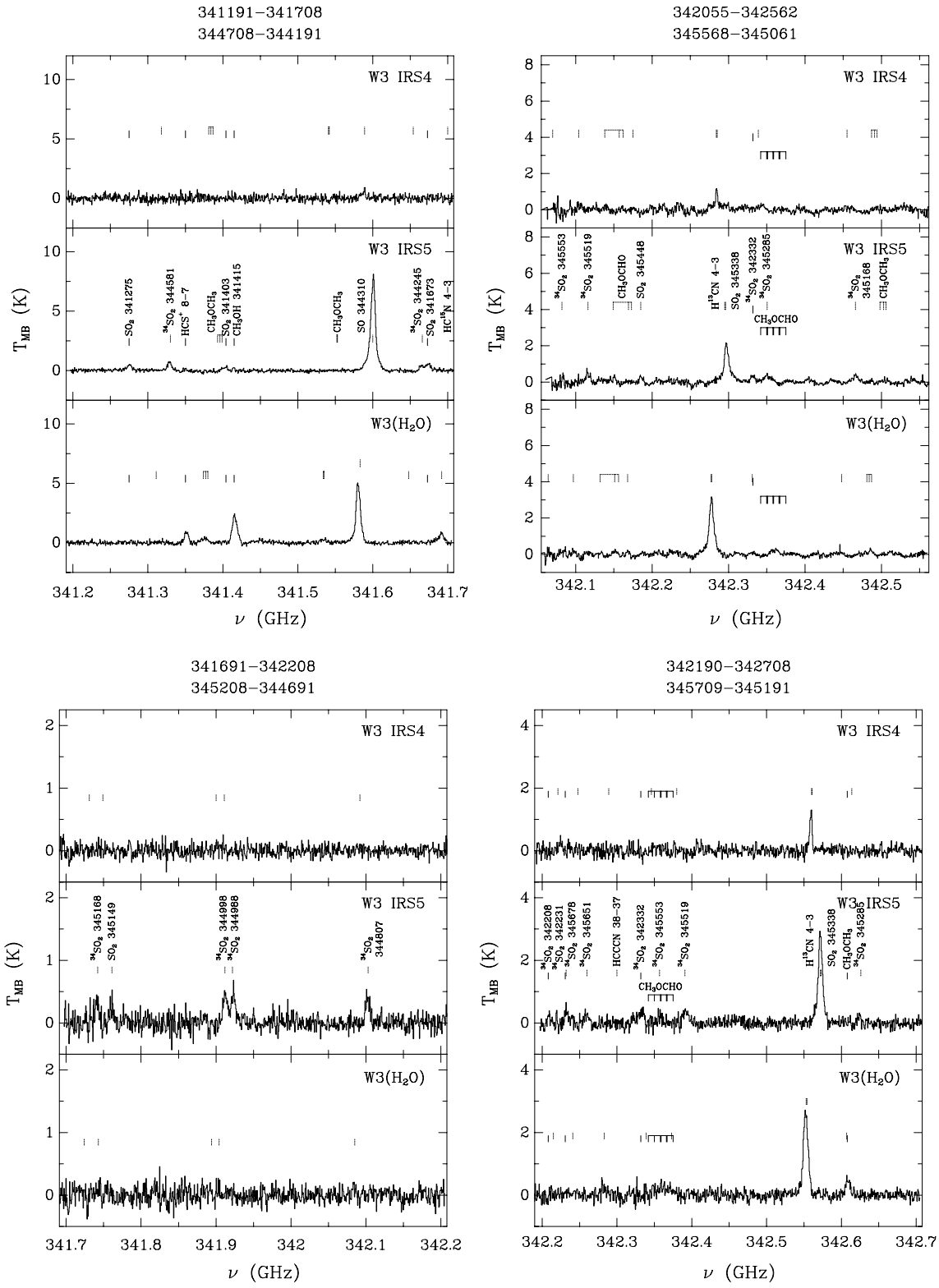

Fig. 4. continued

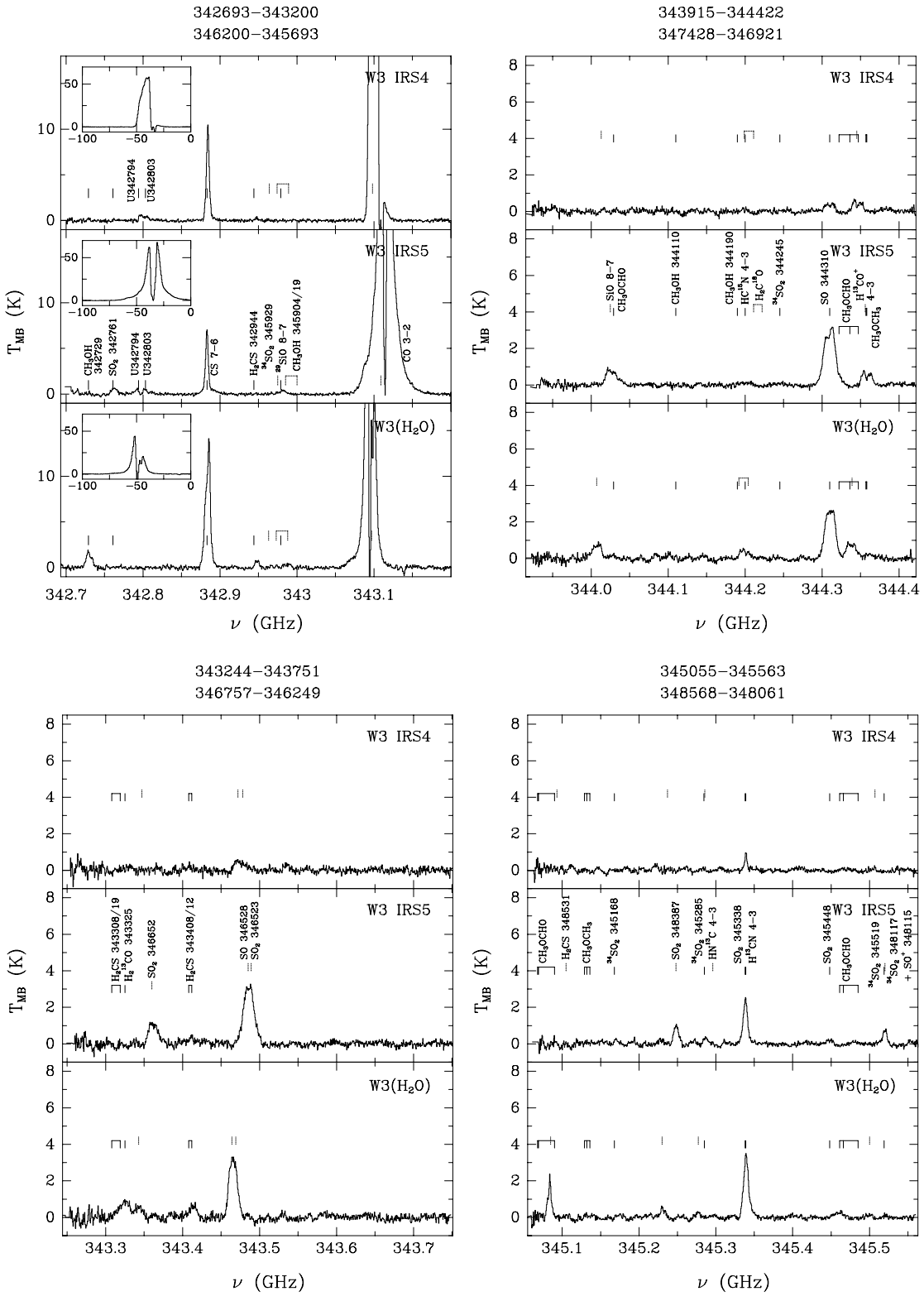

Fig. 4. continued

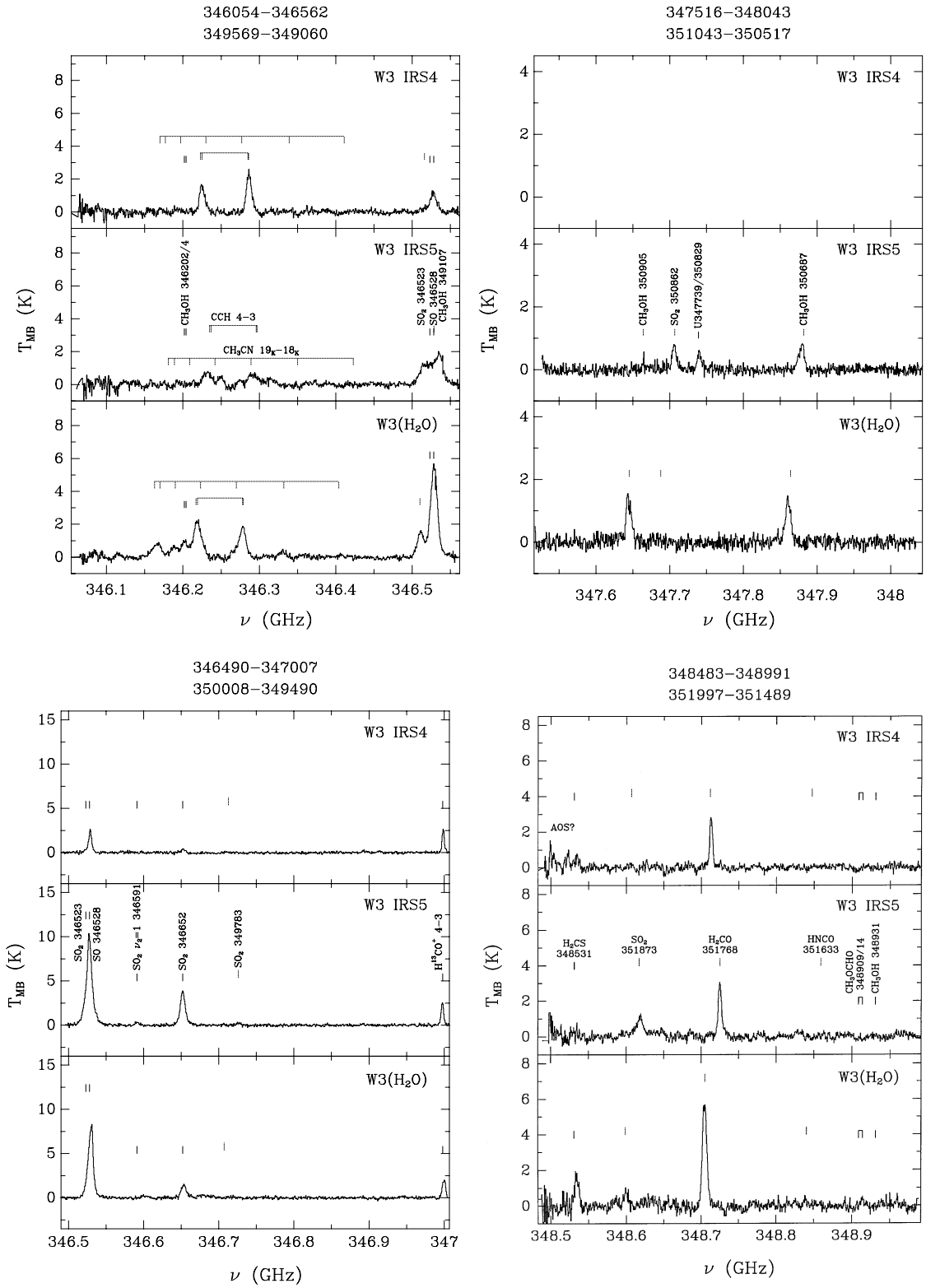

Fig. 4. continued

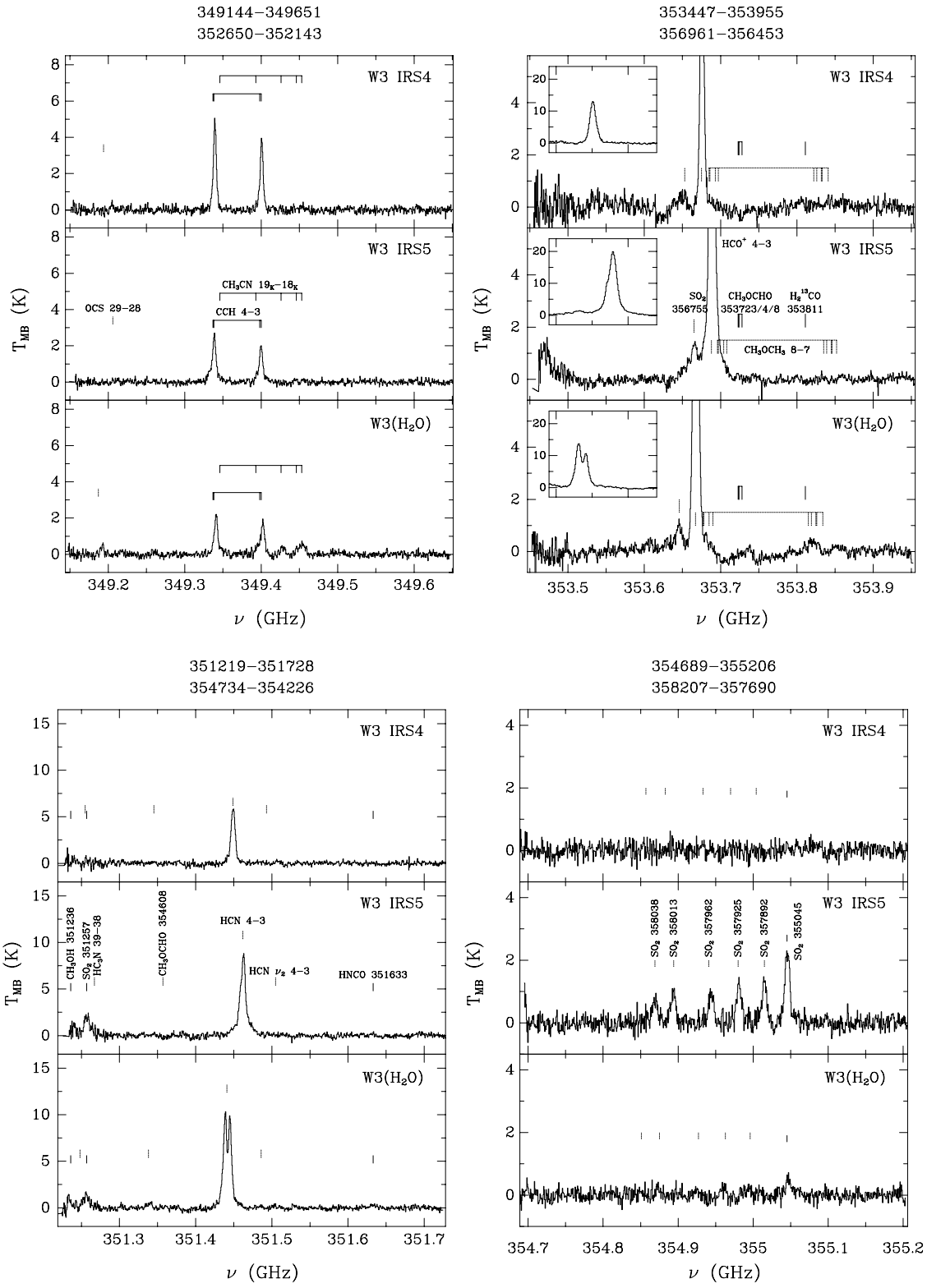

Fig. 4. continued

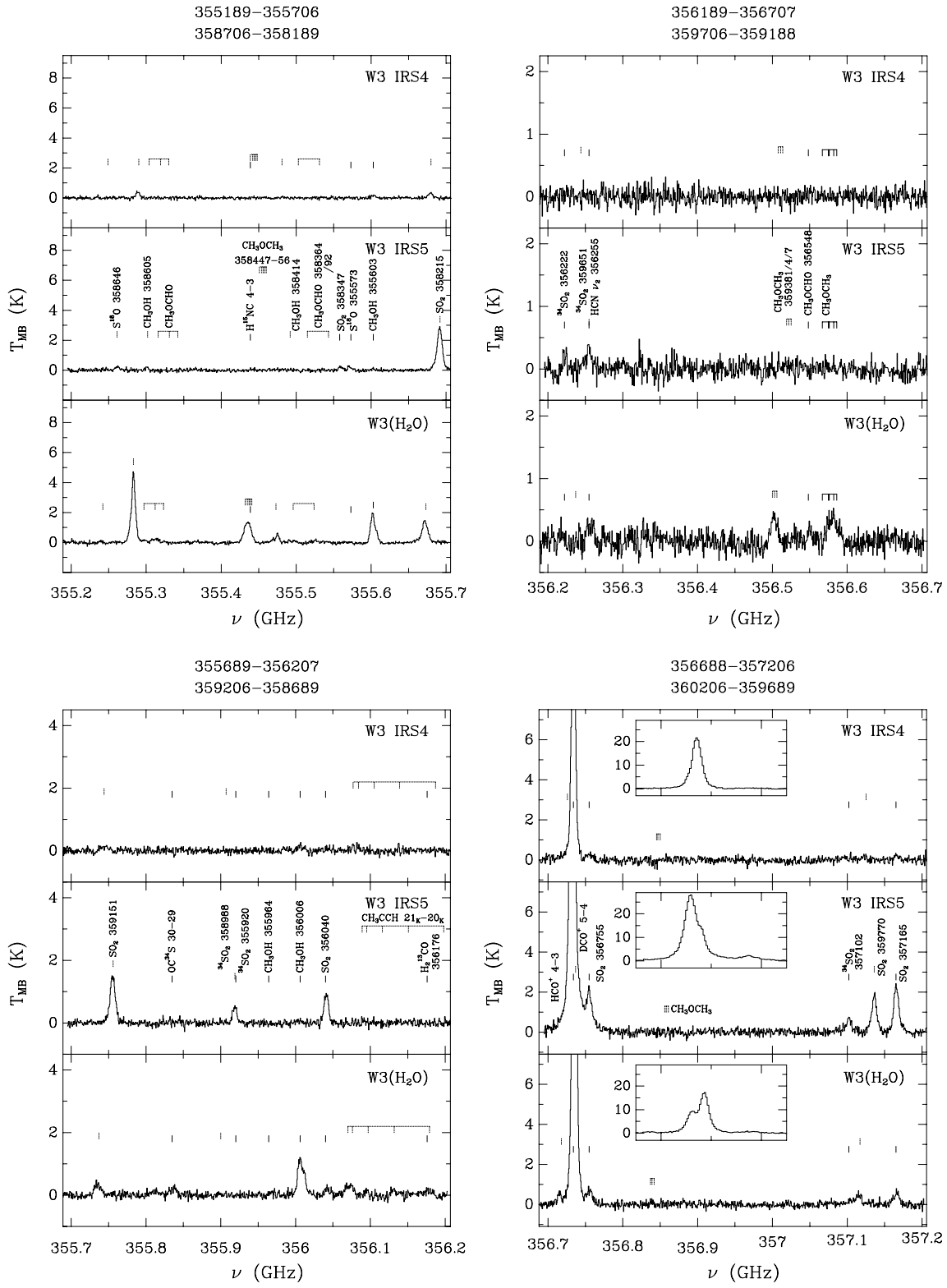

Fig. 4. continued

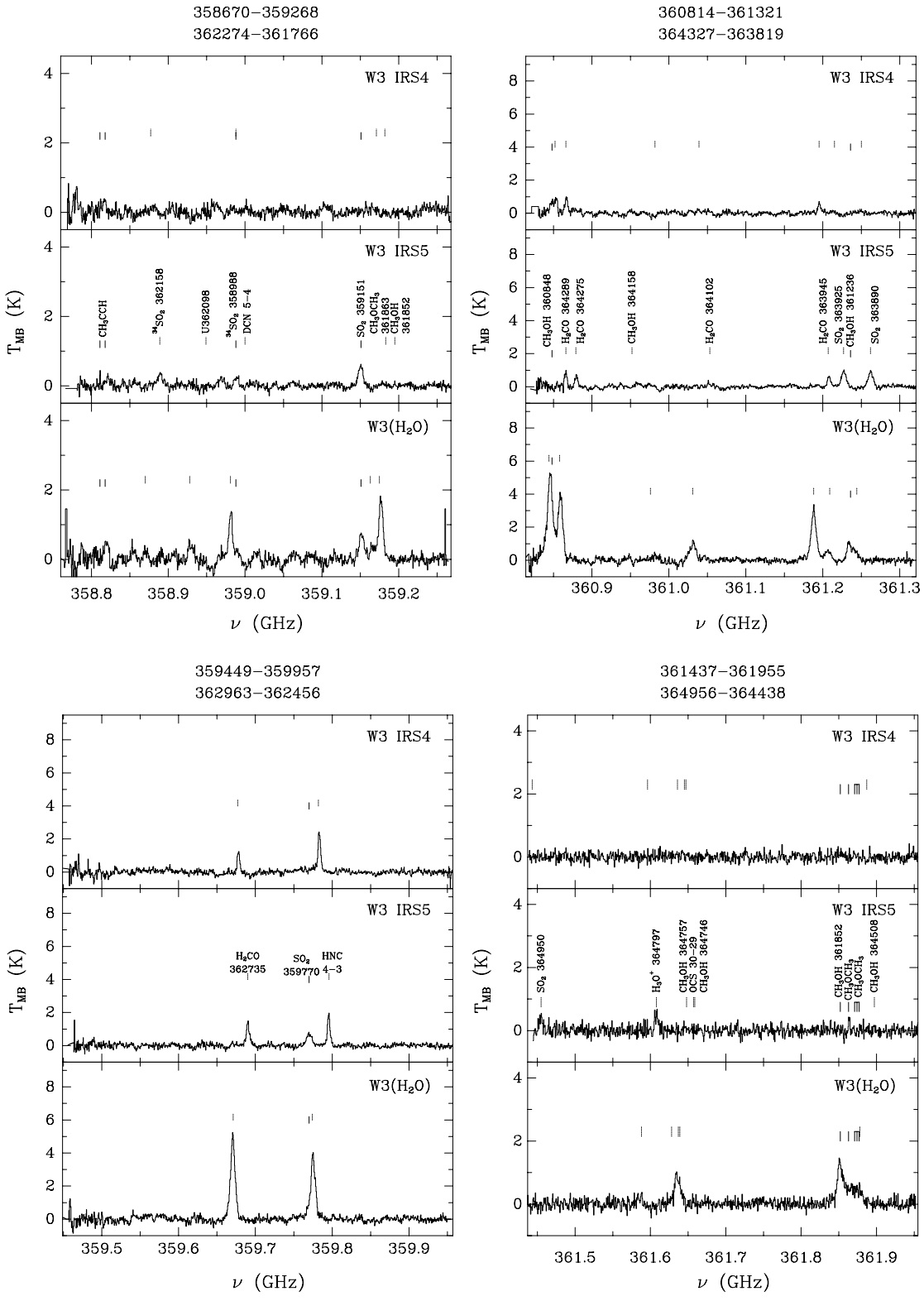

Fig. 4. continued